



National Library
of Canada

Bibliothèque nationale
du Canada

Canadian Theses Service

Services des thèses canadiennes

Ottawa, Canada
K1A 0N4

CANADIAN THESES

NOTICE

The quality of this microfiche is heavily dependent upon the quality of the original thesis submitted for microfilming. Every effort has been made to ensure the highest quality of reproduction possible.

If pages are missing, contact the university which granted the degree.

Some pages may have indistinct print especially if the original pages were typed with a poor typewriter ribbon or if the university sent us an inferior photocopy.

Previously copyrighted materials (journal articles, published tests, etc.) are not filmed.

Reproduction in full or in part of this film is governed by the Canadian Copyright Act, R.S.C. 1970, c. C-30.

**THIS DISSERTATION
HAS BEEN MICROFILMED
EXACTLY AS RECEIVED**

THÈSES CANADIENNES

AVIS

La qualité de cette microfiche dépend grandement de la qualité de la thèse soumise au microfilmage. Nous avons tout fait pour assurer une qualité supérieure de reproduction.

S'il manque des pages, veuillez communiquer avec l'université qui a conféré le grade.

La qualité d'impression de certaines pages peut laisser à désirer, surtout si les pages originales ont été dactylographiées à l'aide d'un ruban usé ou si l'université nous a fait parvenir une photocopie de qualité inférieure.

Les documents qui font déjà l'objet d'un droit d'auteur (articles de revue, examens publiés, etc.) ne sont pas microfilmés.

La reproduction, même partielle, de ce microfilm est soumise à la Loi canadienne sur le droit d'auteur, SRC 1970, c. C-30.

**LA THÈSE A ÉTÉ
MICROFILMÉE TELLE QUE
NOUS L'AVONS REÇUE**

THE UNIVERSITY OF ALBERTA

SOLVENT EXTRACTION-FLOW INJECTION ANALYSIS AND
COPPER ION SPECIATION BY ION EXCHANGE

by

JAMAL A. SWEILEH

A THESIS

SUBMITTED TO THE FACULTY OF GRADUATE STUDIES AND RESEARCH
IN PARTIAL FULFILMENT OF THE REQUIREMENTS FOR THE DEGREE
OF DOCTOR OF PHILOSOPHY

DEPARTMENT OF CHEMISTRY

EDMONTON, ALBERTA

SPRING 1986

Permission has been granted to the National Library of Canada to microfilm this thesis and to lend or sell copies of the film.

The author (copyright owner) has reserved other publication rights, and neither the thesis nor extensive extracts from it may be printed or otherwise reproduced without his/her written permission.

L'autorisation a été accordée à la Bibliothèque nationale du Canada de microfilmer cette thèse et de prêter ou de vendre des exemplaires du film.

L'auteur (titulaire du droit d'auteur) se réserve les autres droits de publication; ni la thèse ni de longs extraits de celle-ci ne doivent être imprimés ou autrement reproduits sans son autorisation écrite.

ISBN 0-315-30204-6

THE UNIVERSITY OF ALBERTA

RELEASE FORM

NAME OF AUTHOR JAMAL A. SWEILEH

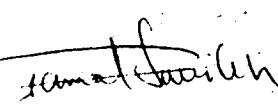
TITLE OF THESIS SOLVENT EXTRACTION-FLOW INJECTION ANALYSIS
AND COPPER ION SPECIATION BY ION EXCHANGE

DEGREE FOR WHICH THESIS WAS PRESENTED PH.D.

YEAR THIS DEGREE GRANTED 1986

Permission is hereby granted to THE UNIVERSITY OF ALBERTA LIBRARY to reproduce single copies of this thesis and to lend or sell such copies for private, scholarly or scientific research purposes only.

The author reserves other publication rights, and neither the thesis nor extensive extracts from it may be printed or otherwise reproduced without the author's written permission.

(Signed) 

PERMANENT ADDRESS:

P.O. Box 921 701
Jebel Al-Nuzha
Amman, Jordan

DATED

April 16

1986

THE UNIVERSITY OF ALBERTA
FACULTY OF GRADUATE STUDIES AND RESEARCH

The undersigned certify that they have read, and
recommend to the Faculty of Graduate Studies and Research,
for acceptance, a thesis entitled SOLVENT EXTRACTION-FLOW
INJECTION ANALYSIS AND COPPER ION SPECIATION BY ION EXCHANGE
submitted by JAMAL A. SWEILEH
in partial fulfilment of the requirements for the degree of
DOCTOR OF PHILOSOPHY.

F. F. Cantwell

F.F. Cantwell, Supervisor

B. Kratochvil

B. Kratochvil

G. Horlick

G. Horlick

R. B. Jordan

R.B. Jordan

J. A. Rogers

J.A. Rogers

J. Hubert
J. Hubert, External Examiner

DATE April 4th 1986

This thesis is dedicated to my wife,
my children, and my parents for their
endless love, understanding, patience, and
encouragement during the course of this work

ABSTRACT

Part I of this thesis deals with three aspects of the technique of solvent extraction/flow injection analysis (FIA) utilizing a porous membrane phase separator. First, solvent extraction/FIA is examined as a means of sample introduction to a flame atomic absorption spectrometer (AAS) in order to eliminate matrix and spectral interferences. As an example, a method is developed for the removal of matrix and spectral interferences of iron in the determination of trace amounts of zinc. The method involves prereduction of iron(III) to iron(II) followed by extraction of zinc as a thiocyanate complex into an organic solvent which is directly and continuously aspirated into the AAS nebulizer.

Second, a quantitative relationship between peak height and sample concentration in solvent extraction/FIA is derived and experimentally verified. The equation takes into account such factors as detector sensitivity, dilution due to band dispersion in the flow stream, fraction of analyte extracted and various flow rates in the flow injection and detection systems.

Third, the segmentation process, which produces small alternate segments of the two immiscible phases in solvent extraction/FIA, is studied as a function of total flow rate for a 1:1 phase ratio. A semiquantitative

physicochemical model is developed to describe this process which is based on the hydrodynamic and interfacial forces operative in the phase segmentor.

In Part II of this thesis a previously developed ion exchange flow-through column equilibration method for the determination of free (hydrated)-copper(II) ion is investigated in detail. The theoretical basis of the method of free metal ion speciation in the flow-through column equilibration mode is described and various experimental parameters are characterized and optimized.

At high pH values the formation of colloidal copper hydroxides tend to sorb onto the ion exchange resin column so that it is not possible to determine the free form.

The method is useful at lower pH (<6).

The method is also tested for specificity for free copper in the presence of various organic and inorganic ligands which may be found in natural water systems. The results are compared with those obtained by the use of a copper ion selective electrode method (ISE) and by speciation modelling calculations. The detection limit of the method is 2×10^{-8} M (1.3 parts per billion) with a relative standard deviation of 16%. The ion exchange column equilibration method is used to determine both free-copper concentration and the complexing capacity of a lake water sample from Québec.

ACKNOWLEDGEMENTS

I wish to express my deepest gratitude to Dr. Frederick F. Cantwell for his supervision, encouragement, and guidance during the course of this work and for his helpful suggestions in the presentation of this manuscript.

I wish also to express my sincere thanks to Dr. B. Kratochvil for his co-supervision, encouragement, and guidance of the second part of this work.

Sincere thanks are also extended to Miss A. Wiseman for her excellent work in typing this manuscript.

The author would like also to acknowledge the Inland Waters Directorate, Quebec Region for supplying the lake water sample.

Finally, the author is indebted to the University of Alberta for their financial support, to Dow Chemicals Canada Inc. for their contribution towards the preparation of this thesis and especially to the Natural Sciences and Engineering Research Council of Canada for a strategic grant to F.F.C. and B.K. in support of the work in Part II of this thesis.

TABLE OF CONTENTS

CHAPTER	PAGE
PART I. SOLVENT EXTRACTION/FLOW INJECTION ANALYSIS..	1
1. INTRODUCTION.....	2
2. SAMPLE INTRODUCTION BY SOLVENT EXTRACTION/FLOW INJECTION ANALYSIS TO ELIMINATE INTERFERENCES IN ATOMIC ABSORPTION SPECTROSCOPY.....	11
2.1 Introduction.....	11
2.2 Experimental.....	16
2.2.1 Chemicals and Reagents.....	16
2.2.2 Apparatus.....	17
2.2.3 Zinc Determination.....	20
2.3 Results and Discussion.....	25
2.3.1 FIA/AAS Interface.....	25
2.3.2 Extraction Characteristics.....	27
2.3.3 Flow Characteristics.....	32
2.3.4 Efficiency of the Membrane Phase Separator.....	34
2.3.5 Determination of Zinc in Iron Matrix.....	37
3. USE OF PEAK HEIGHT FOR QUANTIFICATION IN SOLVENT EXTRACTION/FLOW INJECTION ANALYSIS.....	43
3.1 Introduction.....	43

CHAPTER	PAGE
3.2 Experimental.....	44
3.2.1 Chemicals and Reagents.....	44
3.2.2 Apparatus.....	45
3.2.3 Sensitivity Curve.....	47
3.2.4 Effect of F_C	47
3.3 Results and Discussion.....	48
3.3.1 Derivation.....	48
3.3.2 Calibration Curve.....	51
3.3.3 Sensitivity Curve.....	52
3.3.4 Relative Dilution, R_V	54
3.3.5 Effect of F_{Carrier} on Peak Height....	57
3.3.6 Effect of F_{Reagent} on Peak Height....	59
3.3.7 Effect of F_O on Peak Height.....	61
3.3.8 Effect of F_C on Peak Height.....	63
3.3.9 Other Studies.....	63
4. HYDRODYNAMIC AND INTERFACIAL ORIGIN OF SEG- MENTATION IN SOLVENT EXTRACTION/FLOW INJECTION ANALYSIS	66
4.1 Introduction.....	66
4.2 Experimental.....	67
4.2.1 Solvents.....	67
4.2.2 Apparatus.....	67
4.2.3 Contact Angles.....	68

CHAPTER	PAGE
4.3 Results and Discussion.....	68
4.3.1 Contact Angles.....	68
4.3.2 Segmentation.....	69
PART II. EVALUATION OF A SEMIAUTOMATED ION EXCHANGE/ATOMIC ABSORPTION SYSTEM FOR FREE COPPER ION DETERMINATION IN NATURAL WATERS.....	80
1. INTRODUCTION.....	81
1.1 The Role of Speciation.....	81
1.2 Species Selective Techniques.....	83
1.2.1 Calculation Methods.....	84
1.2.2 Size Separation Methods.....	85
1.2.3 Voltammetric Methods.....	87
1.2.4 Ion Selective Electrode Methods.....	89
1.2.5 Ion Exchange Methods.....	90
1.2.6 Miscellaneous Methods.....	94
1.3 Research Objectives.....	95
2. THEORY OF SPECIATION MEASUREMENT BASED ON ION EXCHANGE.....	98
2.1 Ion Exchange Equilibria.....	98
2.2 Flow-Through Column Equilibration Method.....	101
2.3 Effect of Sorption of MOH^+	104
2.4 Effect of Metal Complexation with Electrolyte Anion.....	110

CHAPTER	PAGE
3. CHARACTERIZATION OF ION EXCHANGE/ATOMIC ABSORPTION SYSTEM FOR FREE COPPER DETERMINATION.....	116
3.1 Introduction.....	116
3.2 Experimental.....	117
3.2.1 Chemicals and Resins.....	117
3.2.2 Reagents and Solvents.....	118
3.2.3 Apparatus.....	119
3.2.4 Cleaning of Equipment.....	122
3.2.5 Resin Preparation.....	122
3.2.6 Sulfonation of XAD-4 Resin.....	123
3.2.7 Esterification of Amberlyst 15 Resin.....	124
3.2.8 Column Construction.....	125
3.2.9 Instrumental Conditions.....	127
3.2.10 Test Solution Preparation.....	127
3.2.11 Free Metal Determination.....	129
3.3 Results and Discussion.....	130
3.3.1 Choice of Eluent.....	130
3.3.2 Buffering of the Test Solutions.....	131
3.3.3 Effect of Copper Concentration on Column-Test Solution Equilibration Times at $\text{pH} \leq 6$	135
3.3.4 Effect of pH on Column-Test Solution Equilibration Times.....	136

3.3.5	Testing for Presence of Copper- Containing Colloids.....	141
3.3.6	Effect of Aging of Test Solutions.....	147
3.3.7	Assessment of a Larger Ion Exchange Resin Column to Increase Sensitivity..	149
3.3.8	Effect of Ionic Strength.....	151
3.3.9	Calibration Curve, Detection Limit, and Precision.....	158
4.	EFFECT OF COMPLEXING LIGANDS ON FREE-COPPER DETERMINATION BY THE ION EXCHANGE COLUMN EQUILIBRATION/AAS METHOD.....	161
4.1	Introduction.....	161
4.2	Experimental.....	164
4.2.1	Chemicals.....	164
4.2.2	Reagents.....	164
4.2.3	Apparatus.....	166
4.2.4	Calculation of Copper Species Distributions as a Function of Ligand Concentration.....	166
4.2.5	Preparation of Test Solutions and Blanks.....	168
4.2.6	Determination of Free Copper by Ion Selective Electrode (ISE) Potentiometry.....	169

4.2.7	Treatment of the Bonneville Lake Water Sample and Standard.....	170
4.2.8	Preparation of Sample Solutions for the Determination of the Com- plexing Capacity of the water Sample..	171
4.3	Results and Discussion.....	172
4.3.1	Effect of Chloride on Free-Copper Determination.....	172
4.3.2	Effect of Orthophosphate on Free- Copper Determination.....	175
4.3.3	Effect of Sulfate on Free-Copper Determination.....	179
4.3.4	Effect of Glycine on Free-Copper Determination.....	184
4.3.5	Effect of Phthalate on Free-Copper Determination.....	186
4.3.6	Effect of Citrate on Free-Copper Determination.....	189
4.2.7	Effect of Salicylate on Free-Copper Determination.....	192
4.3.8	Effect of Fulvic Acid on Free-Copper Determination.....	196
4.3.9	Determination of Free Copper in a Lake Water Sample.....	200

CHAPTER

PAGE

4.3.10	Determination of the Complexing Capacity of a Bonneville Lake Water Sample by Copper Titration.....	201
4.3.11	Determination of the Total Copper Concentration in Lake Water by Graphite Furnace AAS.....	203
5	CONCLUSIONS AND FUTURE WORK.....	206

REFERENCES.....	211
APPENDIX A: CALCULATION OF METAL SPECIES DISTRIBUTION.....	231
APPENDIX B: DERIVATION OF AN EXPRESSION FOR THE EFFECT OF SORPTION OF ANOTHER SPECIES IN ADDITION TO FREE METAL.....	236

LIST OF TABLES

TABLE	PAGE
1. Instrument parameters used with the PE 290B and PE 4000 spectrophotometers for direct aspiration and for FIA.....	24
2. Assay of synthetic samples containing 2% iron for their zinc content by direct aspiration AAS and by extraction/FIA/AAS.....	40
3. Effect of compensating flow rate on signal and constancy of $(F_M + F_C)$	64
4. Instrumental parameters of the PE 4000 spectrophotometer for the determination of free metals by the ion exchange column equilibration method.....	128
5. Effect of test solution aging on pH for copper and nickel.....	150
6. Composition of test solutions used to test for CuNO_3^+ formation.....	156
7. Instrumental conditions for the PE 5000 graphite furnace AAS for the determination of total copper in lake water sample.....	167
8. Species distributions of sodium and sulfate at constant total sodium concentration but variable total sulfate concentration.....	182

TABLE

PAGE

9. Chemical composition of Bonneville Lake water, Quebec, and a pothole lake near Erickson, Manitoba.....	204
---	-----

LIST OF FIGURES

FIGURE		PAGE
1.	Block diagram of a simple solvent extraction/FIA system showing an expanded section of the segmented flow.....	6
2.	Solvent extraction/FIA apparatus for elimination of interferences in the determination of traces of zinc in iron matrix.....	18
3.	A three-dimensional view of the membrane phase separator.....	21
4.	Diagram of the Kel-F segmentor showing the Teflon inserts.....	22
5.	Effect of extraction coil length on peak height.....	28
6.	Variation of peak height with sample volume injected.....	30
7.	Variation of sensitivity of the AA spectrophotometer with flow rate into the nebulizer.....	33
8.	Variation of maximum membrane phase separator efficiency and flow rate through the membrane with total flow rate of both phases.....	36
9.	Calibration curves for the determination of zinc in iron matrix by direct aspiration of	

the aqueous solution and by solvent extraction/FIA/AAS.....	38
10. The absorbance of pure iron solutions at the wavelength of zinc resonance line with (A) and without (B) D_2 background correction.....	42
11. Sensitivity curves for zinc thiocyanate in MIBK as a function of flow rate into the nebulizer of the AA spectrometer.....	53
12. Effect of sample volume injected on peak height for different concentrations of o- nitroaniline in water using Version II instrument.....	55
13. Effect of Carrier stream flow rate on peak height (A) and peak width at half height (B).....	58
14. Effect of Reagent stream flow rate on peak height.....	60
15. Effect of organic phase flow rate on peak height.....	62
16. Segment length <u>vs</u> total flow rate for chloroform-water (A) and methylisobutyl- ketone-water (B).....	71
17. Diagram of segment formation at the "tee".....	72

18. Diagram of the flow-through column ion exchange equilibration system for free-copper determination..... 120
19. Details of column construction..... 126
20. Absorption spectrum of 2,6-lutidine (A), of 2,6-lutidine plus $\text{Cu}(\text{NO}_3)_2$ (B1), of $\text{Cu}(\text{NO}_3)_2$ (B2), and the net subtraction of B2 from B1 (B3)..... 134
21. Effect of copper concentration on equilibration time at pH 6..... 137
22. Effect of pH of test solution on column equilibration time..... 139
23. Calculated copper species distributions as a function of pH for total copper concentrations of 10^{-7} M (A) and 10^{-4} M (B)..... 140
24. Effect of filtration of the test solution on the shape of the equilibration curve..... 143
25. Equilibration curves for different total copper concentrations..... 146
26. Effect of aging of test solution on the relation between metal uptake and pH for copper and nickel..... 148
27. The distribution coefficient of free copper between the resin and the aqueous phases as a function of ionic strength..... 153

28. Chart recorder tracings for a calibration curve for free-copper determination by the ion exchange column equilibration method..... 159
29. Copper species distribution as a function of chloride concentration and the decrease in relative free copper with chloride concentration..... 173
30. Copper species distribution as a function of orthophosphate concentration and the decrease in relative free copper with phosphate concentration..... 177
31. Copper species distribution as a function of sulfate concentration and the decrease in relative free copper with sulfate concentration..... 180
32. Copper species distribution as a function of glycine concentration and the decrease in relative free copper with glycine concentration..... 185
33. Copper species distribution as a function of phthalate concentration and the decrease in relative free copper with phthalate concentration..... 188

FIGURE

PAGE

34. Copper species distribution <u>vs</u> total citrate concentration and the decrease in relative free copper with citrate concentration.....	191
35. Copper species distribution <u>vs</u> total salicylate concentration and the decrease in relative free copper with salicylate concentration.....	194
36. The decrease in relative free copper as a function of fulvic acid concentration.....	198
37. Relation between the total copper concentration in the sample solution and the free-copper concentration as determined by the ion exchange column equilibration/AAS method.....	202

LIST OF SYMBOLS

SYMBOL	DESCRIPTION
A	aqueous
a	ionic activity, or minor axis of ellipse
α_i	fraction of a component present as species i
AAS	atomic absorption spectrophotometry
AR	area of the drop of organic phase facing the aqueous stream
ASV	anodic stripping voltammetry
AUSF	absorbance units full scale
β	formation constant of metal-ligand complex
β'	conditional formation constant of metal-ligand complex
C	concentration
C_{pk}	concentration at the peak maximum
CIT	citrate ion
D	distribution ratio between two phases
D_C	internal diameter of the extraction coil
D_H	internal diameter of the horizontal branch of the tee segmentor
D_V	internal diameter of the vertical branch of the tee segmentor

SYMBOL	DESCRIPTION
ΔP	pressure drop across the organic drop in the segmenter
$\Delta \rho$	density difference between the organic solvent and water
en	ethylenediamine
η	viscosity
F	volumetric flow rate
F_A, F_a	total volumetric flow rate of the aqueous phase
F_C	volumetric flow rate of the compensating stream
F_M	volumetric flow rate of the organic phase through the membrane
F_O	total volumetric flow rate of the organic phase
F_T	total volumetric flow rate ($F_A + F_O$)
F_W	volumetric flow rate to waste
f_{HYD}	hydrodynamic force
f_{INT}	interfacial force
FIA	flow injection analysis
ϕ	fraction of the analyte extracted into the organic phase
G	weight of dry ion exchange resin in the column

SYMBOL	DESCRIPTION
GLY	glycinate anion
g	gravitational constant or gram
γ	surface tension or activity coefficient
$\gamma_{O/W}$	liquid-liquid interfacial tension between the organic and water phases
h	height of the capillary rise
ISE	ion selective electrode
i.d.	internal diameter
K_{IE}	concentration ion exchange equilibrium constant
K_{IE}^{Th}	thermodynamic ion exchange equilibrium constant
k_w	autoprotolysis constant of water
k_{an}	nth acid dissociation constant ($n > 1$)
L	segment length or ligand or litre
λ_O	resin distribution coefficient of free metal ion.
λ_i	resin distribution coefficient of species i
<u>M</u>	molarity (moles/litre)
M_T	total metal concentration
μ	ionic strength
O	organic
o.d.	outer diameter

SYMBOL	DESCRIPTION
P_1	upstream pressure across the drop of organic phase
P_2	downstream pressure across the drop of organic phase
P.A.	peak area
P.H.	peak height
PTH	phthalate ion
R	equivalent radius of ellipse or resin fixed charge site
R_v	relative dilution of the injected sample due to dispersion
r.s.d.	relative standard deviation
ρ	density
S	sensitivity of the atomic absorption detection system ($\text{absorbance} \cdot \text{mL} \cdot \text{mole}^{-1}$)
S_F	sensitivity of the atomic absorption detection system ($\text{cm} \cdot \text{mL} \cdot \mu\text{g}^{-1}$)
SAL	salicylate ion
s	second
θ	the solid-liquid-liquid contact angle

PART I

SOLVENT EXTRACTION/FLOW INJECTION ANALYSIS

CHAPTER 1

INTRODUCTION

Since the introduction of flow injection analysis (FIA) in the mid-seventies by Ruzicka and Hansen [1] and independently by Stewart et al. [2], the FIA method has found a wide range of application as a novel approach for automation of wet chemical methods of analysis. This is evident in the numerous reviews on the technique which appeared in the scientific literature [3-12] and a monograph [13].

Specifically, FIA involves the reproducible injection of the sample in a continuously flowing non-segmented carrier stream. The carrier stream may contain a reagent which reacts with the sample component. FIA is based on a combination of three fundamental features; sample injection, controlled dispersion, and reproducible timing. The key feature is the use of flow-induced dispersion of the sample "slug" as it moves through a narrow bore tube. This produces controlled mixing of the sample solution with the carrier stream. Flow-induced dispersion of the sample is highly reproducible as long as the flow rate is constant and a consistent injection

technique is used. Furthermore the extent of dispersion can be controlled by varying the flow rate, the sample volume injected, and the dimensions of the tube.

Under laminar flow conditions, dispersion in narrow bore tubes arises from the fact that the linear velocity of the injected sample solution zone in the centre of the tube is twice the mean velocity of the liquid, whereas the layers closer to the wall are progressively more retarded [14]. Thus mixing between the carrier stream and the sample solution is always incomplete, but because the mixing pattern is highly reproducible, FIA yields reproducible results. Reijn et al. [14] semiquantitatively described the dispersion process in open tubes; they showed that non-uniform velocity distribution (wall drag) is the prime cause of dispersion. Lateral relaxation of the parabolic flow occurs because of diffusion but it can be markedly enhanced by inducing lateral convection by either coiling the tube [15] or more efficiently by making use of packed bed reactors [14,16].

The basic components of a flow injection system are: (a) a device for propelling the flowing streams such as a pulse-free peristaltic pump or a pneumatic pump; (b) a means of sample injection such as a rotary valve; (c) suitable reaction manifolds for various chemical

operations such as sample dispersion, reagent addition, solvent extraction, etc. and (d) a suitable detector. The most attractive features of FIA include reduction of analysis time, sample volume, and reagent consumption; minimal need for sample pretreatment; feasibility of automation; high precision; high sampling rate; and minimization of contamination.

FIA is quite different from air-segmented continuous flow analysis (CFA). FIA involves injection of a highly reproducible volume of the sample in a flowing stream. This is unlike the aspiration approach taken in CFA, which is relatively imprecise. The incorporation of the compressible air segments in the CFA renders the system more complex and causes pulsation of the flow. This in turn causes irregularities in dispersion which are minimized in CFA systems by allowing a steady state plateau to be closely approached [17]. This requires a relatively large volume of sample solution with consequent reduction in sampling rate.

Automation of solvent extraction by CFA and FIA is especially valuable for metallurgical, geological, and clinical analysis where a large number of samples is to be handled. As with manual solvent extraction techniques, analyte may be preconcentrated or various interferents eliminated by careful choice of the chemistry involved and

the extraction conditions (Chapter 2). Although solvent extraction/CFA has been in use for quite some time [18], solvent extraction/FIA was introduced fairly recently by Karlberg and Thelander [19] and independently by Bergamin F° et al. [20]. Figure 1 shows the essential components of a solvent extraction manifold for flow injection analysis; a Teflon extraction coil is generally used together with two special devices, a segmentor and a phase separator. The sample is injected in the carrier stream, A (usually aqueous). In its simplest form the segmentor, S, is a standard Kel-F tee piece [21,22] in which the stream of organic phase, O, is merged with carrier stream, A. A regular pattern of alternate segments of the two phases emerges from the segmentor and flows through the extraction coil, C, to the phase separator, P. A portion of the extract and/or the raffinate flow through the phase separator to a detector, D.

Various types of tees have been used as the segmentors; Karlberg et al. [19] used a modified A8T standard connector (Technicon). In this segmentor the organic phase was introduced through a platinum capillary while the aqueous phase entered through a glass inlet. The segment length is variable, being determined by the position of the end of the Teflon tube connected to the outlet arm. Kawase et al. [23] used an A10T standard

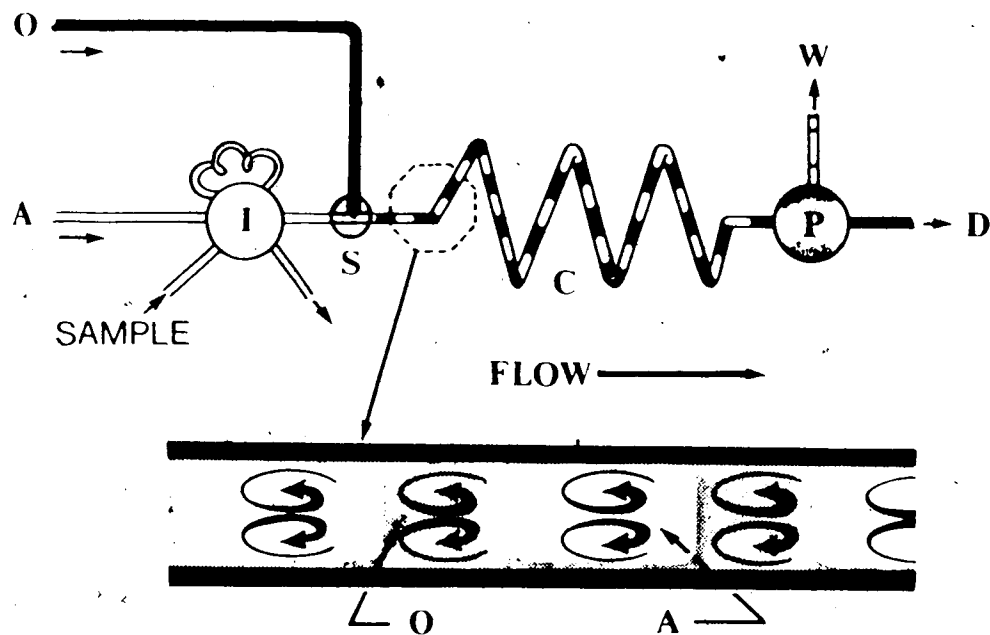


Figure 1. Diagram of a solvent extraction/FIA system. O is the organic phase, A is the aqueous phase, I is the injection valve, S is the segmentor, C is the extraction coil, P is the phase separator, D is the detector, and W is waste. The lower part of the diagram is an enlarged section of the extraction coil showing individual segments; the spiral arrows refer to the direction of liquid flow in each segment.

connector (Technicon) without any modification. Bengtsson et al. [24] reported a specially designed segmentor with a variable (1-15 mm) segment length. Segment length was found to vary with flow rate and there was hysteresis when flow rate was decreased. The relation between segment length and flow rate was critically examined by Cantwell and Sweileh [25] (Chapter 4) for a tee segmentor. They modified the standard Kel-F tee piece by inserting small narrow Teflon tubes in all arms, thereby obtaining a regular segmentation pattern at total flow rates up to 13 mL/min [26] (Chapter 2).

The extraction coil is generally a few-meter long Teflon tube through which the segmented stream travels. The sample, occupying many aqueous segments, will extract into neighbouring organic segments as it moves along the extraction coil. The organic phase will wet the wall of the Teflon coil, and it is believed that the aqueous phase segments are separated from the wall of the extraction coil by a thin film of the organic phase [24,27-29].. Extraction from the aqueous to the organic phase occurs by diffusion across the interfaces. As for air-segmented CFA, wall drag causes bolus flow within each segment, which promotes efficient mixing of the liquid [18]. Figure 1 shows an enlarged section of the segmented stream; the spiral arrows indicate the direction of bolus

flow within the segment. The thickness of the arrow is proportional to flow rate within the liquid, which is greatest in the centre of the extraction coil. As mentioned earlier coiling of the extraction tube promotes convective lateral mixing (not shown in Figure 1) [15,30].

At the end of the extraction coil the segmented stream is fed to the phase separator which allows part of the phase of interest to pass to the detector, D, yielding a peak-shaped sample zone, while rejecting the rest of the two-phase stream to waste. A variety of phase separators are employed in FIA; the simplest is a conventional glass tee piece where separation of the two phases is based on the difference in specific gravity [20]. In another design the glass tee was modified by incorporating some Teflon strands to guide the wetting organic phase from the inlet of the tee to the outlet [19]. In this case separation is achieved by both gravity and phase guidance.

A major breakthrough in solvent extraction/FIA has been the development of the porous membrane phase separators [21,23,31-33]. As for the tee phase separators, the membrane phase separators have an internal chamber, one inlet, and two outlets. However the outlet for the phase of interest is separated from the internal chamber by a porous membrane which is permeable to that

phase but impermeable to the other. In general, Teflon membranes are used for separation of the organic phase, while cellulose membranes are used for separation of the aqueous phase.

The porous membrane phase separators are characterized by a high separation efficiency even with high flow rates. The device generally has a low internal volume in order to avoid excessive broadening of the peak-shaped sample zone. A dual membrane phase separator has been described by Fossey and Cantwell [22]. This permits simultaneous monitoring of both phases. In an alternative approach, Burguera and Burguera [34] used a tee-type membrane phase separator for complete separation of the two phases.

In Part I of this thesis studies of three aspects of solvent extraction/FIA are described. In Chapter 2 solvent extraction/FIA is examined as a means of sample introduction and elimination of interferences in flame atomic absorption spectrophotometry. As an example, the matrix and spectral interferences in the determination of traces of zinc in iron matrix were eliminated. In Chapter 3 the quantitative relationship between peak height and sample concentration in solvent extraction/FIA is established and experimentally verified [35]. The derived equation takes into consideration such factors as detector

sensitivity, dilution due to band dispersion, fraction extracted, and various flow rates in the flow injection and detection systems. In the last chapter, the segmentation process in solvent extraction/FIA is studied as a function of flow rate and a semiquantitative physicochemical model is developed to describe this process. The model is based on hydrodynamic and interfacial forces operative in the tee phase segmentor.

CHAPTER 2

SAMPLE INTRODUCTION BY SOLVENT EXTRACTION/FLOW INJECTION ANALYSIS TO ELIMINATE INTERFERENCES IN ATOMIC ABSORPTION SPECTROSCOPY

2.1 Introduction

Several types of interference plague flame atomic absorption spectrophotometry (AAS). Physical interference arises from differences in viscosity and surface tension which lead to sample-to-sample changes in rate and efficiency of aspiration and atomization as well as changes in the vapor pressure of the solid and liquid components of the sample [36]. Physical interferences can be eliminated by matching the physical properties of all standard and sample solutions and by the "standard addition" technique. Another interference commonly encountered in flame AAS is chemical in nature. It arises from incomplete vaporization and atomization of the analyte due to formation of highly stable chemical compounds at the flame temperature. A classical example here is the depression of the calcium atomic absorption signal in the presence of phosphate, silicate or aluminum ions [37]. Several strategies are routinely used to

eliminate chemical interference. Using a hotter flame such as nitrous oxide/acetylene increases the extent of vaporization and atomization. Addition of releasing agents is another method of eliminating chemical interference. Releasing agents (e.g. lanthanum) tend to preferentially react with an interfering anion thus preventing the analyte atom from forming a refractory compound. Finally chemical interferences are reduced by the addition of masking agents (e.g. EDTA) which form easily atomized compounds with the analyte.

Ionization interference is a third type of interference which is usually encountered in the analysis of the alkali metals. A substantial amount of the easily ionized elements will be in the ionized state in the flame leading to a lower atomic absorption signal. Ionization can be suppressed [38] by addition of a more easily ionized element to the samples and standards. This shifts the analyte ionization equilibrium towards the atomic form by providing a high electron density in the flame.

Ionization can also be reduced by using a cooler flame.

Spectral interference arises from any non-specific radiation, emission or absorption that falls within the spectral bandpass of the monochromator [39]. It can be subdivided into three main types:


- (a) Light scattering [40] is due to incomplete atomization of the test solution so that the flame contains solid particles and solvent droplets which tend to scatter the light beam falling on them. This gives erroneous absorption signals by attenuating the intensity of the incident light.
- (b) Molecular spectral interference is a common type of spectral interference in AAS, and arises from absorption of molecules in the flame such as CaOH, OH, H₂O and flame gases such as CO₂, CO, N₂, CN, etc.
- (c) Spectral line interference is relatively uncommon in AAS but is sometimes, reported in the literature [39,41-43]. It may arise from the presence of more than one absorbing or emitting line in the spectral bandpass of the monochromator, from a non-absorbable line emitted by the source (e.g. filler gas line), or from direct total or partial overlap of two absorption lines of different elements. Lovett et al. [39] listed cases of potential spectral line overlap. Experimental results confirmed the presence of such interference in some cases.

Both light scattering and molecular absorption spectral interferences are almost constant in intensity over the spectral bandpass and can be compensated for by various methods of background correction [44-46]. In some

cases of "highly structured" background absorption, correction even by the most elegant method may not be satisfactory [43,47] and may lead to over or undercorrection. The only methods available for overcoming spectral line interference are either to choose another analytical line where there is no spectral interference or to separate the interfering element [42].

Solvent extraction is one of the most commonly used separation techniques prior to AAS [48-51]. The vast body of literature on the solvent extraction of metals serves as a readily available source of extraction systems to separate almost any metallic element from other metals or nonmetals [52-57]. However manual solvent extraction procedures are operator-intensive and relatively time consuming so that, where possible, alternative approaches to minimize interference in AAS, which do not involve separation, are generally preferred.

In the past few years devices have been reported for performing automated solvent extraction in the flow injection analysis (FIA) mode (Chapter 1). Such devices can be flow-coupled to the nebulizer of an AA spectrophotometer to provide a rapid and convenient means of performing solvent extraction separations prior to atomic absorption determinations. Solvent extraction/FIA systems have been described for metal assays in



conjunction with various detector systems including molecular absorption spectrophotometry by extracting the neutral complexes [20,34,58], flame [26,32,59,60], and graphite furnace atomic absorption spectrophotometry [24,61]. Flame AAS has also been used for the indirect determination of perchlorate by liquid-liquid extraction/FIA [62].

The solvent extraction/FIA system used here is based on one previously described [21,22] which employs constant pressure pumping and a porous membrane phase separator. The organic extract is methylisobutylketone (MIBK) which, after it extracts the analyte element, is introduced directly and continuously into the nebulizer. Pure MIBK is used to compensate the disparity between the flow rate of the organic extract stream and the aspiration rate of the nebulizer. As an example, zinc has been determined in the presence of a large excess of iron. This determination is known to suffer from several interferences [39,42,43,63,64]. The nature of these interferences was investigated [42] and found to be due to a combination of background absorption and/or light scattering and a spectral line interference due to the presence of a weakly absorbing iron line at 213.859 nm partially overlapping the zinc principal analytical line at 213.856 nm. A second zinc atomic absorption line at 307.6 nm is 7×10^3

times less sensitive than the principal line and is not suitable for trace zinc determination [65].

Chemically the extraction/FIA determination of zinc developed here involves the prereduction of Fe(III) to Fe(II) by ascorbic acid followed by extraction of $\text{Zn}(\text{SCN})_2$ into MIBK. The Fe(II) remains unextracted. Quantification is based on peak height of the AA signal for the extracted zinc. The method is analogous to the manual procedure used by Headridge and Sowerbutts for the determination of tin in steel [66].

2.2 Experimental

2.2.1 Chemicals and Reagents

All chemicals used were reagent grade unless otherwise stated. Glassware was soaked in 30% nitric acid (Fisher Scientific Limited, Fair Lawn, NJ) for 24 h prior to use. Distilled, deionized water was used in the preparation of all aqueous solutions.

Iron solution (2%) was prepared by slowly dissolving 2 g of Specpure iron powder (Spex Industries Inc., Metuchen, NJ) according to the procedure reported by Headridge et al. [66]. Hydrochloric acid (Fisher Scientific Limited) and formic acid (Baker & Adamson, supplied by Allied Chemicals, Morristown, NJ) were used in

the digestion procedure.

Zinc stock solution (1000 $\mu\text{g/mL}$) was prepared by dissolving 1 g of zinc granules (Shawinigan, distributed by McArthur Chemical Co., Montreal, Quebec) in 0.1 M HCl solution and diluting to 1 L with 0.1 M HCl.

Potassium thiocyanate solution (0.5 M) was prepared by dissolving the salt (Fisher Scientific Co., Fair Lawn, NJ) in 0.1 M HCl solution.

Solid L(+) ascorbic acid (Anachemia, Montreal, Quebec) was used as received.

Methylisobutylketone and acetone (Fisher Scientific Co., Fairlawn, NJ) were used without further purification.

All reagents used were vacuum filtered through a 10-20 μm sintered glass buchner funnel in order to remove any solid particles which otherwise might block the flow system.

2.2.2 Apparatus

The extraction/FIA system used was similar to the one described in earlier reports [21,22], and is shown schematically in Figure 2. Organic reagents to be pumped were kept in 1.7-L glass bottles placed inside aluminum cylinders which were pressurized with nitrogen. Aqueous solutions were kept in 2-L polyethylene bottles in the pressurized cylinders instead of in glass bottles. Flow

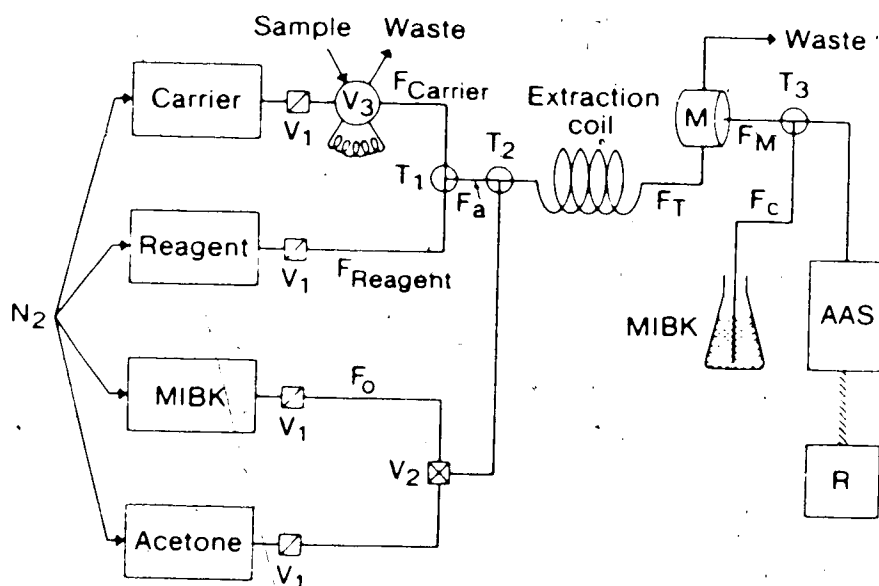


Figure 2. Solvent extraction/FIA/AAS system for elimination of spectral interference in the determination of traces of zinc in an iron matrix. Carrier is 0.1 M HCl, reagent is 0.5 M KSCN in 0.1 M HCl, V_1 and V_2 are two- and three-way valves respectively, V_3 is the injection valve, T_1 and T_3 are tees, T_2 is the segmentor, C is the extraction coil, M is the membrane phase separator, F_c is a compensating flow, and R is a recorder. See text for details.

rates of aqueous carrier F_{Carrier} , of the aqueous reagent F_{Reagent} , of total MIBK F_0 and of MIBK through the membrane F_M are identified on the diagram. Flow rates F_{Carrier} , F_{Reagent} and F_0 were adjusted by inserting suitable lengths of 0.3 mm i.d. Teflon tubing immediately downstream of valves V_1 . Except where it is desired to minimize sample bandbroadening, 0.8-mm i.d. Teflon tubing was used throughout the system. Two-way valves, V_1 (part no. CAV 2031, Laboratory Data Control (LDC), Riviera Beach, FL), placed in the solvent and reagent delivery lines served as on-off valves. A three-way valve V_2 (part no. CAV 3031, LDC) allows selection of either MIBK or acetone. The latter is used to flush the system whenever necessary.

The sample injection valve V_3 (Altex, model 202-00, Altex Inc., Berkeley, CA) allows manual injection of the sample into the carrier stream (0.1 M HCl). The reagent stream (0.5 M KSCN, 0.1 M HCl) mixes with the carrier stream at the Cheminert tee fitting, T_1 (part no. CJ-3031, LDC). The combined aqueous stream joins the MIBK stream at the segmentor, T_2 , and the resulting segmented flow stream passes through the extraction coil, C, in which $\text{Zn}(\text{SCN})_2$ is extracted into the MIBK segments. As previously, the extraction coil is made of 0.8-mm i.d. Teflon tubing. In the membrane phase separator, M, which

has been described in Chapter 1 [21] (Figure 3), a fraction of the MIBK phase passes through the porous Teflon membrane and is directed to the nebulizer of the AA spectrophotometer (either a Model 290B or a Model 4000, Perkin-Elmer Corp., Norwalk, CT). Because the aspiration rate of the nebulizer is usually higher than the flow rate of MIBK through the membrane (F_M), a flow compensator tee (T_3) provides for the difference to be made up by a compensating flow (F_C) of MIBK from the flask. The flow rate of the aqueous phase, F_a , is equal to F_{Carrier} plus F_{Reagent} and the total flow rate through the extraction coil, F_T is equal to F_a plus F_O . The strip chart recorder, R, is a model 7127A (Hewlett Packard).

The phase segmentor, T_2 , is shown in enlarged detail in Figure 4. It was made by drilling out the small bore cylindrical chamber of a commercially available Kel-F tee (part no. CJ-3031, LDC) to 1/16 in i.d. and inserting 2-mm long flared pieces of 0.8-mm i.d. \times 1/16 in o.d. Teflon tubing into the three branches of the tee.

2.2.3. Zinc Determination

Following is the general procedure for the determination of trace zinc in the presence of a large excess of iron. If the sample is a solid it is first dissolved by the procedure described by Headridge and

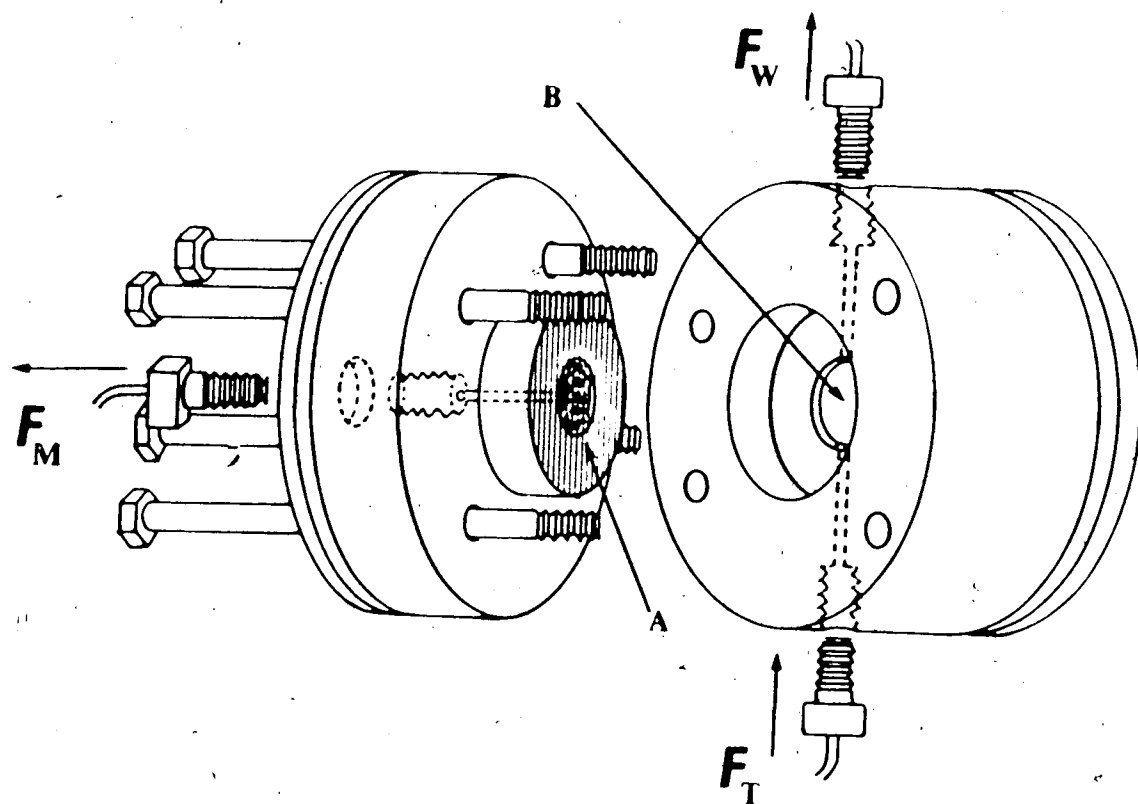


Figure 3. A three-dimensional view of the membrane phase separator used in this work. The porous Teflon membrane (A) is sandwiched between two Kel-F blocks thus partitioning the organic phase outlet from the internal separation chamber (B). The two blocks are pressed together with four screws and two metal end plates. The radial and circular grooves in the left hand membrane support direct the organic phase to the outlet hole.

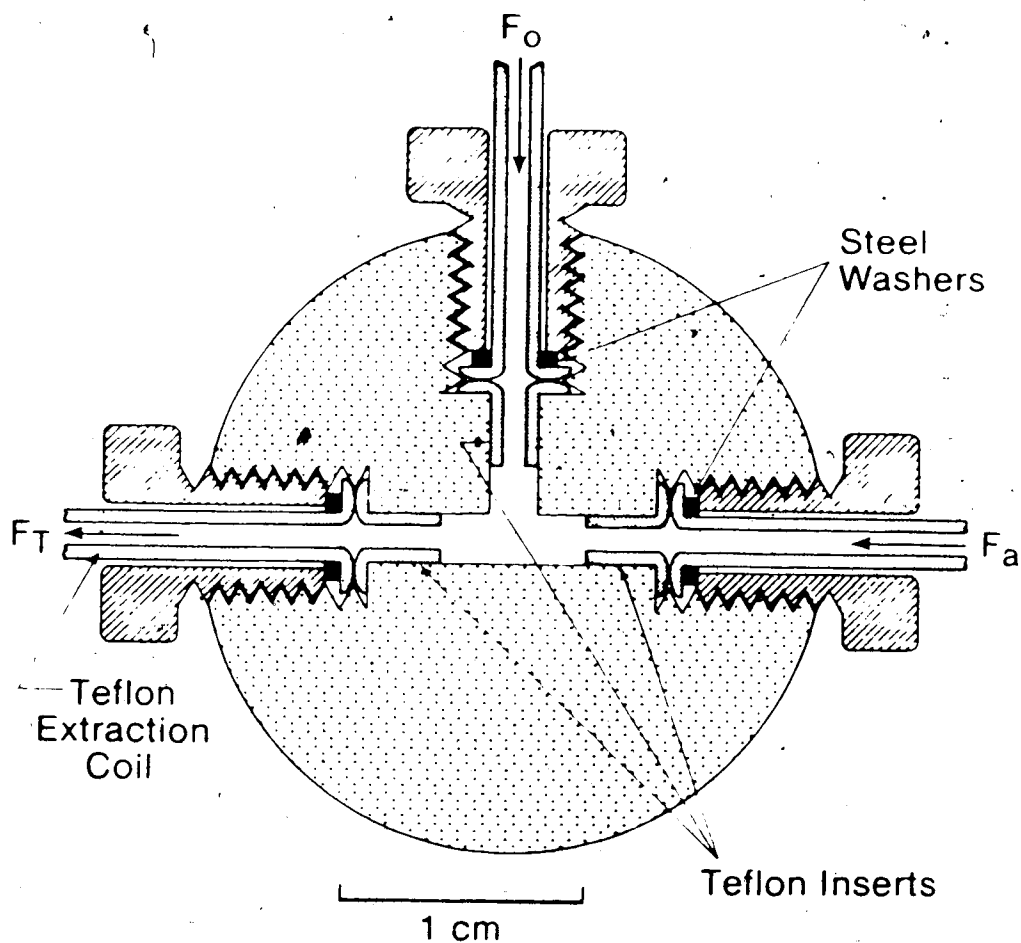


Figure 4. Diagram of the Kel-F segmentor showing the Teflon inserts and upstream end of the extraction coil. F_a = aqueous (reagent plus carrier) flow rate, F_o = organic phase flow rate, F_T = total flow rate.

Sowerbutts [66]. To 25 mL of the 0.1 M HCl solution containing up to 1 g of iron is added 4 g of solid L(+)-ascorbic acid. The solution is diluted to 50 mL with 0.1 M HCl, mixed, and allowed to stand for 10 minutes. A volume of 300-400 μ L, precisely controlled, is injected via valve V_3 shown in Figure 2. Attempts to incorporate the required high concentration of ascorbic acid in the acid/thiocyanate reagent led to occasional breakthrough of the aqueous phase through the porous Teflon membrane.

Assays of synthetic samples containing various trace concentrations of Zn in the presence of a large excess of Fe were performed both by direct aspiration AAS and by solvent extraction/FIA/AAS, using the PE 4000 spectrophotometer. Instrumental parameters for the PE 4000 were optimized in both cases at the values shown in Table 1. Extraction/FIA conditions employed were as follows: carrier 0.1 M HCl; reagent 0.5 M KSCN in 0.1 M HCl; N_2 pump pressure \approx 25 psig; extraction coil length 300 cm; $F_O = 3.2$ mL/min; $F_a = 6.0$ mL/min; $F_M = 2.1$ mL/min; sample volume injected, 335 μ L; sample injection rate 1/min. The injector loop was filled for \approx 10 s with the valve in the load position, the valve was switched to the inject position and held there for \sim 40 s, until the entire peak had been recorded, and it was then switched back to the load position.

Table 1. Instrument parameters used with the PE 290B and the PE 4000 spectrophotometers for direct aspiration and for FIA.

	Direct Aspiration AAS	Solvent Extraction/FIA/AAS	
Instrument	PE 4000	PE 4000	PE 290B
Lamp current	10 mA	10 mA	8 mA
Wavelength	213.9 nm	213.9 nm	213.9 nm
Spectral slit width	7 Å	7 Å	7 Å
Aspiration rate	5.5 mL/min	2.7 mL/min	2.5 mL/min
Acetylene pressure	12 psig	12 psig	8 psig
Air pressure	23 psig	23 psig	55 psig
Recorder full scale	50 mV	50 mV	50 mV
Recorder speed	1.25 cm/min	1.25 cm/min	2.50 cm/min

Synthetic samples for this study were prepared by first spiking 0.1 M HCl solutions containing 1 g of Specpure iron (TMI 10 purity) per 25 mL with accurately known quantities of Zn. Samples to be assayed by direct aspiration were then diluted to 50 mL with 0.1 M HCl. Samples to be analyzed by FIA/AAS were treated as described above starting with the addition of ascorbic acid. Zinc standard solutions in 0.1 M HCl were prepared to contain the same concentrations of Zn as the synthetic samples, without iron present, and were treated in the same manner as the corresponding synthetic samples for use in direct aspiration or in FIA/AAS.

2.3 Results and Discussion.

2.3.1 FIA/AAS Interface

Important constraints on the present instrument design arise from the following features: (a) the AA spectrophotometer, disconnected from the phase separator, has its own aspiration rate which can be adjusted by altering the position of the nebulizer needle (in the present case it was adjusted to 2.5 mL/min); (b) for given values of F_0 and F_a the FIA system, disconnected from the AA spectrophotometer, has its own "natural" value of F_M which can be adjusted by changing the lengths of the two

tubes conducting liquids out of the phase separator (usually the natural F_M is 1-2 mL/min [21,22]; (c) the phase separator provides an open-ended parallel-branched flow circuit with flow through the membrane in parallel with flow to waste.

When the FIA system is coupled to the AA spectrophotometer the value of the natural F_M and the aspiration rate should, ideally, be adjusted to the same value in a condition called "matched flow" [67,68]. In our experience, attempts to maintain matched flow at ≈ 2 mL/min as well as attempts at using "flooded flow" [69,70] led to poor reproducibility in AA signals. The use of "starved flow" [71] resulted in the aqueous phase occasionally breaking-through the porous Teflon membrane. An arrangement which yielded reliable and reproducible performance involved the use of flow compensation with MIBK, as shown in Figure 2. To keep the consumption of MIBK from the compensating flask small during routine operation, the aspiration rate was adjusted to about 2.5 mL/min and the natural F_M to about 2.0 mL/min. Attempts to use water as a compensating solvent in place of MIBK [72] led to reduced AA sensitivity, presumably because of the cooling effect of water on the flame, while attempts to use air as a compensating fluid [32,73a] yielded a variable baseline and poor

reproducibility of the AA signal.

2.3.2 Extraction Characteristics

The following characteristics related to the solvent extraction chemistry were investigated systematically: extraction coil length; volume of sample injected; concentration of KSCN in the Reagent; and concentration of ascorbic acid reductant. In all studies the sample solution injected contained 2 ppm Zn^{++} (3×10^{-5} M) in 0.1 M HCl, with no iron added.

Extraction coil length was varied from 30 to 450 cm and a fixed sample volume of 385 μ L was repeatedly injected. F_T was maintained at 10.5 mL/min and F_O/F_a at 0.4. A plot of peak height vs extraction coil length showed a steep rise between 0 and about 100 cm followed by a nearly flat plateau at coil lengths above 100 cm (Figure 5). The peak width variation with extraction coil length was very similar to that observed previously [21] though displaced to larger values, partly because of the use of a 385 μ L injection volume in this study compared to 44 μ L in the previous one and partly because of the different physical properties of the two organic solvents used such as viscosity, η , and interfacial tension, $\gamma_{O/W}$ (see Chapter 4). Nord and Karlberg concluded that the smaller the ratio $\eta/\gamma_{O/W}$ the lower the dispersion in the

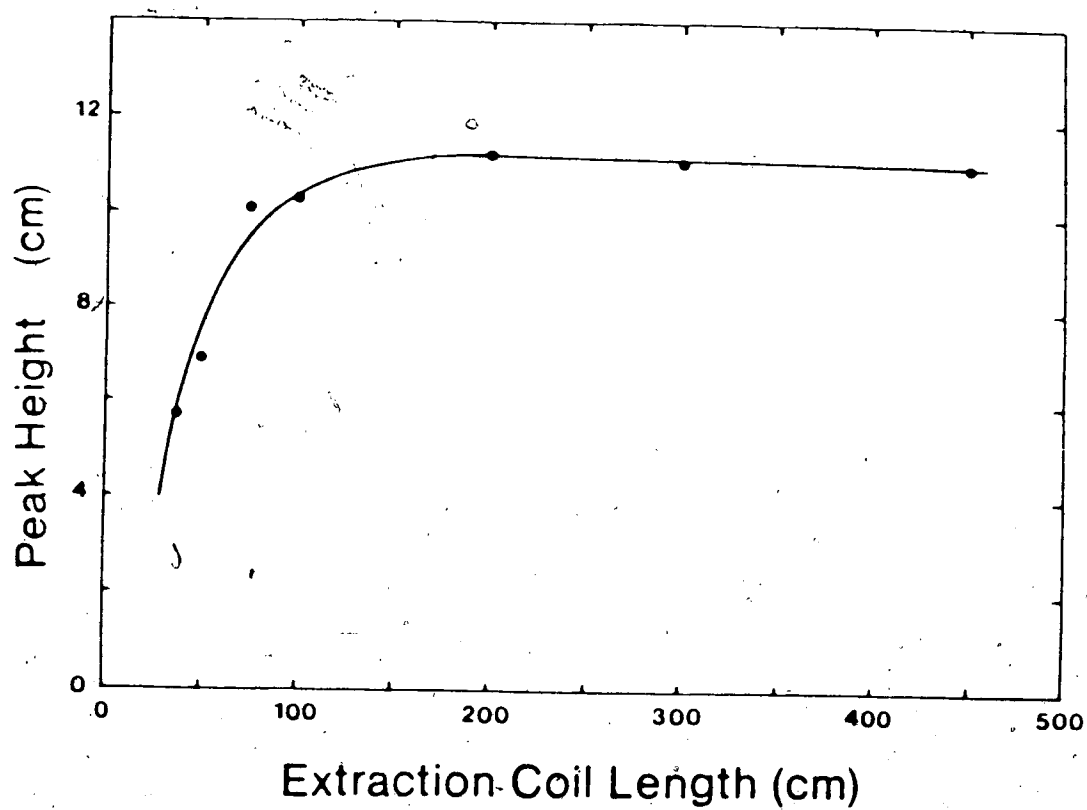


Figure 5. Effect of extraction coil length on peak height for 2 $\mu\text{g/mL}$ Zn solution injected into the flow system in Figure 2. $F_T = 10.5 \text{ mL/min}$, $F_O/F_a = 0.4$ and the sample volume injected was 385 μL .

extraction coil [29]. At 25°C the viscosity of MIBK [73b] is the same as that of chloroform [73c] (0.542 dyne·s/cm²). The interfacial tension of MIBK/H₂O system equals 10.7 dyne/cm while that of chloroform/H₂O system equals 32.8. Substituting these figures it is evident that for the MIBK/H₂O system the film thickness will be three times that of the chloroform/H₂O system. Peak widths were 5.3 s, 6.7 s and 7.4 s for coil lengths of 40 cm, 200 cm and 450 cm, respectively. A coil length of 300 cm, on the peak height plateau, was used in all subsequent studies.

Sample volume injected was varied from 135 μL to 1385 μL while F_T and F_O/F_A were maintained at 13.8 mL/min and 0.44, respectively. The flow rate F_{Carrier} was kept constant as the length of the 0.8-mm i.d. Teflon sample loop was increased by removing an equal length of 0.8-mm i.d. Teflon tubing from between the carrier reservoir and the injection valve. As seen in Figure 6 peak height increases with sample volume until a plateau is reached at about 500 μL. Peak width at half-height (not shown) approaches a nearly constant value of 5 s at sample volumes below about 200 μL and becomes linear with a slope of 1.6×10^{-3} s/μL and zero intercept for sample volumes above about 400 μL. Peak area, calculated from peak height and peak width at half-height, increases linearly

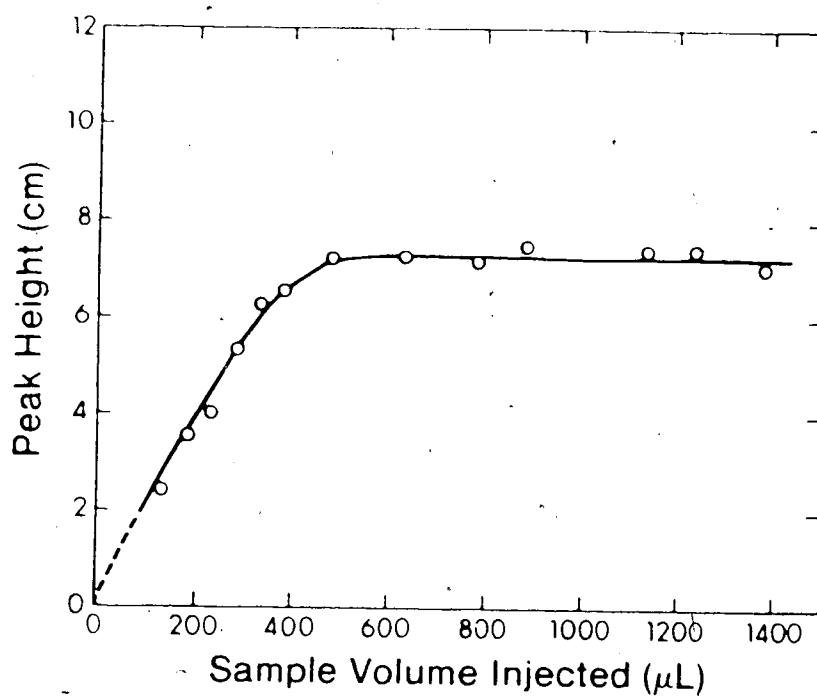


Figure 6. Variation of peak height with sample volume injected:
 sample, $2 \mu\text{g/mL Zn}^{2+}$ in 0.1 M HCl , $F_{\text{Carrier}} = 4.8 \text{ mL/min}$;
 $F_{\text{Reagent}} = 4.8 \text{ mL/min}$; $F_0 = 4.25 \text{ mL/min}$, $F_0/F_a = 0.44$, F_T
 $= 13.8 \text{ mL/min}$; $F_M = 1.7 \text{ mL/min}$; Carrier 0.1 M HCl ; Reagent
 0.5 M KSCN in 0.1 M HCl ; recorder speed, 2.5 cm/min ; study
 performed on PE 4000 AA.

with volume injected from a zero intercept (not shown in Figure 6). The general aspects of the variations of peak height, width, and area with volume injected are similar to those previously described [21]. An injection volume of 385 μL was chosen for all subsequent studies since it represents a favorable compromise between large peak height and small peak width.

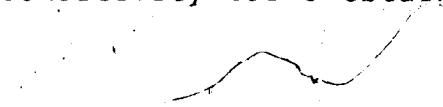
Potassium thiocyanate concentration in the reagent was varied from 0 to 0.5 M. Peak height increased rapidly until a limiting plateau at about 0.11 M KSCN. Peak height at 0.50 M KSCN was identical with that at 0.11 M KSCN. Peak-to-peak baseline noise, expressed as a percentage of the peak height obtained for 2 $\mu\text{g/mL}$ Zn in the injected sample, increased only slightly from 3.1% at 0.11 M KSCN to 4.1% at 0.5 M KSCN. A concentration of 0.5 M KSCN was selected for use in the determination of trace Zn in the presence of Fe. Sample solutions may contain up to 2% (0.35 M) iron and the use of 0.5 M KSCN insures an excess of this reagent over that required by the formation of the non-extractable complex FeSCN^+ in the aqueous phase.

Ascorbic acid was added as a solid in varying amounts to 25 mL portions of a solution containing 4 $\mu\text{g/mL}$ zinc and 4% iron in 0.1 M HCl. The mixtures were then diluted to 50 mL with 0.1 M HCl. After standing for about 10

minutes 385 μ L of each solution was injected into the FIA/AAS system and the concentration of iron extracted into MIBK was measured by atomic absorption using an iron hollow cathode lamp set at 296.7 nm. A 4% (w/v) concentration of ascorbic acid in the sample, which corresponds to about twice the stoichiometric amount of Fe(III) initially present, was sufficient to achieve maximum reduction of the iron. With this or higher concentrations of ascorbic acid the concentration of iron appearing in the MIBK extract was 110 μ g/mL (2×10^{-3} M). The nature of the residual iron extracted was not studied. In aqueous solutions Fe(II) forms a positively charged 1:1 complex with thiocyanate ion [73d] which is unextractable. On the other hand the formation of Fe(II) hydrogen ascorbate ($[\text{FeHAsc}^+]$) complex was reported in perchlorate solution [73e]. In the presence of excess thiocyanate ions a neutral mixed ligand complex (FeHAscSCN) may form and extract.

2.3.3 Flow Characteristics

The sensitivity, S_F , of the AA spectrophotometer, expressed as signal height per unit concentration of absorbing element in the aspirated solution, depends on the flow rate of the solution into the nebulizer [74]. The plot in Figure 7 is the sensitivity curve obtained by



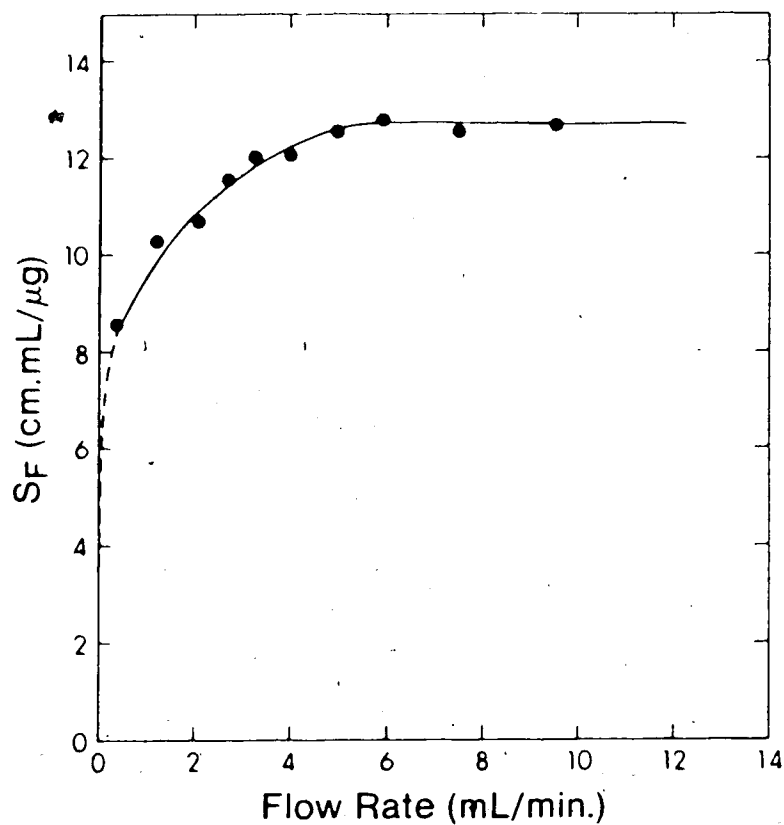


Figure 7. Variation of sensitivity of the AA spectrophotometer with flow rate into the nebulizer; sample, $0.4 \mu\text{g/mL Zn(SCN)}_2$ in MIBK pumped directly into the nebulizer. The instrument conditions are given in Table 1, Column 4.

continuously pumping a $0.4 \mu\text{g/mL}$ solution of Zn(SCN)_2 in MIBK into the AA spectrophotometer at various flow rates. (Flow injection was not involved in collecting these data.) Figure 7 is used as follows: The value of S_F relevant to an FIA/AAS experiment is read off the curve at a flow rate equal to $(F_M + F_C)$. Except in the nearly linear region of the curve at low flow rates, the nebulization efficiency decreases as the flow rate is increased and in the limiting plateau region S_F actually becomes independent of the rate at which solution enters the nebulizer. An equation is derived in Chapter 3 (Equation 3.4) which expresses peak height in extraction/FIA/AAS as a function of S_F and other system variables. Anticipating that equation, in the present case, the distribution ratio, $D \approx 100$ [66] so that $\phi \approx 1$.

2.3.4 Efficiency of the Membrane Phase Separator

Membrane phase separation efficiency is the fraction of the organic phase that can be separated by the membrane (F_M/F_O). Maximum efficiency of the membrane phase separator is the maximum value of F_M/F_O which can be achieved before breakthrough of water. The maximum efficiency was studied as a function of the total flow rate, F_T . The flow rate ratio (F_O/F_a) was kept constant at 3.2 while the total flow rate, F_T was varied from 4.2

to 10.7 mL/min. The flow system used did not involve sample injection or detection. At the segmentor T_2 in Figure 2, the aqueous (0.1 M HCl) stream flowing at F_a was merged with the organic (MIBK) stream flowing at F_o , and the segmented flow in the extraction coil, C, was fed to the membrane phase separator M. For each F_T value the efficiency of the membrane phase separator was adjusted to its maximum value by changing the length of the Teflon tubing connected to the waste outlet. F_M , F_a and F_o were measured using two standard burets receiving the liquids at both outlets of the membrane phase separator.

Figure 8 is a graphical representation of the results obtained. Curve A shows that the efficiency of the membrane phase separator is decreased as the total flow rate is increased. The reason for this has not been investigated but there is evidently a correlation between maximum F_M/F_o and pressure across the membrane. At higher F_T the pressure in the phase separator is greater if the Teflon tubing exiting to waste is kept at the same length. At low F_T high efficiency of separation is obtained while F_M drops almost linearly (Curve B). Thus in a typical experiment in which compensating flow is employed it is better to work at high F_T conditions despite the lower efficiency of separation. This allows operation at a total organic flow rate into the nebulizer

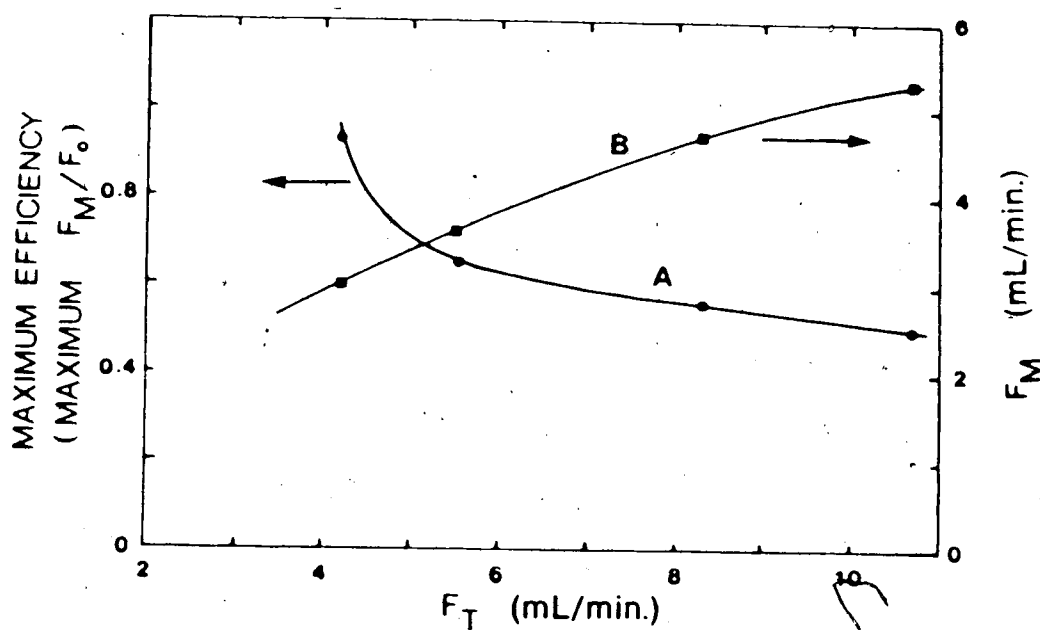


Figure 8. Variation of membrane phase separator efficiency F_M/F_O , (A) and flow rate through the membrane, F_M , (B) with total flow rate of both phases ($F_T = F_O + F_A$). At all total flow rate values the phase ratio, F_O/F_A , was kept constant at 3.2 and the flow system was adjusted to maximize F_M values without breakthrough of the aqueous phase. Aqueous phase was 0.1 M HCl, while organic phase was MIBK.

($F_M + F_C$) as close as possible to the plateau region of Figure 7 with minimum dilution by the compensating flow. The phase separator was designed with a small internal volume in order to minimize bandbroadening and it has been used successfully with molecular absorption detectors [21,22]. In such detectors, unlike an atomic absorption detector, the signal is independent of the flow rate into the detector, and a low F_M value will be as good as a high one.

2.3.5 Determination of Zinc in Iron Matrix

The data shown with open symbols in Figure 9 were obtained by analyzing iron-free zinc standard solutions in 0.1 M HCl (Section 2.2.3), either by directly aspirating the aqueous phase (circles) or by solvent extraction/FIA/-AAS (squares). The data shown with solid symbols were obtained by analyzing synthetic samples containing 2% Fe and various concentrations of zinc by direct aspiration (circles) or by solvent extraction/FIA/AAS (squares). Synthetic samples assayed by direct aspiration are always higher than those of the iron-free standards. At every zinc concentration the sample signal height (absorbance or cm) lies above the corresponding standard signal height obtained for the same zinc concentration, by about the same amount. This height (or absorbance), which is

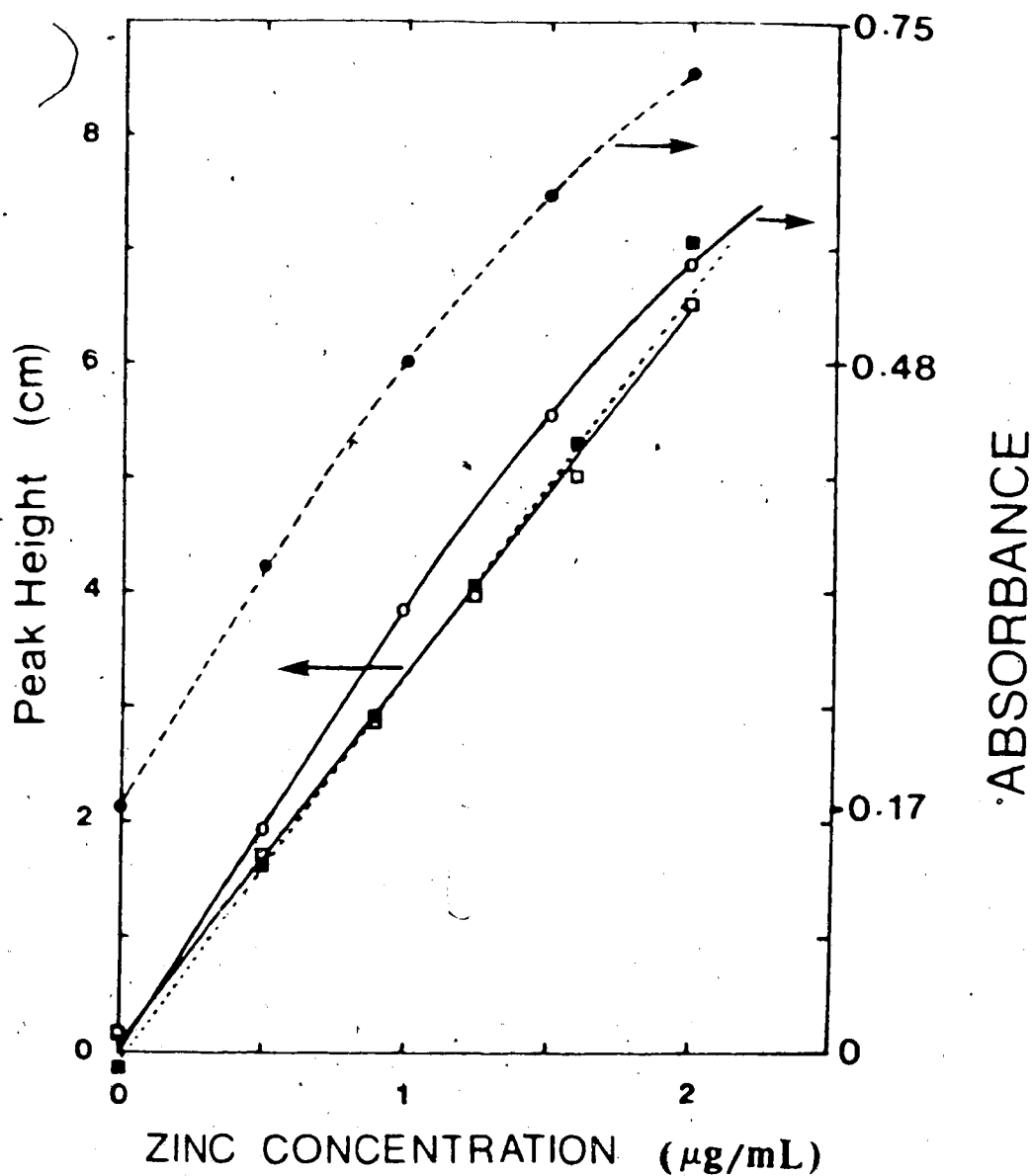


Figure 9. Calibration curves for the determination of zinc in iron matrix by directly aspirating the aqueous solution (●) and by solvent extraction of the zinc-thiocyanate complex into MIBK using FIA/AAS (■) as described in Section 2.2.3. The open symbols were obtained for zinc standards in 0.1 M HCl analyzed as for the solid symbols except for the absence of ascorbic acid in the FIA/AAS method. Experimental conditions are presented in Table 1, Columns 2 and 3.

necessarily the intercept of the sample plot on the peak height axis, corresponds to $0.42 \mu\text{g/mL}$ Zn in the linear part of the plot.) In the curved part of the plots the same signal height difference between the sample signal height and the standard signal height corresponds to a greater difference between actual and added zinc concentrations (see data in Table 2). The positive intercept of the sample plot in the direct aspiration method of course arises from the absorbance of Fe at 213.9 nm . Thus a Zn-free solution containing 2% Fe appears to contain $21 \mu\text{g}$ of Zn per gram of Fe (i.e. 21 ppm): This is consistent with the previously reported [47] spectral interference of Fe in the determination of Zn.

In contrast, the assay values obtained for Zn in the samples by the extraction/FIA/AAS method is essentially free of interference from Fe. Peak heights obtained for the samples and standards are the same within experimental error (Table 2). The minimum detectable quantity of zinc is $0.2 \mu\text{g/mL}$, taken as three times the peak-to-peak noise in the baseline.

Background correction techniques are frequently used to compensate spectral interferences in AAS, but they usually under-correct in cases of spectral line interference where line overlap is extensive [76,77].

Deuterium background correction was tested in the present

Table 2. Assay of synthetic samples containing 2% iron for their zinc content by direct AAS and by extraction/FIA/AAS.

Direct AAS			FIA/AAS		
Added Zn ($\mu\text{g/mL}$)	Found Zn ($\mu\text{g/mL}$) ^a	Difference ($\mu\text{g/mL}$) ^b	Added Zn ($\mu\text{g/mL}$)	Found Zn ($\mu\text{g/mL}$) ^{a, c}	Difference ($\mu\text{g/mL}$)
0.00	0.42	0.42	0.00	-0.02 \pm 0.01	0.02
0.50	0.92	0.42	0.50	0.47 \pm 0.01	0.03
1.00	1.51	0.51	0.90	0.90 \pm 0.02	0.00
1.50	2.15	0.65	1.25	1.28 \pm 0.04	0.03
2.00	2.76	0.76	1.60	1.66 \pm 0.06	0.06

a. As read off from the aqueous standard calibration curve.

b. Added Zn - Found Zn.

c. \pm are standard deviations based on three replicates.

case on the PE 4000 spectrophotometer using direct aspiration. The interference was reduced only by about 32% indicating that, as expected, D_2 background correction is not suitable for compensating Fe spectral interference on Zn (Figure 10).

While spectral line interference is relatively rare in AAS, the extraction/FIA/AAS approach can be used routinely to eliminate all kinds of matrix effects in addition to spectral interferences. Also, use of the technique in conjunction with inductively coupled plasma (ICP) emission spectroscopy, where spectral interferences are more common, should provide an attractive means of eliminating them. Flow rates of the organic extract in FIA are in the same range as aspiration rates commonly used in ICP spectroscopy [78] and, while the use of organic solvents is more problematic with the ICP than with AAS, they are now routinely employed [79,80].

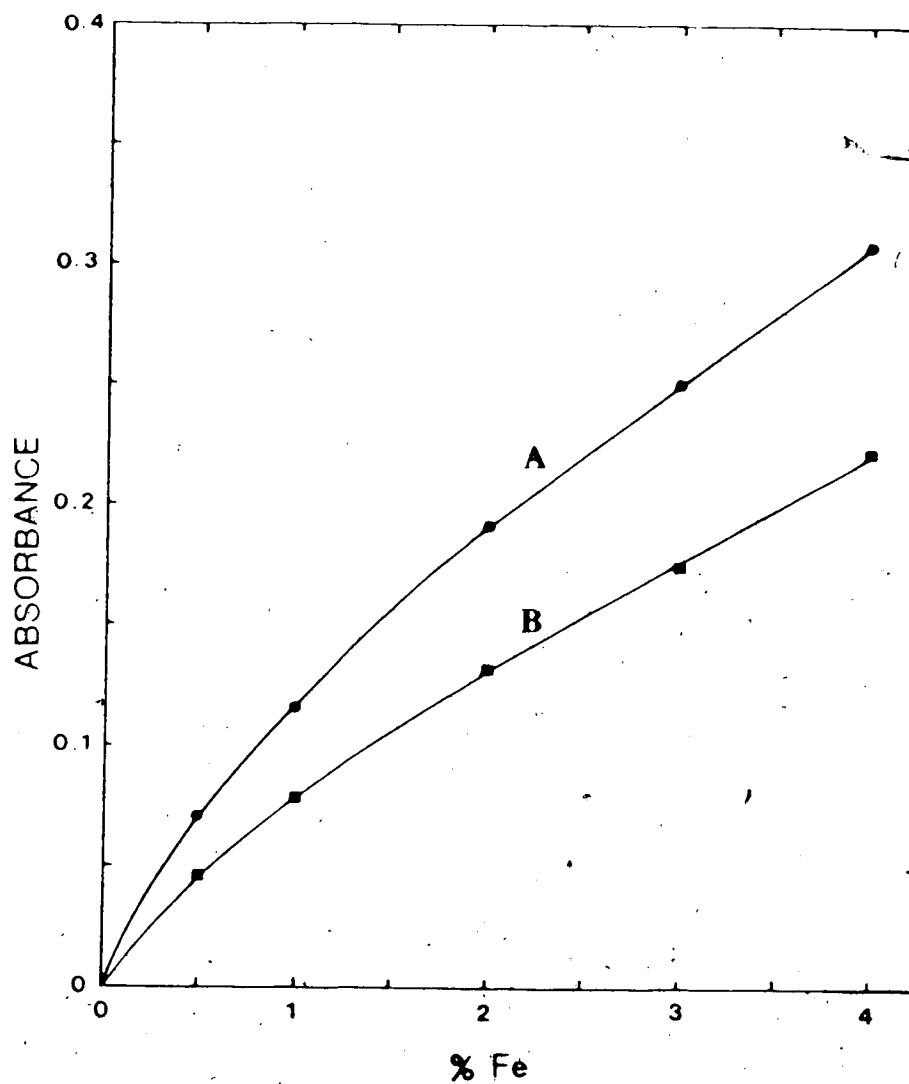


Figure 10. The absorbance of pure iron solutions at the wavelength of the zinc resonance line at 213.9 nm. The experimental conditions were those presented in Table 1, Column 2. Curve A was obtained without background correction while Curve B was obtained with D₂ background correction.

CHAPTER 3

USE OF PEAK HEIGHT FOR QUANTIFICATION IN SOLVENT EXTRACTION/FLOW INJECTION ANALYSIS

3.1 Introduction

The performance of automated solvent extraction in the FIA mode has been studied both in terms of its principles of operation and its application to quantitative determination [21,22,25,26 and references therein]. Quantification in solvent extraction/FIA is based on either peak height or peak area. The quantitative relationship between peak area and various system parameters was derived and experimentally verified for systems employing a concentration sensitive detector [21]. This chapter deals with the quantitative relationship between peak height and such system parameters as detector sensitivity, peak dispersion, flow rates of various streams, and sample distribution coefficients.

Some types of detectors, such as molecular absorption spectrophotometers, can simply be attached to the organic extract line exiting the phase separator [21], while other detectors, such as atomic absorption spectrophotometers (AAS) may require additional plumbing to provide flow

compensation to the extract entering the nebulizer, as described in Chapter 2 [26,32]. Furthermore, while the detector sensitivity is independent of flow rate with a molecular absorption spectrophotometer, it exhibits a complex flow rate dependence with AAS detectors [26,74]. Both situations are included in the equation which is derived and experimentally verified in this chapter.

3.2 Experimental

3.2.1 Chemicals and Reagents

Ortho-nitroaniline stock solution (5.0×10^{-3} M) was prepared in water from the reagent grade chemical (BDH, Montreal). The sample solution (4×10^{-5} M) was prepared by dilution of the above stock. Phosphate buffer (0.01 M, pH = 7.0) was prepared in water by titrating a solution of KH_2PO_4 (McArthur Chemical Co., Montreal) to pH = 7.0 with NaOH and diluting to 2 L. Reagent grades of CHCl_3 (Mallinckrodt) and MIBK (Fisher Scientific Co.) were used without further purification. Other reagents and chemicals were reagent grade and have been described in Chapter 2.

3.2.2 Apparatus

Two versions of the extraction/FIA instrument are considered, one with an AAS detector and the other with a molecular absorption spectrophotometric detector. The former, which has been used in the atomic absorption determination of zinc following solvent extraction of $\text{Zn}(\text{SCN})_2$, is shown in Figure 2 and described in Chapter 2. It will be referred to as Version I of the instrument. The aqueous carrier is 0.10 M HCl, the aqueous reagent is 0.50 M KSCN in 0.10 M HCl and the immiscible organic solvent is methylisobutylketone (MIBK). Samples consist of dilute solutions of Zn in 0.1 M HCl which are injected via a sample injection valve V_3 . During passage of the segmented aqueous-organic flow stream through the extraction coil the complex $\text{Zn}(\text{SCN})_2$ is quantitatively extracted into MIBK. The AA signal peak is due to Zn.

The aqueous flow rate F_a is the sum of carrier flow rate F_{Carrier} and reagent flow rate F_{Reagent} ; the total flow rate F_T is equal to F_a plus the MIBK flow rate F_o ; flow rate of MIBK phase passing through the membrane phase separator is F_M and compensating flow rate of MIBK from the flask is F_c . It was found (see below) that use of the flow compensator resulted in the total flow rate of MIBK entering the nebulizer ($F_M + F_c$) remaining constant for a

given nebulizer setting, even when F_M was purposely varied during experiments. The value of $(F_M + F_C)$ is governed by the "natural" aspiration rate demanded by the particular nebulizer setting as demonstrated in this study.

The second version of the extraction/FIA instrument, called Version II, was used in studies where some flow rates were varied while others were kept constant and where it was desired to use a detector whose sensitivity is flow rate independent. The design was similar to that in Figure 2 except for the following changes: (a) The constant pressure pumps were replaced by three constant flow rate liquid chromatography pumps (Model 6000A, Waters Assoc. and Model 396 Minipump, LDC); (b) Methanol was used, instead of acetone, as a flushing solvent; (c) T_3 and the compensating solvent were absent; (d) A uv absorbance detector (Model 770, Schoeffel Instrument Corp.) was used at 410 nm, in place of the AAS; (e) A peristaltic pump (Minipuls 2, Gilson Instruments) was placed in the outlet line from the detector flow cell in order to gate the flow F_M , as described previously [21]; (f) Carrier was water, reagent was phosphate buffer, organic solvent was $CHCl_3$, and the sample solution was o-nitroaniline in water.

In both versions of the instrument flow rates were measured by collecting the liquids in burets at the outlet

end of the system. Therefore, reported values of F_{Carrier} , F_{Reagent} , F_{O} , F_{a} and F_{M} are for mutually saturated phases. Also, the extraction coil was sufficiently long that extraction equilibrium was always achieved for both $\text{Zn}(\text{SCN})_2$ and o-nitroaniline.

3.2.3 Sensitivity Curve

This was measured by pumping a solution of $\text{Zn}(\text{SCN})_2$ in MIBK into the nebulizer. The "natural" aspiration rate of the nebulizer was set at 2.5 mL/min by suitable adjustment of the position of the nebulizer tip. The $\text{Zn}(\text{SCN})_2$ solution was pumped from a constant pressure pump directly and continuously into the nebulizer - no solvent extraction or FIA was involved. $\text{Zn}(\text{SCN})_2$ concentrations of 0.40 $\mu\text{g/mL}$ and 0.70 $\mu\text{g/mL}$ were used.

3.2.4 Effect of F_{c}

Variation of peak height with flow rate of compensating solvent was studied by pumping 0.4 $\mu\text{g/mL}$ $\text{Zn}(\text{SCN})_2$ solution in MIBK from a constant pressure pump through a tee junction, where it merged with the compensating flow of MIBK, and then into the nebulizer. No solvent extraction or FIA was involved in this study. The "natural" aspiration rate of the nebulizer was set at about 5 mL/min. A baseline for the AA signal was obtained

by shutting off the flow of $\text{Zn}(\text{SCN})_2$ solution so that the nebulizer aspirated only MIBK compensating solvent. The flow rate of $\text{Zn}(\text{SCN})_2$ solution was then set, in turn, at several values by varying the nitrogen pressure in the pumps. Flow rate of the $\text{Zn}(\text{SCN})_2$ solution from the pump was measured for each run by switching a three-way valve (No. CAV 3031, LDC) located between the pump and compensating tee so that the $\text{Zn}(\text{SCN})_2$ solution was diverted to a measuring buret. The flow rate of compensating solvent during each run was measured as the rate of reduction in liquid level in the compensating solvent container.

3.3. Results and Discussion

The derivation of an equation relating peak height to various system parameters in solvent extraction/FIA is first presented and then each of the terms in the equation is examined experimentally.

3.3.1 Derivation

Peak height (P.H.) is related to the maximum concentration in the sample zone (peak) entering the detector, C_{pk} , by the expression:

$$\text{P.H.} = S_F \cdot C_{pk} \quad (3.1)$$

in which S_F is the sensitivity of the detector in units of height per unit concentration of sample component.

Depending on the detector used S_F may depend on [26,74], or be independent of [21,22] flow rate into the detector. The peak concentration C_{pk} can be calculated from the concentration of sample component in the sample solution injected, C_{SAMP} , by taking into account the dilution steps, the extraction efficiency and the dilution resulting from band dispersion. These are considered here for the instrument shown in Figure 2. Dilution resulting from merging of Carrier stream with Reagent stream is given by $(F_{Carrier}/F_a)$. Dilution resulting from extraction into the organic phase is given by the product of the ratio F_a/F_o times the fraction of sample component extracted, ϕ . The fraction extracted can be calculated from the distribution ratio, D , and the phase ratio [21,22]:

$$\phi = \frac{D \cdot (F_o/F_a)}{1 + D \cdot (F_o/F_a)} \quad (3.2)$$

Dilution caused by band dispersion through the system is the result of laminar flow in connecting tubing and

mixing chamber effects in the phase separator and detector [81]. The relative dilution, R_V , of the sample due to dispersion is measured experimentally from a plot of peak height versus volume of sample solution injected as described below.

In flow sensitive detectors, such as an AAS, a compensating flow, F_C , merges with the flow of organic extract from the phase separator, F_M , before it enters the detector [26]. Dilution of sample component concentration from this source is given by $(F_M / (F_M + F_C))$.

Combining all of the above factors accounting for dilution of the sample component allows C_{pk} to be calculated:

$$C_{pk} = C_{SAMP} \cdot R_V \cdot \frac{F_{Carrier}}{F_a} \cdot \frac{F_a}{F_o} \cdot \phi \cdot \frac{F_M}{F_M + F_C} \quad (3.3)$$

Simplifying this expression and substituting into equation 3.1 gives:

$$P.H. = C_{SAMP} \cdot S_F \cdot R_V \cdot \frac{F_{Carrier}}{F_o} \cdot \phi \cdot \frac{F_M}{F_M + F_C} \quad (3.4)$$

The quantity ϕ depends on F_a and F_o (equation 3.2), but in the usual situation in which D is large and F_a/F_o is close to unity $\phi \approx 1$ so that both ϕ and P.H. become

independent of F_a . It should also be noted that with flow rate sensitive detectors S_F depends on $(F_M + F_C)$ but, as mentioned above, when flow compensation is used with the AAS detector, $(F_M + F_C)$ remains essentially constant and equal to the "natural" aspiration rate of the nebulizer even when F_M is varied. Thus the appropriate value of S_F is read from the sensitivity curve (see below) at a flow rate equal to the nebulizer aspiration rate.

3.3.2 Calibration Curve

Using Version I of the instrument in which an atomic absorption detector is employed, a calibration plot of peak height versus zinc concentration injected, C_{SAMP} , was found to be linear with zero intercept and a correlation coefficient of 0.9996 up to peak heights corresponding to an absorbance of about 0.5 (Figure 9, Chapter 2). The negative deviation observed above this absorbance is found also when samples of Zn^{2+} are aspirated directly into the flame in the normal, non-FIA manner of performing atomic absorption. This, therefore, arises from a negative deviation from Beer's Law at higher absorbances which is a well known phenomenon in atomic absorption spectroscopy. The linearity of P.H. vs C_{SAMP} observed in the linear absorbance range of the spectrophotometer is consistent with the prediction of equation 3.4.

3.3.3 Sensitivity Curve

In Figure 11 are presented plots of detector sensitivity versus flow rate into the nebulizer. The experiment was performed by pumping MIBK solutions containing two different concentrations of $\text{Zn}(\text{SCN})_2$ directly and continuously into the nebulizer. The solid triangles are the same points presented in Figure 7. It is seen that S_F , which is the AA signal divided by $\text{Zn}(\text{SCN})_2$ concentration, is essentially independent of sample concentration. The general shape of this type of curve has previously been discussed [74]. It clearly demonstrates the flow rate dependence of S_F for an AAS detector. Presumably, the leveling-off of the value of S_F at higher flow rates derives from the decreasing efficiency of the nebulizer at producing a fine aerosol from the aspirated liquid [82]. The appropriate value of S_F for use in equation 3.4 is read from the curve at a flow rate equal to the value of $(F_M + F_C)$ being used (i.e. at the nebulizer aspiration rate).

Some workers have chosen to keep the nebulizer aspiration rate at the optimum value (plateau region in Figure 11) and adjust the FIA stream to match that flow rate [32,37,83]. With the currently used porous membrane phase separators in which F_M is about 2 mL/min, operating on the sensitivity plateau at 6 mL/min would require a

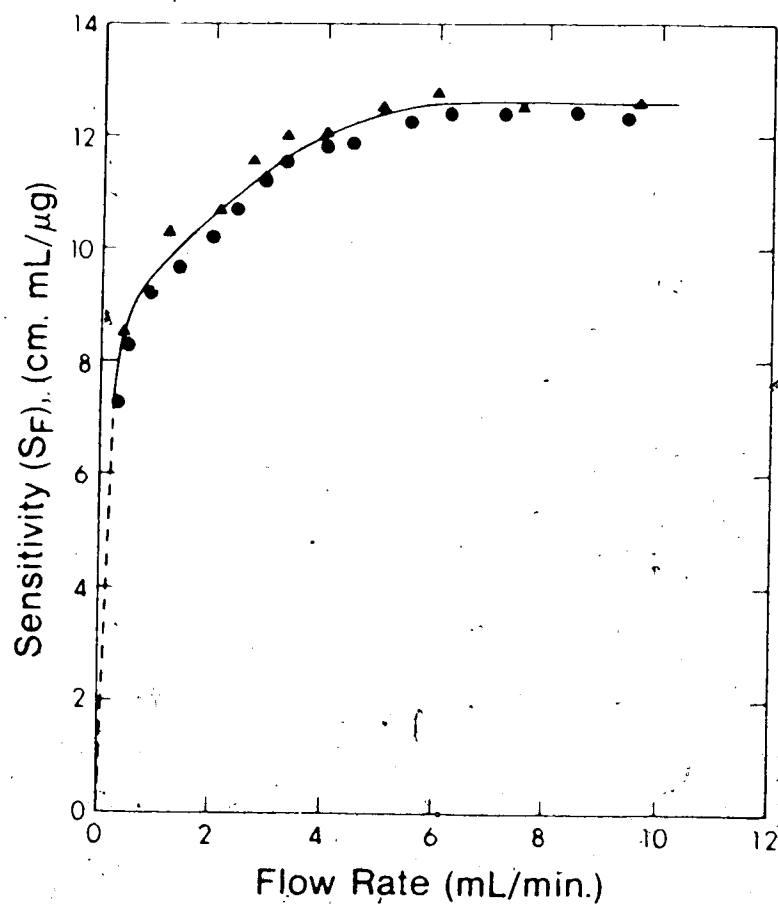


Figure 11. Sensitivity curve for Zn obtained by pumping 0.7 $\mu\text{g/mL}$ (▲) and 0.4 $\mu\text{g/mL}$ (●) of $\text{Zn}(\text{SCN})_2$ in MIBK directly into the nebulizer of the AAS. Nebulizer "natural" aspiration rate was fixed at 2.5 mL/min.

dilution by compensating solvent of 2/6 and a corresponding decrease in peak height. Alternatively it is possible to adjust the nebulization rate to a value lower than 6 mL/min such as 2.5 mL/min with only a 20% sacrifice in sensitivity (Figure 11). In this case a compensating flow of 0.5 mL/min will cause a dilution of only 2/2.5. Thus operating at a natural aspiration rate of 2.5 mL/min rather than 6 mL/min yields a substantial net increase in signal.

3.3.4 Relative Dilution, R_v

Band dispersion resulting from flow of the sample zone through the system causes a broadening and decrease in height of the peak. In addition, as the volume of sample injected is made larger it too contributes to the width of the peak [21]. To study this phenomenon both Version I and Version II instruments were used. Relative dilution R_v is evaluated from the dependence of peak height on sample volume injected. A plot of this type for measurements made on the Version I instrument has been published [26]. Three plots of this type for measurements made on the Version II instrument are presented in Figure 12. All plots have the same general shape. The evaluation of R_v is done as follows: Consider first curve A in Figure 12. The limiting plateau seen in this curve

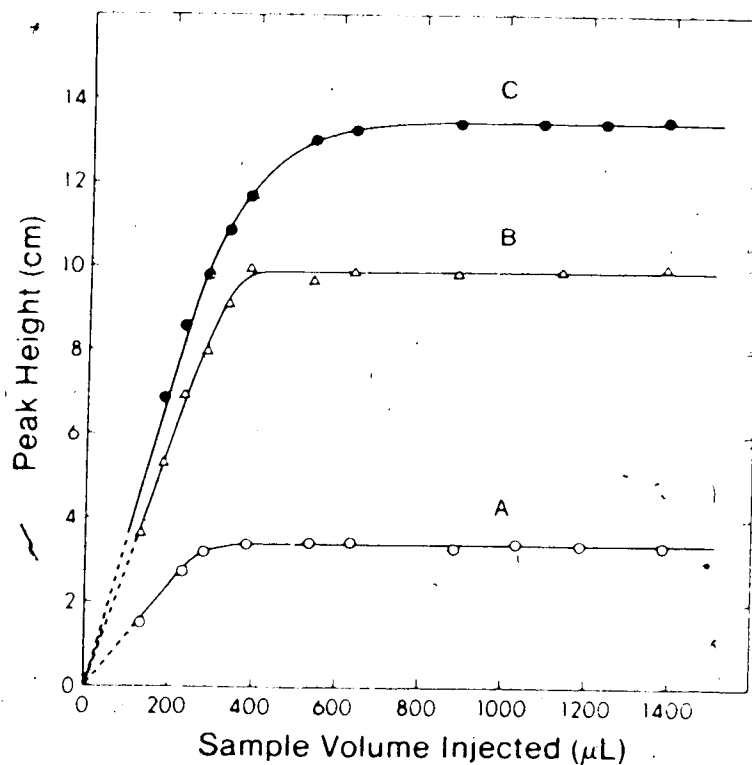


Figure 12. Effect of sample volume injected on peak height for a sample containing 4×10^{-5} M o-nitroaniline. Version II instrument. Flow rates, mL/min, are: Curve A, $F_o = 3.0$, $F_{\text{Carrier}} = 0.9$, $F_{\text{Reagent}} = 0.4$, $F_M = 1.2$, $F_o/F_a = 2.3$, Detector AUFS = 0.01; Curve B, $F_o = 3.0$, $F_{\text{Carrier}} = 2.0$, $F_{\text{Reagent}} = 2.0$, $F_M = 1.1$, $F_o/F_a = 0.75$, Detector AUFS = 0.02; Curve C, $F_o = 1.5$, $F_{\text{Carrier}} = 2.0$, $F_{\text{Reagent}} = 2.0$, $F_M = 0.9$, $F_o/F_a = 0.375$, Detector AUFS = 0.02. Full scale = 25.0 cm.

at large injection volumes exists because the "slug" of injected sample is sufficiently long that dilution due to band dispersion does not reach the centre of the zone [21]. Hence, there is no dilution due to dispersion on this plateau. For a system in which $F_0/F_a = 2.3$ the value of R_v corresponding to any injection volume is calculated as the ratio of the peak height seen in Figure 12 at the corresponding injection volume divided by the peak height on the limiting plateau. Defined in this way R_v is analogous to the concept of "dispersion" used by some workers in FIA [75].

Comparison of curves A, B and C in Figure 12, each of which was obtained at a different value of F_0/F_a , shows that R_v is somewhat sensitive to large changes in F_0/F_a . This is not surprising in view of the processes giving rise to band dispersion. It means, in a practical sense, that the curve used to calculate the value of R_v to be used in a given extraction/FIA determination should have been obtained under similar experimental conditions to those used in the determination. The increase in the plateau peak height seen on going from curve A to curve C is a consequence of the increase in (F_{Carrier}/F_0) as seen in equation 3.4 and as discussed below. (Note change in detector sensitivity given in figure caption.) It will be recalled that, since R_v is a ratio of peak heights, it is

the shapes of curves A-C that relate to R_V and not the absolute values of peak heights.

3.3.5 Effect of F_{Carrier} on Peak Height

Equation 3.4 predicts a linear dependence of P.H. on F_{Carrier} provided that S_F , R_V , ϕ , F_O , F_M and $(F_M + F_C)$ remain constant. This was studied using the Version II instrument. For this instrument S_F is constant, independent of flow rate. Since no compensating flow is used the last term in equation 3.4 reduces to 3.1 and F_M is eliminated from the equation. For the sample compound o-nitroaniline $\phi \approx 1$ because K_D is large [84]. In this experiment F_O was fixed at 3.00 mL/min, F_{Reagent} at 0.50 mL/min and F_M at 1.00 mL/min while F_{Carrier} was varied between 0.10 mL/min and 2.50 mL/min. An injection volume of 385 μL was used. Under these conditions F_O/F_A varies between 1 and 5 over the range of F_{Carrier} used. Examination of Figure 12 shows that for $F_O/F_A > 0.75$ an injection volume of 385 μL falls on the plateau so that $R_V = 1$ for all values of F_{Carrier} used. Thus S_F , R_V , ϕ and F_O are constants and F_M is eliminated from equation 3.4. A plot of P.H. vs F_{Carrier} is expected to be linear. The experimentally measured plot, which is presented as Figure 13A, is linear (slope = 8.35 ± 0.12 at 95% confidence limit (C.L.)) with zero intercept (intercept = $0.024 \pm$

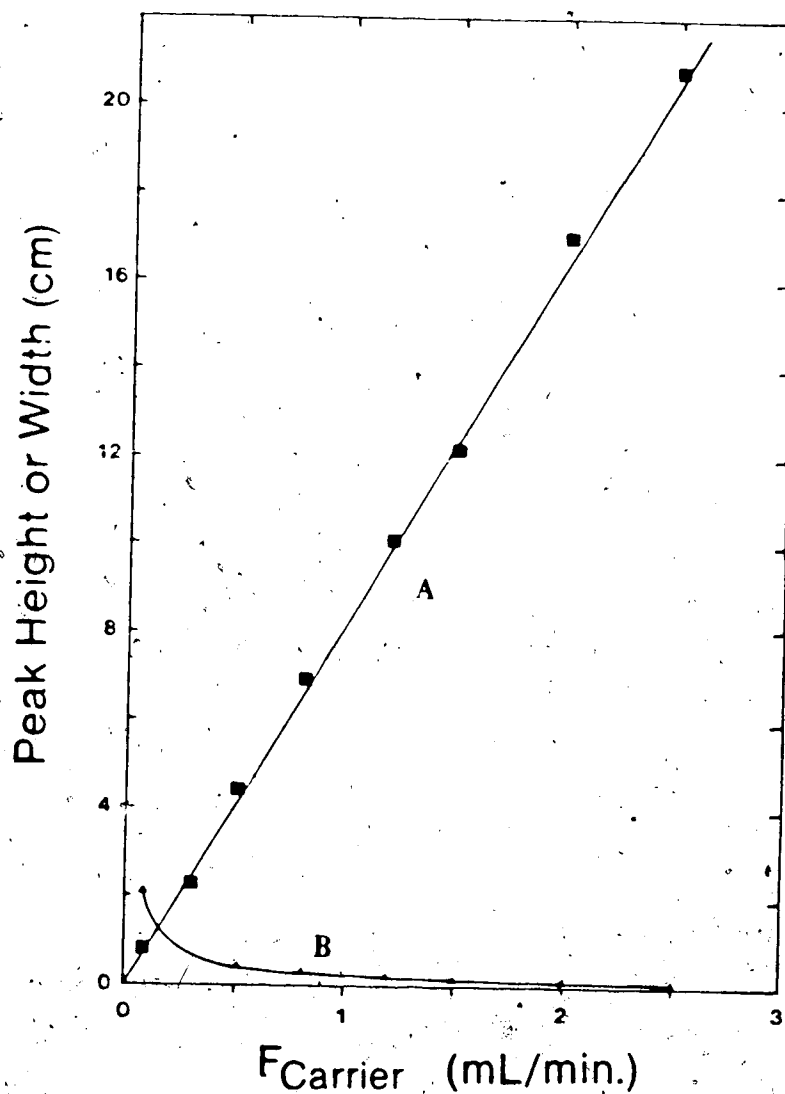


Figure 13. Effect of carrier stream flow rate on peak height (A) and peak width at half-height (B) for a sample containing 7×10^{-5} M o-nitroaniline. Version II instrument. Sample volume injected 385 μ L, $F_{\text{Reagent}} = 0.5$ mL/min, $F_0 = 3.0$ mL/min, $F_M = 1.0 \pm 0.05$, Detector AUFS = 0.02 (full scale = 25.0 cm). The points are averages of duplicate injections (range < 0.4 cm).

0.368 at 95% C.L.) and a correlation coefficient of 0.9995. Peak width at half-height was found to increase with decreasing carrier flow rate (Figure 13B), which is expected since at lower F_{Carrier} the fixed sample slug is segmented and extracted into a greater number of organic phase segments. Since F_M is constant this volume of the organic extract will require a longer time to enter the nebulizer giving rise to a shorter and wider peak signal.

3.3.6 Effect of F_{Reagent} on Peak Height

According to equation 3.4, P.H. should be independent of F_{Reagent} . The Version II instrument was used. F_{Carrier} was held at 1.00 mL/min, F_O at 3.00 mL/min and F_M at 1.45 mL/min while F_{Reagent} was varied from 0.50 to 2.50 mL/min. Injection volume of o-nitroaniline sample solution was 385 μL . Peak height was found to be constant, independent of F_{Reagent} as seen in Figure 14. The slope of a plot of P.H. vs F_{Reagent} was 0.06 ± 0.05 . Peak width at half-height was constant (5.7 ± 0.25) independent of F_{Reagent} . This is because the fixed sample volume injected is segmented at a constant F_{Carrier} yielding a fixed number of segments. Since F_O is constant the segmented sample zone will extract into a fixed number of segments (thus a fixed volume) of the organic phase giving a detector signal of equal height and width.

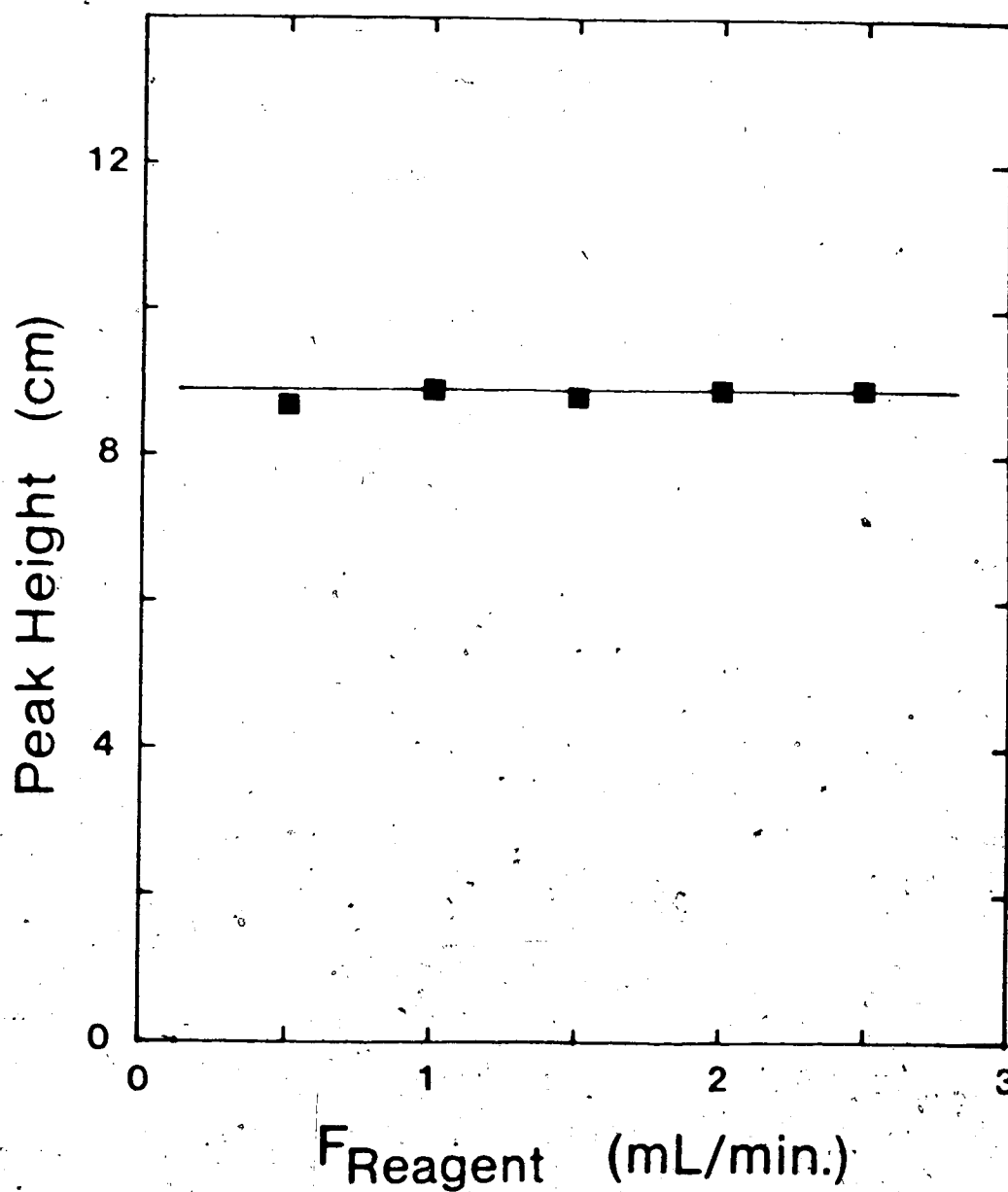


Figure 14. Effect of reagent stream flow rate on peak height for a sample containing 7×10^{-5} M o-nitroaniline. Version II instrument. Sample volume injected 385 μL , $F_{\text{Carrier}} = 1.0$ mL/min, $F_{\text{O}} = 3.0$ mL/min, $F_{\text{M}} = 1.45 \pm 0.05$ mL/min, Detector AUFS = 0.02 (full scale = 25.0 cm). Each point is an average of duplicate injections (range < 0.5 cm).

Increasing F_{Reagent} will simply increase the length of the aqueous segment.

It should be realized that equation 3.4 takes no account of the chemistry or stoichiometry of the reaction upon which an extraction/FIA determination may be based. Thus if the amount of product formed by the reaction between the sample component and the reagent is changed as a result of a change in F_{Reagent} , the peak height would of course change - but this effect is unrelated to the flow dependencies to which equation 3.4 relates.

3.3.7 Effect of F_0 on Peak Height

Using the Version II instrument, F_{Carrier} was fixed at 1.00 mL/min, F_{Reagent} at 0.50 mL/min, and F_M at 1.45 mL/min while F_0 was varied from 1.80 to 3.00 mL/min.

Injection volume of o-nitroaniline solution was 385 μL .

Since all other variables on the right-hand-side of equation 3.4 are constant and F_M is eliminated as discussed earlier, a plot of P.H. vs $1/F_0$ is expected to be linear. The experimental plot, shown in Figure 15, is linear (slope = 25.2 ± 1.3 at 95% C.L.) with a correlation coefficient of 0.996

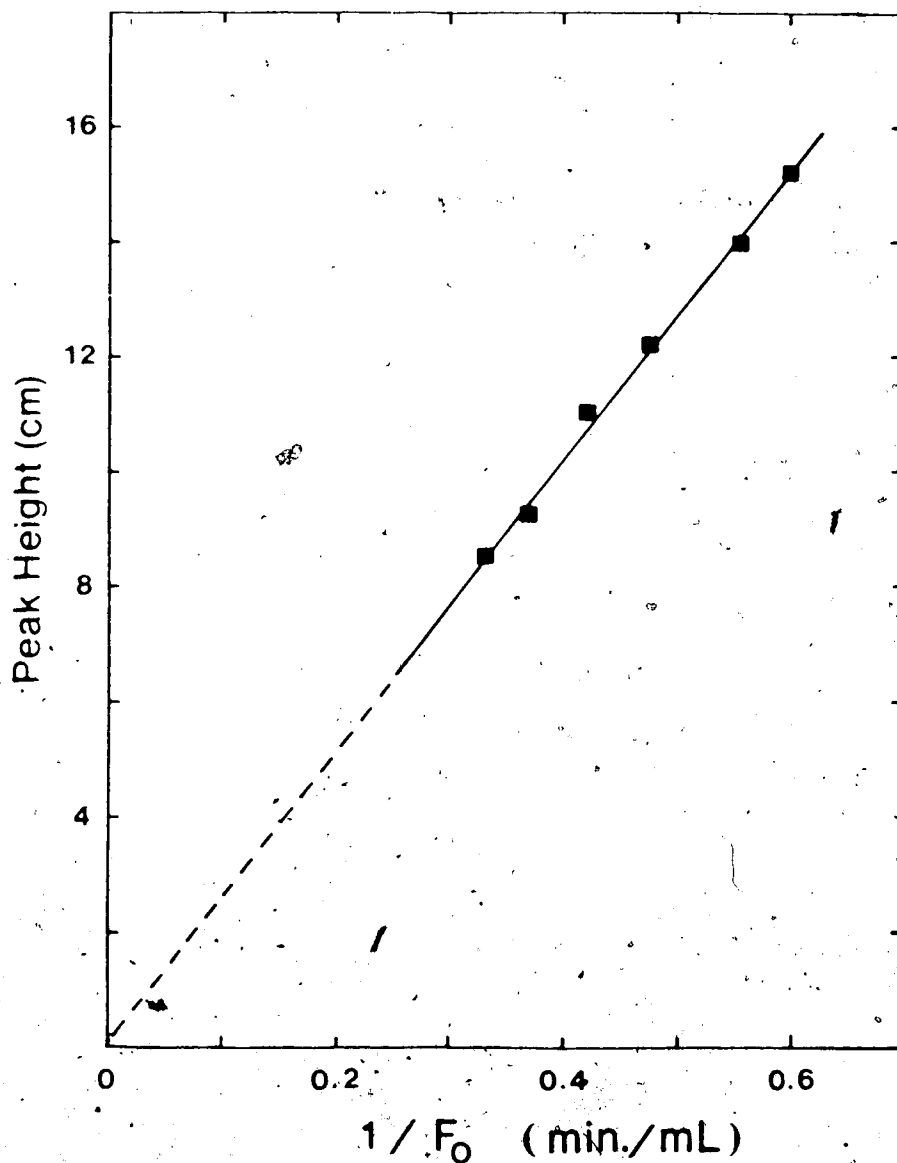


Figure 15. Effect of organic phase flow rate on peak height for a sample containing 7×10^{-5} M o-nitroaniline. Version II instrument. Sample volume injected 385 μ L, $F_{\text{Carrier}} = 1.0$ mL/min, $F_{\text{Reagent}} = 0.5$ mL/min, $F_M = 1.45$ mL/min, Detector AUPS = 0.02 (full scale = 250 cm). The points are averages of duplicate injections (range < 0.3 cm).

3.3.8 Effect of F_C on Peak Height

Variation of peak height with the flow rate of compensating solvent was studied as described in Section 3.2.4. In this experiment the flow rate of $\text{Zn}(\text{SCN})_2$ from the pump is analogous to F_M in the extraction/FIA experiment, while the flow of MIBK from the compensating flask is F_C . The results of this experiment are summarized in Table 3. It can be seen from the first three columns that, at a fixed nebulizer "natural" aspiration rate, $(F_M + F_C)$ remains constant as F_M is changed. From equation 3.4 it is expected that a plot of AA signal vs $F_M/(F_M + F_C)$ should be linear. Using the data in Table 3 a plot (not shown) of AA signal vs $F_M/(F_M + F_C)$ is linear (slope = 5.17 ± 0.12 at 95% C.L.) with zero intercept (intercept = 0.05 ± 0.19 at 95% C.L.) and a correlation coefficient of 0.998.

3.3.9 Other Studies

Several reports on the effect of flow rates on peak height in solvent extraction/FIA have previously appeared [19,20,35,37]. These studies were performed as part of the optimization procedure in the development of extraction/FIA determinations. As such they were not meant to include the effects of all system parameters and, for the most part, no effort was made to keep all other

Table 3. Effect of compensating flow rate on signal and constancy of
 $(F_M + F_C)$.

F_M (mL/min)	F_C (mL/min)	$(F_M + F_C)$ (mL/min)	F_M $(F_M + F_C)$	AA Signal (cm)
1.6 ₀	4.9 ₀	6.5 ₀	0.24 ₆	1.25
2.3 ₀	4.2 ₀	6.5 ₀	0.35 ₄	1.85
2.9 ₀	3.6 ₀	6.5 ₀	0.44 ₆	2.30
3.2 ₅	3.2 ₀	6.4 ₅	0.50 ₄	2.75
4.0 ₀	2.5 ₀	6.5 ₀	0.61 ₅	3.25
4.6 ₀	1.9 ₀	6.5 ₀	0.70 ₈	3.80
5.2 ₀	1.3 ₀	6.5 ₀	0.80 ₀	4.25
6.0 ₀	0.5 ₀	6.5 ₀	0.92 ₃	4.65
6.5 ₀	0.00	6.5 ₀	1.00	5.25

system variables constant while studying the effect of one. Taking this into account, the data obtained in these studies is consistent with the predictions of equation 3.40. For example, data presented in references 20 and 37 give a linear plot of P.H. vs $1/F_0$ in the higher end of the range of F_0 studied, though the plots are non-linear at lower F_0 . Also data in reference 35 shows that P.H. increases with an increase in aqueous phase flow rate.

CHAPTER 4

HYDRODYNAMIC AND INTERFACIAL ORIGIN OF SEGMENTATION IN SOLVENT EXTRACTION/FLOW INJECTION ANALYSIS

4.1 Introduction

Solvent extraction performed in the flow injection analysis mode requires that two immiscible solvent streams undergo a confluence at some sort of segmentor from which they merge into an extraction coil as alternating segments of the two phases, typically organic, O, and aqueous, A (Chapter 1). Segment length in the extraction coil seems to be an important factor in optimizing solvent extraction/FIA [30] and experimental evidence indicates that the segmentor design and geometry play a major role in determining segment length [19,23,24,85]. Another factor affecting segment length is the flow rates of the two immiscible solvents. In all systems in which flow rates of the confluent streams are maintained constant and uninterrupted the volumes of the O and A segments, and hence their lengths in the extraction coil, are governed by a combination of hydrodynamic and interfacial forces. In this chapter the theoretical basis for understanding the segment formation process is presented and the

resulting model is experimentally tested [25]. The segmentor design employed is based on a simple tee made of Kel-F which has been used successfully in several applications for solvent extraction/FIA [21,22,26,86], but the underlying theory will apply, with suitably modified parameters, to all constant flow segmentors.

4.2 Experimental

4.2.1 Solvents

Reagent grade chloroform and methylisobutylketone (MIBK) were used as received. Water was distilled, deionized, and distilled from alkaline permanganate.

4.2.2 Apparatus

Solvents were pumped by two liquid chromatography pumps (Model 6000A, Waters Associates and Mini-Pump Model 396, LDC) to insure constancy of flow rates. The solvents met in the tee segmentor shown in Figure 4. Attached to the exit of the segmentor was a 300-cm long coil of 0.8-mm i.d. Teflon tubing which served as the extraction coil. Segment length in the extraction coil was studied as a function of flow rate. To do this both pumps were first set to identical flow rates and pumping was continued for several minutes. The two pumps were then turned off at the same time and the lengths of the stationary segments

were measured near the downstream end of the extraction coil. Solvents were not pre-equilibrated before being pumped to the segmentor. Teflon inserts, consisting of short segments of 0.8-mm i.d. tubing, were placed in three branches of the tee to improve the regularity of segmentation as discussed below (see Figure 4).

4.2.3 Contact Angles

Solid-liquid-liquid contact angles, θ [87], were measured in a 4-cm long by 0.16-cm i.d. capillary machined from Kel-F. They were measured for MIBK/H₂O and for CHCl₃/H₂O by the capillary rise technique [88].

4.3 Results and Discussion

4.3.1 Contact Angles

The solid-liquid-liquid contact angle, θ , is related to the height of capillary rise, h , by the expression [88]:

$$\cos \theta = \frac{\Delta \rho \cdot g \cdot h \cdot r}{2 \cdot \gamma_{O/W}} \quad (4.1)$$

when $\Delta \rho$ is the density difference between the organic solvent and water, $\gamma_{O/W}$ is the liquid-liquid interfacial tension between organic and aqueous phases, g is the

gravitational constant, and r is the radius of the measurement capillary. In the 0.079 ± 0.001 cm radius capillary used the MIBK/H₂O interface was depressed by 1.2 ± 0.08 cm and the CHCl₃/H₂O interface was elevated by 1.7 ± 0.06 cm, which give $\cos \theta$ of 0.88 ± 0.06 and 0.98 ± 0.04 , respectively, for MIBK/H₂O with $\gamma_{O/W}$ of 10.7 dyne/cm [89] and for CHCl₃/H₂O with $\gamma_{O/W}$ of 32.8 dyne/cm [90]. For MIBK/H₂O $\theta = 29^\circ \pm 7^\circ$. In CHCl₃/H₂O $\theta = 11^\circ$ as an average value but, because of the closeness of $\cos \theta$ to 1, the range of θ within the experimental uncertainty of $\cos \theta$ is 0° to 20° . The fact that a larger value of θ is observed for a solvent system with a smaller value of $\gamma_{O/W}$ is consistent with observations on other hydrophobic solids at low $\gamma_{O/W}$ [91].

4.3.2 Segmentation

The phase segmentor differs from those used in earlier studies [21,22] by the inclusion of short inserts of 0.08-cm i.d. Teflon tubing in the three branches of the tee. In their absence, irregular segmentation patterns sometimes developed in which usually long and short segments appeared. This was observed to be due to creeping of the organic phase along the wall into the aqueous inlet branch of the tee where it formed an adherent droplet located a millimeter or two into the branch. The droplet

grew in size until it formed a constriction large enough to occasionally facilitate breakage of the aqueous stream at that point rather than at the junction of the three branches of the tee where it normally occurs. Inclusion of the Teflon tubing inserts in the tee eliminated the problem over a wide range of flow rates. With F_O/F_A maintained at 1.0 the lengths of the aqueous and organic segments are necessarily equal when segmentation is regular.

The experimentally measured dependence of segment length L on total flow rate F_T is shown as points in Figure 16A for $\text{CHCl}_3/\text{H}_2\text{O}$ and in Figure 16B for $\text{MIBK}/\text{H}_2\text{O}$ over the ranges of F_T where segmentation is regular. At higher F_T than those shown the segmentation patterns are regular at the segmentor but were irregular at the measurement point as the result of coalescence of segments during passage through the extraction coil. It is evident from Figure 16 that shorter segments are produced at higher flow rates and that, at a given flow rate, longer segments are obtained with $\text{MIBK}/\text{H}_2\text{O}$ than with $\text{CHCl}_3/\text{H}_2\text{O}$.

These two features of the L vs F_T curves are a consequence of the physical processes responsible for segment formation at the tee, which can be described in the following terms by reference to Figure 17. The vertical and horizontal orientation of the branches of the

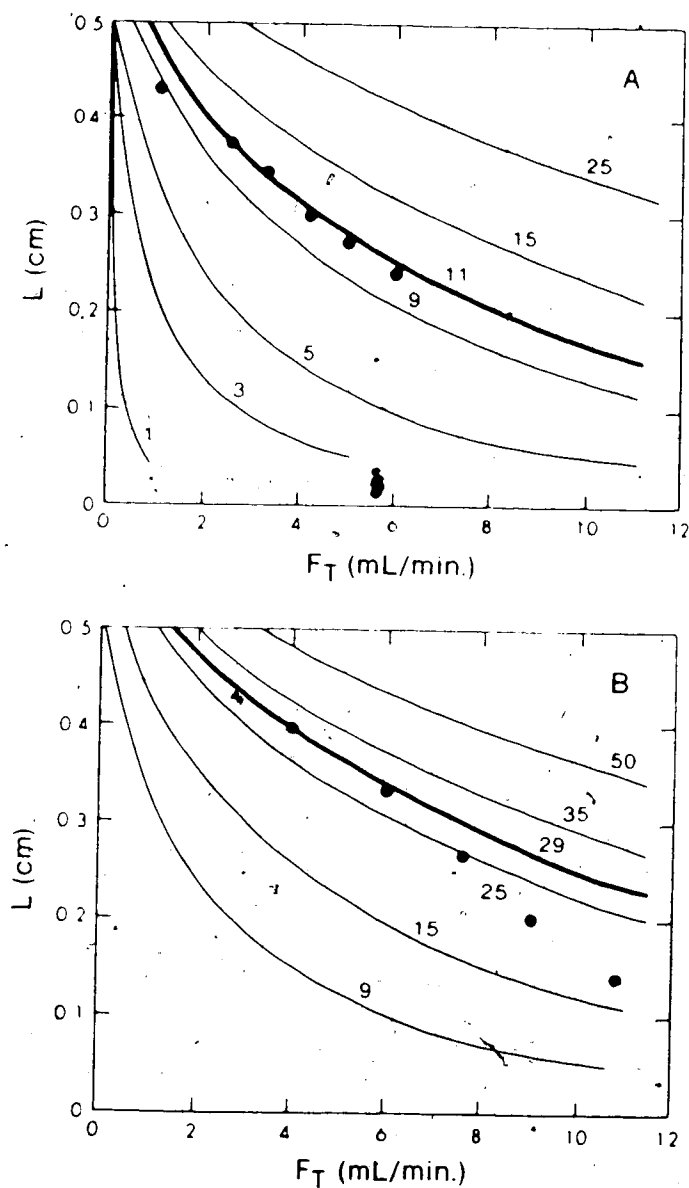


Figure 16: Segment length, L , versus total flow rate, F_T , for chloroform-water (A) and methylisobutylketone-water (B). $F_O/F_a = 1$. Points are experimental and lines are theoretical for the contact angles shown.

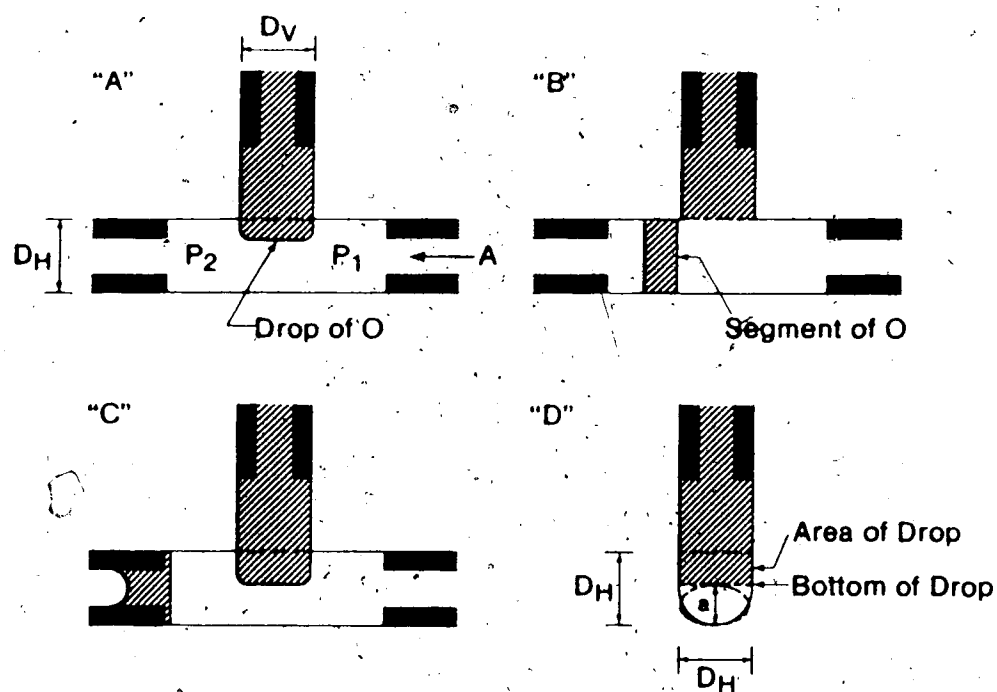


Figure 17. Diagram of segment formation at the "tee". A-C are side views, D is end view of tee. Organic phase is shaded. P_1 and P_2 are upstream and downstream pressures across the drop of organic phase. D_H is the internal diameter of the horizontal branches of the tee and D_V is the internal diameter of the vertical branch.

tee in Figure 17 are merely for ease of reference in the following discussion. Gravity probably plays a negligible role in the segment forming process. As shown in Figure 17A, the flow of organic solvent phase (O) into the aqueous phase (A) flow stream has the appearance of a drop of O. It should be realized, however that, since the diameters of the vertical and horizontal branches of the tee are equal, the sides of the drop of O are in contact with the side walls of the horizontal branch at the crossing of the tee. This is shown in end view in Figure 17D where the growing drop of O is seen to descend like a gate across the aqueous flow stream. A hydrodynamic force is exerted on the drop of O as a result of the perpendicular flow of A. This force tends to dislodge (break off) the drop of O from the column of O above it and "slide" it along the surface of the left horizontal branch of the tee. The drop will be dislodged in this way when the hydrodynamic force pushing it is equal to the interfacial force holding it onto the vertical column of O. When the drop of O finally is dislodged and moves into the horizontal branch it tends to minimize its contact area with A and maximize its contact area with the Kel-F wall, on which it is a wetting-solvent. This results in a rearrangement of the dislodged drop to form a segment of O (Figure 17B) which subsequently is pushed along into the

0.8-mm i.d. Teflon insert and extraction coil (Figure 17C).

Before providing quantitative descriptions of the hydrodynamic and interfacial forces involved, several assumptions of the model should be clarified: (a) Because both O and A are always flowing there will continue to be flow of O into the drop during the time that it is dislodging. It is assumed in subsequent calculations that once the drop has started to dislodge it does so very rapidly, so that the volume of O flowing into it during the transition from drop to segment (Figure 17A to 17B) is negligible. (b) Visual observation of the tee at very slow flow rates showed that spreading of O along the walls of the horizontal branches did not occur during drop growth (before dislodgment). It can safely be assumed that such spreading does not occur at the flow rates used in Figure 16 since they are even closer to the critical jetting velocity [92]. (c) The drop is assumed to grow straight down, along the extrapolated axis of the vertical branch. In fact, visual observation at very low flow rates, where drops grow to a large size before dislodging, shows that they bend somewhat toward the left (downstream). Presumably this drop distortion occurs to some extent at all flow rates, but it will be neglected in calculating the hydrodynamic force. (d) The effect of the

Teflon inserts in the tee on flow streamlines, especially in the upstream horizontal branch, are ignored [93-96].

(e) To facilitate calculations, the cross section of the space below the growing drop is assumed to be elliptical, as shown in Figure 17D, with its major axis equal to the diameter of the horizontal tube ($D_H = 0.16$ cm) and its minor axis, a , equal to the difference between D_H and the vertical length of the drop at any time. Vertical drop length is calculated from the geometry of the space at the crossing point of the tee into which the drop is growing and from F_0 and time. Use of D_H as the major axis is justified by the fact that the largest segment length observed in the experiments reported in Figure 16 corresponds to ($a > D_H/2$), so that the meniscus never got further than about the position shown in Figure 17D. (f) Interfacial tensions and contact angles were measured on pre-equilibrated phases, while the liquids pumped in the segmentation studies were not pre-equilibrated.

Segment formation is quantitatively described as follows: The hydrodynamic force tending to dislodge the drop is the product of the area of the drop facing the aqueous stream (A_R ; Figure 17D) times the pressure difference across the drop due to the aqueous flow ($\Delta P = P_1 - P_2$; Figure 17A). Drop area may be expressed in terms of L as:

$$AR_q \equiv \frac{D_H \cdot \pi \cdot L \cdot D_C^2}{4 \cdot D_V^2} \quad (4.2)$$

where D_C and D_V are the internal diameters of the extraction coil (0.08 cm) and the vertical branch of the tee (0.16 cm), respectively. The pressure difference ΔP is composed of two contributions: The first arises from the viscous drag on the aqueous phase as it flows through the elliptical "capillary tube" beneath the organic phase drop, and the second arises from the kinetic energy loss of the aqueous phase flowing through the same elliptical "orifice". The relationship of ΔP to volumetric flow rate F_A through a short elliptical tube is given as a combination of Poiseuille's Law and Bernoulli's Law by the following expression [96]:

$$\Delta P \equiv \frac{F_A \cdot 8 \cdot \eta_A \cdot (D_V + 1.64 \cdot R)}{\pi \cdot R^4} + \frac{1.12 \cdot \rho_A \cdot F_A^2}{\pi^2 \cdot R^4} \quad (4.3)$$

in which η_A is the viscosity of A, ρ_A is the density of A and R is the equivalent radius of the ellipse [96] given by:

$$R \equiv \frac{a^2 \cdot D_H + a \cdot D_H^2}{2a^2 + 2D_H^2} \quad (4.4)$$

The minor axis of the ellipse can be calculated from:

$$a = D_H - \frac{\pi \cdot L \cdot D_C^2}{4 \cdot D_V^2} \quad (4.5)$$

The hydrodynamic force f_{HYD} exerted by the flow of A on the growing drop of O is given by:

$$f_{HYD} = AR \cdot \Delta P \quad (4.6)$$

The drop will be dislodged when this force equals the interfacial force holding the drop onto the column of O.

The interfacial force is the force required to take an area of $\pi(D_V/2)^2$ of O which is in contact with the vertical column of O and move it into contact with the Kel-F wall. This interfacial force f_{INT} is given by the following form of the Tate equation [87,88]:

$$f_{INT} = 2 \cdot \pi \left(\frac{D_V}{2} \right) \cdot \gamma_{O/W} \cdot (1 - \cos \theta) \quad (4.7)$$

The value of f_{INT} is independent of drop size. It is thus evident in a qualitative way that when a larger aqueous flow rate F_A is used f_{HYD} will be equal to f_{INT} at a smaller drop size so that, as is seen experimentally, L is

smaller at higher F_A . A quantitative expression for F_A in terms of L can be obtained by substituting f_{INT} from equation 4.7 for f_{HYD} in equation 4.6 and combining the result with equations 4.2-4.5. Since D_H , D_V and D_C are known from the design of the system, η_A and ρ_A can be looked up in tables, a and R can be calculated for any value of L , and θ has been measured experimentally for $CHCl_3/H_2O$ and for $MIBK/H_2O$, it is possible to calculate the values of F_A expected for various values of L . F_T is readily obtained from

$$F_T = F_A + F_O \quad (4.8)$$

where $F_O = F_A$ in this case.

The solid points in Figure 16 show the experimentally measured dependence of L on F_T . The lines, calculated via equations 4.2-4.8 for various assumed values of θ , are theoretical predictions. The two dark lines are the theoretical predictions for $CHCl_3/H_2O$ ($\theta = 11^\circ$, $\gamma_{O/W} = 32.8$ dyne/cm) and $MIBK/H_2O$ ($\theta = 29^\circ$, $\gamma_{O/W} = 10.7$ dyne/cm) based on their experimentally measured θ . The remarkably good fit of the experimental points to the theoretical line for $\theta = 11^\circ$ in the $CHCl_3/H_2O$ system must be considered to be somewhat fortuitous in light of the large experimental uncertainty in θ for the system. For both of

the solvent systems the experimental points describe more nearly straight lines than are predicted by the hydrodynamic-interfacial model. A substantial discrepancy between theory and experiment is not surprising in view of the simplifying assumptions (a)-(f) that were necessary. However, the model does predict the main features of the data - the decrease of L with increasing F_T and the displacement of the MIBK/H₂O curve to higher L than the CHCl₃/H₂O curve (this being mainly a consequence of the larger contact angle for Kel-F/MIBK/H₂O). The proposed semiquantitative model represents a viable basis for a theoretical understanding of the segmentation process and will serve as a guide in the design of new and modified segmentors in continuous flow systems.

It may be noted, in this connection, that in segmentors designed around a jet in which the drop grows and breaks off in such a way that it is not in contact with the wall at the time of dislodgment, $\cos \theta$ is absent from equation 4.7. The resulting equation for f_{INT} would have the more conventional form of the Tate equation [87-88] which corresponds to very much higher value of f_{INT} for a given jet diameter (D_V) than those encountered in the tee segmentor.

Conclusions and suggestions for future work are presented in Chapter 5 of Part II of this thesis.

PART II

EVALUATION OF A SEMIAUTOMATED ION EXCHANGE/ATOMIC
ABSORPTION SYSTEM FOR FREE COPPER ION DETERMINATION
IN NATURAL WATERS

CHAPTER 1

INTRODUCTION

In this chapter the role of speciation is briefly discussed followed by an overview of the most important speciation-sensitive techniques. The last section outlines the research objectives of Part II.

1.1 The Role of Speciation

Unpolluted natural water systems contain metals at well below their toxic concentrations. Usually significant fractions of the metals are adsorbed on organic or inorganic colloidal particles [97]. Human activity has dramatically increased these levels either by direct introduction through waste disposal of the metal (e.g. copper from mine dust and liquid waste [98,99]) or by lowering the pH of water with acidic industrial and domestic effluents and acid rain so that the metals are leached from otherwise insoluble forms [100,101]. It has been calculated that 10,000 tonnes of the most abundant heavy metals are discharged to sewer systems in the United Kingdom every year [102].

Trace metals in natural waters may exist in a variety

of different forms; free (hydrated), complexed with various organic and inorganic ligands, adsorbed on inorganic particles and organic colloids, and incorporated in living organisms [97,103,104]. The distribution of a given trace element among these forms is determined by several factors, including the presence of other metals, the presence of various ligands, the pH, and biological uptake of various species by organisms. The determination of the concentrations of these individual forms of an element is termed chemical speciation. Measurement of the total concentration of a trace element does not provide the required information about its influence on aquatic life because only a fraction of the total concentration of the metal is involved in the uptake process of a given organism. This is called the bioavailable fraction [97]. There is considerable evidence in the literature that free ionic copper is the most toxic form to aquatic life [105-109], and there is more limited data supporting this conclusion for cadmium [110], lead [111], nickel [112], and zinc [110,113,114]. Growth of microorganisms has been shown to decrease as a result of complexation of essential trace nutrients [113]. For copper there are also reports of biological availability of hydroxo complexes [115-117], amino acid complexes [118], and lipid-soluble complexes [119].

Physicochemical behavior of trace elements is also

highly affected by the species present. Adsorption to sediment can either be enhanced or reduced depending on the chemical form. As an example, it is reported that lead carbonate is much more strongly adsorbed on silica than are free lead ions [120]. Feick et al. [121] found that run-off of road de-icing salt tends to release mercury from contaminated fresh water sediments by formation of soluble chloro complexes of mercury.

From another point of view, metals affect the speciation of the ligand(s) to which they are coordinated which, in turn, can influence species toxicity, biodegradability, and transportation in aquatic systems [121]. Most natural waters have the capacity to reduce the toxic effect of added trace metals. This detoxification is generally attributed to complexation of the added metal by the available ligands; the ability of water to complex metals is quantified as the "complexing capacity" of the water [122]. This topic has been a subject of two major reviews [120,122].

1.2 Species Selective Techniques

The present awareness of the important role of speciation has triggered increased activity in development of analytical techniques for the determination of various

chemical forms of environmentally important elements. The wide variety of techniques now available which provide some discrimination between the different forms of trace elements have been reviewed by several workers [97,120,122,123-126]. In this section the most important species selective techniques are outlined.

1.2.1 Calculation Methods

This method involves calculation of various species concentrations (or percentages) by simultaneous solution of equations representing the thermodynamic equilibria in the system. This would seem to be a very attractive method since all the problems associated with method selectivity immediately disappear. However, this method is generally not applicable to natural water samples. For one thing, it requires analytical determination of all components in the sample. In addition, the element can be divided among both a particulate and a soluble fraction, each of which may be composed of several species.

Adsorption of metal ions or various complexes on the solid phase is a complicating factor which cannot be accounted for in the calculation method. Furthermore many of the equilibrium constants and corrections for ionic strength are subject to considerable uncertainty even for inorganic complex formation [97,127]. Another complication arises

from the presence, in water samples, of significant quantities of undefined soluble and dispersed colloidal organic polymeric materials (fulvic and humic acids) [128] which interact strongly with some trace elements in the sample [97,129,130]. Although progress is now being made in studying these interactions [131-133] the difficulty in characterizing the humic and fulvic materials in each particular sample means that the calculation methods cannot be used for speciation in real samples. For artificial test solutions where the exact composition is known the calculation method can be a powerful tool depending on the accuracy of the thermodynamic constants and equilibria considered. A variety of computer programs are available for this purpose [97,134,135].

1.2.2 Size Separation Methods

These methods include ultrafiltration, dialysis, and size exclusion chromatography [136-141]. Filtration through a 0.45 μm filter is frequently used to separate the solid phase of the sample from the operationally defined "soluble phase" [97]. Even ultrafilters (e.g. 0.015 μm pore size) are not absolute filters; Laxen and Harrison showed that significant amounts of colloidal materials may pass through them [142]. Guy and Chakrabarti compared several techniques of metal

speciation and concluded that sorption of species on the filter is a serious limitation of ultrafiltration [143]. Species separation by dialysis involves transport of soluble species across a membrane into the dialysis bag containing pure water. Equilibration for the dialysis of cationic and neutral species is considerably faster than for anionic species because the latter are repelled by the negatively charged membrane [138]. This effect can be overcome by addition of a high concentration of electrolyte [143]. Cox et al. [140] developed a rapid (1 h) dialysis method for estimation of the total free plus labile complexes as well as the non-labile complexes of metals. They demonstrated that dialysis of the metal into salt solution yields the sum of the concentrations of the free metal plus the labile complexes, while dialysis into strongly acidic or chelating receiving solutions yields free metal plus labile and non-labile complexes of the metal.

Heavy metal speciation by size-exclusion chromatography (gel filtration chromatography) has been discussed by Neubecker and Allen [120] and by de Mora and Harrison [144]. Large complexes which are formed between macromolecules and metal ions are eluted more rapidly than the free metal ions and thus a separation of the two categories can be achieved [145]. One major disadvantage

of the method is the excessive dilution of the sample upon elution. The metal concentration in the sample to be analyzed should be at least 50 times the detection limit of the analytical technique used for determination in the eluted fraction [126]. Furthermore, charged species sometimes behave anomalously, either being retarded to some extent or eluted rapidly due to the weak ion-exchange characteristics of the gel used. Gel filtration chromatography may be perturbing to the equilibrium system because kinetically labile species will dissociate upon fractionation.

1.2.3 Voltammetric Methods

A variety of voltammetric techniques can be used for speciation of trace metals in solution including differential pulse polarography [146,147], anodic stripping voltammetry (ASV) [142,147-149], and differential pulse anodic stripping voltammetry [141,146,150-152]. Application of voltammetry to the determination and speciation of metals in natural systems has been the subject of several reviews [97,154,155]. ASV is sufficiently sensitive for direct determination of the very low levels of heavy metals in natural waters (10^{-8} to 10^{-9} M) [153]. Pulsed ASV techniques are able to achieve detection limits approximately an order of magnitude lower.

[155]. Advantages of voltammetric methods include relatively modest initial cost, simultaneous multi-element capability, and minimal sample pretreatment [156].

ASV speciates metals on the basis of electrochemical lability. The signal obtained is proportional to the free metal ion plus any contribution from kinetically labile complexes which may dissociate during the deposition step [157]. Thus, depending on the deposition time, ASV techniques may perturb the sample by lowering the free metal ion concentration in the vicinity of the electrode, thereby providing a driving force for dissociation of metal-ligand complexes. The result is that the signal measured is higher than predicted [159]. Metal carbonate and hydroxide complexes, which are abundant in natural waters [146], are electrochemically indistinguishable from the free metal by ASV [160]. Correction of such an error is possible given accurate formation constants of the relevant species, the carbonate concentration and the pH. Still other problems may be encountered in ASV, such as formation of intermetallic compounds in or on the electrode which bring about inter-element interferences [150,161]. Dissolved organic matter may be adsorbed onto the electrode surface causing a change in reversibility of electrode reaction, a wave shift to more cathodic potentials, and multiple waves [147,162]. These problems,

have resulted in considerable controversy concerning the application of ASV for the determination of complexing capacity and the interpretation of the results [158,163,164].

Depending on the reduction potential used, certain complexes may be reduced irreversibly [158]. This is especially problematic in titration experiments used to measure complexing capacity in which the same sample is analyzed after each incremental addition of the titrant. The effect can be overcome by careful choice of the electrolysis condition or by using a fresh sample for each addition of titrant.

1.2.4 Ion Selective Electrode Methods

Ion selective electrode (ISE) methods are probably the most ideal techniques for monitoring free metal ion concentrations without affecting solution equilibria. Although direct measurements of free copper in natural systems by ISE's have been attempted [165-167] the concentrations of copper and most trace elements in these systems are far too low to be reliably measured in this way [123]. Nevertheless, ISE methods remain an important technique for basic speciation studies which involve free metal ion concentration determination at higher levels, such as the determination of the formation constants of

metal-ligand complexes and hydrolysis studies [128,131,141,168-171].

Ion selective electrodes are available for only a limited number of transition metals. Those that are available generally suffer from non-Nernstian response below 10^{-6} M (e.g. 0.06 $\mu\text{g/mL}$ for Cu^{2+}) [166,172]. The copper ion selective electrode is the most widely used; it has been tested for response to submicromolar levels [172]. The steady state potential response is very dependent on the method of electrode cleaning and conditioning. The rate of approach to steady state potential is a function of the copper concentration. Smith and Manahan [173] used a copper ISE plus the method of standard addition for the determination of copper in tap water by ISE potentiometry. They added an excess of an acetate-fluoride complexing buffer to adjust the pH to 4.7 and to prevent iron interference. This method is obviously inapplicable to speciation work. Halide interference with copper ISE response [174-178] and the electrode's anomalous response in the presence of chelating ligands [179] and in natural water [180,181] have been reported in the literature.

1.2.5 Ion Exchange Methods

Cation/exchange resins have been incorporated in a

number of schemes designed to differentiate free and labile complexes of metals from strongly bound complexes and particulate metal forms [142,182,183]. Figura and McDuffie [184] used ASV and Chelex-100 ion exchange resin in the calcium form in their scheme of metal speciation. They used both batch and column methods to classify trace metal species as "very labile", "moderately labile", "slowly labile", or "inert" depending on the time scale of the measuring technique. Laxen and Harrison [142] used Chelex-100 in their speciation studies of lake water and preferred the term Chelex-labile metal fraction for the species sorbed onto the resin during a 48 h batch equilibration.

Schubert's ion exchange method has been used as a batch technique for the determination of the stability constants of metal complexes in various systems [186,187] and for the determination of the metal complexation capacity of sewage [188]. The method usually yields the free metal ion concentration provided that certain conditions are met [184,186,187,189]:

- (a) The solution ionic strength must remain constant.
- (b) The free ligand concentration must remain nearly constant.
- (c) There should be no sorption of ligand or complexes on the ion exchange resin.

- (d) The system must reach equilibrium.
- (e) Only a very small fraction of the free metal is sorbed so that the equilibria in the sample solution are not perturbed in the presence of the ion exchanger. The perturbation effect can be eliminated by successive equilibration of the same portion of resin with several fresh aliquots of the sample solution.

Van den Berg and Kramer [190] used very small amounts of a weak inorganic cation exchanger (manganese dioxide) in their speciation measurements of natural waters. Although the method may be specific for free copper uptake, perturbation is expected since the free copper is removed from solution.

Perturbation can be eliminated conveniently by using a column-equilibration method rather than a batch method of equilibration. Flow through column or successive batch equilibration methods were used for the determination of cation activities in milk [191]. In contrast to the Schubert method the authors did not employ addition of a "swamping" electrolyte so that the effect of other cations on the accuracy of the method was pronounced.

Cantwell et al. [189] determined free nickel ion concentrations in raw sewage by a flow through column equilibration version of the Schubert method using a

strong cation exchange resin. They compared this method with the batch method. The batch method requires either multiple equilibration with fresh portions of sample solution or that the sample be well buffered with respect to free metal ion so that sorption of a small fraction of Ni^{2+} will not significantly alter its concentration in the sample. In contrast, the column equilibration method does not require this condition since the sample is continuously pumped through the resin bed until no further nickel ions are sorbed, such that the entire resin bed is finally in equilibration with unperturbed sample solution. The free nickel is determined by elution of the equilibrated resin after a brief wash with water. Unlike the ASV or ISE methods the ion exchange method is not limited to a small number of elements. It can be applied to the speciation of many different metals with adequate sensitivity for environmental work. Detection limits can be as low as 10^{-10} M [184] depending on the experimental conditions and the metal detection system used. One disadvantage of the method is that maintaining trace ion exchange conditions requires addition of an inert electrolyte salt to the sample. This changes the activity coefficients of the ions and possibly shift chemical equilibria in the system.

1.2.6 Miscellaneous Methods

Solvent extraction has been applied to the determination of kinetically inert lipid-soluble organometallic complexes in combination with other separation techniques such as gas chromatography [192]. Various tin alkyls have also been separated and determined by high pressure liquid chromatography with AAS detection [193]. Metal speciation using AAS as a chromatographic detector have been reviewed by Fernandez [194]. In general, chromatographic techniques can be used to separate only kinetically inert species since it severely perturbs equilibria involving labile species.

An important feature of several elements is their existence in more than one oxidation state of different toxicity. This is true of chromium and arsenic [123]. Lynch et al. [195] reported a FIA system with sequential visible molecular absorption spectrophotometric and AA detectors for the determination of the stable oxidation states of chromium and iron. The visible molecular absorption spectrophotometric detector selectively determined the Cr(VI)-diphenylcarbazide complex or the Fe(II) 1,10-phenanthroline complex. The same speciation principle was also used by Burguera and Burguera for the determination of iron(II) and total iron [196]. This speciation technique by FIA has been the subject of a

recent review [197].

UV-Vis spectrophotometry involves no direct contact between the sample and the measuring device so that many possible causes of error are eliminated. Unfortunately this technique generally lacks the required sensitivity and specificity. The theoretical basis of a modified form of UV-Vis absorption spectrophotometry for measurement of free ion concentrations was presented by Fulton and Kratochvil [198] who also reviewed earlier work. The method has been used for the determination of unbound iron in blood serum [199]. Fluorescence quenching also has been used to measure complexation capacity of fulvic acid and the stability constants of Cu-fulvic acid complexes [200,201].

1.3 Research Objectives

Copper sulfate is the most widely used chemical for controlling algal growth in water supplies, recreational lakes, and reservoirs [167,202]. It is estimated that over 9 million kilograms of copper sulfate are annually applied for algal control in the United States. Copper ions are also the most toxic form of copper species to aquatic life (Section 1.1) and many cases of fish kill have been reported after application of copper sulfate to

lakes [202]. Metallic copper, widely used because of its excellent conductivity and mechanical properties, likely contributes appreciable quantities of waste Cu^{2+} to sewer systems, lakes, rivers, and seas. With the ever-mounting problem of acid rain in aquatic systems [100], a larger fraction of copper is likely to be solubilized, and to remain in the free toxic form.

Copper is a well studied element both from the chemical and the environmental points of view so that there is ample information in the literature about its formation constants with many important ligands. Furthermore, the element can be analyzed by various methods of speciation such as ASV, ISE, and ion exchange. Copper is often the element of choice for the basic speciation studies.

Because of all the above mentioned reasons copper was the metal chosen for a detailed investigation of the ion exchange method of determining free M^{2+} species in the presence of its kinetically labile complexes. As mentioned earlier, a previous report from this laboratory dealt with the determination of free nickel ion concentrations in raw sewage by the ion exchange equilibration technique [191]. Later the method was miniaturized, made semiautomatic, and applied to the determination of free copper in aqueous solutions [74].

In Chapter 2 of this work the theoretical basis of this semiautomated method will be described. In Chapter 3 various experimental parameters will be characterized and optimized. In Chapter 4 the specificity of the method for free-Cu²⁺ determination will be examined in the presence of various organic and inorganic ligands commonly found in natural waters. Finally, the method will be used for the determination of free-copper concentration and for the determination of the complexing capacity of a lake water sample from Quebec.

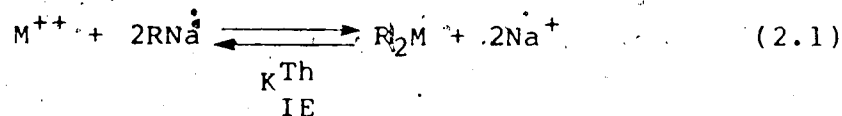
CHAPTER 2

THEORY OF SPECIATION MEASUREMENT BASED ON ION EXCHANGE

The theoretical treatment presented in this chapter is specific to the ion exchange column equilibration method of speciation. Detailed theory as applied to the batch method is presented elsewhere [189].

2.1 Ion Exchange Equilibria

Consider a simple equilibrium system containing trace amounts of a divalent metal ion, M^{++} , a high concentration of an inert electrolyte (e.g. 0.1 M $NaNO_3$), a non complexing buffer, and a few milligrams of a strong acid type cation exchange resin (e.g. Dowex 50W-X8). If the pH is so low that no hydroxide species are formed then the following equilibrium will prevail:



where R represents a resin fixed charge site, k_{IE}^{Th} is the thermodynamic ion exchange equilibrium constant for the metal ion distributed between the solution and the resin

phases, defined as follows:

$$K_{IE}^{Th} = \frac{a_{R_2M} \cdot a_{Na^+}^2}{a_{M^{++}} \cdot a_{RNa}^2} \quad (2.2)$$

Here a_i is the activity of the species i . Equation 2.2 can be written in terms of species concentrations, $[i]$, and activity coefficients, γ_i :

$$K_{IE}^{Th} = \frac{[R_2M][Na^+]^2}{[M^{++}][RNa]^2} \cdot \frac{\gamma_{R_2M} \cdot \gamma_{Na^+}^2}{\gamma_{M^{++}} \cdot \gamma_{RNa}^2} \quad (2.3)$$

where γ_{R_2M} and γ_{RNa} are the respective activity coefficients of R_2M and RNa in the resin phase.

If it is assumed that all test solutions are "swamped" with a high concentration of non-complexing strong electrolyte, it can be safely stated that ionic strength is constant, and the activity coefficients are therefore constant too. The trace amount of metal in any form is not expected to change the total ionic strength of the system and equation 2.3 can be written in the form

$$K_{IE} = K_{IE}^{Th} \cdot \frac{\gamma_{M^{2+}} \cdot \gamma_{RNa}^2}{\gamma_{R_2M} \cdot \gamma_{Na^+}^2} = \frac{[R_2M][Na^+]^2}{[M^{2+}][RNa]^2} \quad (2.4)$$

where K_{IE} is the concentration equilibrium constant of the metal ion between the aqueous and the resin phases.

A second assumption necessary to the method is that only a small fraction ($<1\%$) of the exchange sites on the resin will be occupied by the metal, i.e. $R_2M \ll RNa$. This is controlled by the electrolyte concentration. One should have high enough Na^+ to guarantee the above condition. The upper limit of the Na^+ concentration is governed by the desire to maintain adequate sensitivity (related to resin uptake) of the metal ion, M^{2+} , and to avoid flow problems associated with increased viscosity.

The two assumptions above provide for "trace" ion exchange conditions [189,203]. Thus, upon changing the metal ion concentration the amount of Na^+ released from or sorbed by the resin is negligible in comparison with the total Na^+ concentration in the system. Under these conditions both $[Na^+]$ and $[RNa]$ may be considered constant. These constants can be incorporated in K_{IE} and upon rearrangement equation 2.4 will take the following form:

$$\frac{[R_2M]}{[M^{++}]} = K_{IE} \cdot \frac{[RNa]^2}{[Na^+]^2} = \lambda_0 \quad (2.5)$$

where λ_0 is the distribution coefficient of the free metal ion between the solution and resin phases. λ_0 will be constant as long as trace ion exchange conditions are maintained, and the swamping electrolyte concentration is held constant. If the swamping electrolyte concentration is changed both the $[\text{Na}^+]$ and the K_{IE} value will change. The K_{IE} change is due to the direct effect of ionic strength on the activity coefficients in both the solution and the resin phases. Thus the value of λ_0 will change as a result of both changing K_{IE} and changing $1/[\text{Na}^+]^2$.

A third assumption is that only the free metal ion is sorbed onto the resin. This assumption is not likely to be met since, in principle, any cationic species is likely to undergo ion exchange to some extent. However it is predicted that complexes with lower charge than the free metal will sorb to a lower extent. Uncharged species also may sorb onto ion exchange resins [203]. In this work the extent of sorption of species other than free copper (e.g. CuL_2^{2+} , CuL^+ , and CuL_2) is being tested (see below).

2.2 Flow-Through Column Equilibration Method

This method involves passing a test solution, which has been swamped with NaNO_3 , through a known weight of a strong cation exchange resin in the sodium form until the

total metal concentration in the effluent is the same as that of the test solution. Thus the resin in the column is brought to equilibrium with the unperturbed test solution. That is, the resin is in equilibrium with a solution from which no metal species of any form have been taken up by the resin. Any further passage of fresh test solution will cause no change in the metal species distribution in either phase.

It should be made clear that the addition of the swamping electrolyte to the sample solution somewhat perturbs the original sample solution composition because it lowers the activity coefficients. This will shift the ion exchange equilibrium system (equation 2.4) and thus change the K_{IE} . It will also shift the solution equilibria by decreasing the acid dissociation constants of organic ligands and the conditional stability constants of metal complexes [204,205].

A more pronounced perturbation of the equilibrium system is expected if the electrolyte anion complexes with the metal ion of interest (section 2.4). The swamping electrolyte cation may also compete with the metal of interest for complexing ligands in the system.

The addition of swamping electrolyte to the natural aquatic sample containing colloidal clay particles enhances coagulation and precipitation with consequent

perturbation. Because swamping electrolyte compresses the electrical "double layer" around the particles and thus, decreases the electrostatic repulsion forces among them [206].

The swamping electrolyte also competes with the free metal ions for adsorption and exchange sites on hydrated clay particles in the sample and may cause the release of various adsorbed metal species [206].

Under trace ion exchange conditions and assuming that M^{2+} is the only species of the metal M that is sorbed onto the resin, the amount of metal sorbed onto the resin is directly proportional to the free metal ion concentration in the solution phase. The value of the distribution coefficient, λ_0 (in L/g), can be obtained from the slope of a calibration curve obtained in the absence of complexing ligands. The area under the peak measured upon elution of the equilibrated column (P.A.), in units of absorbance \cdot sec, is proportional to the metal ion concentration in the resin phase, $[R_2M]$ (moles/gram of resin).

$$P.A. = \frac{G \cdot S}{F} \cdot [R_2M] \quad (2.6)$$

The proportionality constant includes the sensitivity of the atomic absorption detection system, S

(absorbance/mole/mL), the weight of the resin in the column, G (grams), and the flow rate of the eluate into the nebulizer, F (mL/sec). It has been found that S is a function of F [35,74]. Substituting for $[R_2M]$ from equation 2.5

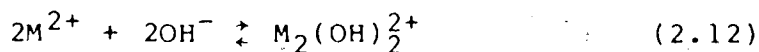
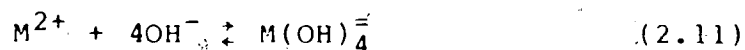
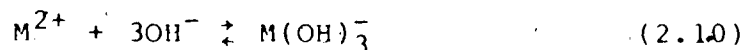
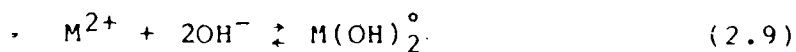
$$P.A. = \frac{G \cdot S \cdot \lambda_0}{F} \cdot [M^{2+}] \quad (2.7)$$

Thus peak area is proportional to the free metal ion concentration in the test solution.

2.3 Effect of Sorption of MOH^+

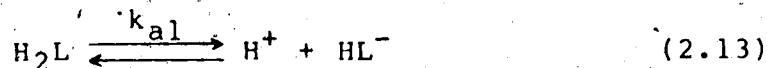
In Section 2.1 it is assumed that the pH is so low that hydrolysis products of the metal ion are absent. In natural water samples the pH may vary from 4 to 9, consequently, the hydrolysis product of the metal ion cannot be neglected. Since some of the metal-hydroxyl species are positively charged they are likely to participate in the resin ion exchange process. In this section it will be shown that ion exchange of the positively charged species, MOH^+ will not impair the specificity of the method for free metal ion determination.

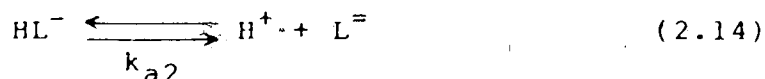
The most important hydrolysis products of the metal M^{2+} are listed below.



Of the above species those that are negatively charged are likely to be excluded from the resin phase. Polynuclear complexes are unlikely to form to a significant extent at the low metal concentration considered here. Positively charged MOH^{+} exchange on the resin occurs to an extent that depends on its distribution coefficient value.

In the presence of an excess of a weakly acidic complexing ligand new equilibria will be established. For the sake of simplicity, assume a dibasic acid H_2L which forms a single complex (ML) , with the metal. Under these conditions equilibria such as the following need to be considered as well:





where k_{a1} and k_{a2} are the first and second acid dissociation constants of the ligand respectively and β_{ML} is the conditional formation constant of ML [207].

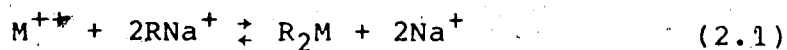
Assuming a simple system where MOH^+ is the only hydrolysis product of the metal ion M^{2+} , consider two cases; in Case I MOH^+ is not sorbed and in Case II MOH^+ is sorbed:

Case I: (MOH^+ does not sorb onto resin):

In the absence of any complexing ligand, L^{2-} :

$$M_T = [\text{M}^{2+}] + [\text{MOH}^+] \quad (2.16)$$

where M_T is the total concentration of metal in solution



$$\alpha_{\text{M,OH}} = \frac{[\text{M}^{++}]}{[\text{M}^{++}] + [\text{MOH}^+]} = \frac{[\text{M}^{++}]}{M_T} \quad (2.17)$$

where $\alpha_{M,OH}$ is the fraction of the metal in solution that is in the free form.

$$\lambda_o = \frac{[R_2M]}{M_T} = \frac{[R_2M]}{[M^{++}] + [MOH^+]} \quad (2.18)$$

Combining equation 2.17 and equation 2.18 we get

$$[M^{++}] = M_T \cdot \alpha_{M,OH} = \left(\frac{R_2M}{\lambda_o} \right) \alpha_{M,OH} \quad (2.19)$$

In the presence of H_2L

$$M_T = [M^{++}] + [MOH^+] + [ML] \quad (2.20)$$

The distribution ratio, D_I of the metal between the resin and the aqueous phases is given by

$$D_I = \frac{[R_2M]}{[M^{++}] + [MOH^+] + [ML]} \quad (2.21)$$

from equation 2.15

$$\beta_{ML} = \frac{[ML]}{[M^{++}][L^-]} \quad (2.22)$$

substituting for $[ML]$, equation 2.21 will take the form

$$D_I = \frac{[R_2M]}{[M^{++}] + [MOH^+] + \beta_{ML} \cdot [M^{++}][L^-]} \quad (2.23)$$

substituting the value of $[M^{++}] + [MOH^+]$ from equation 2.18 and the value of $[M^{2+}]$ from 2.19 we get:

$$D_I = \frac{[R_2M]}{\frac{R_2M}{\lambda_O} + \beta_{ML} \cdot \left(\frac{R_2M}{\lambda_O}\right) \cdot \alpha_{M,OH} \cdot [L^-]} \quad (2.24)$$

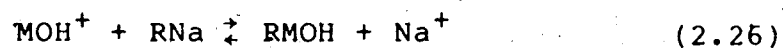
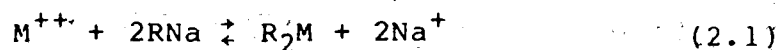
simplifying

$$D_I = \frac{\lambda_O}{1 + \beta_{ML} \cdot \alpha_{M,OH} \cdot [L^-]} \quad (2.25)$$

Case II (MOH^+ sorbs onto resin):

In the absence of a complexing ligand

$$M_T = [M^{++}] + [MOH^+] \quad (2.16)$$



$$\alpha_{M,OH} = \frac{[M^{++}]}{[M^{++}] + [MOH^+]} = \frac{[M^{++}]}{M_T} \quad (2.17)$$

$$\lambda_o = \frac{[R_2M] + [RMOH]}{[M^{++}] + [MOH^+]} = \frac{[R_2M] + [RMOH]}{M_T} \quad (2.27)$$

In the presence of a complexing ligand H_2L

$$M_T = [M^{++}] + [MOH^+] + [ML] \quad (2.20)$$

$$D_{II} = \frac{[R_2M] + [RMOH]}{[M^{++}] + [MOH^+] + [ML]} \quad (2.28)$$

Rearranging equation 2.27 we get

$$([M^{++}] + [MOH^+]) = \frac{[R_2M] + [RMOH]}{\lambda_o} \quad (2.29)$$

Substituting from equations 2.29, 2.17, 2.22 and 2.27 in equation 2.28 we get:

$$D_{II} = \frac{[R_2M] + [RMOH]}{\left(\frac{[R_2M] + [RMOH]}{\lambda_o} \right) + \beta_{ML} \cdot \left(\frac{[R_2M] + [RMOH]}{\lambda_o} \right) \cdot \alpha_{M,OH} \cdot [L^-]} \quad (2.30)$$

Simplifying

$$D_{II} = \frac{\lambda_o}{1 + \beta_{ML} \cdot \alpha_{M,OH} \cdot [L^-]} \quad (2.31)$$

In both Case I and Case II, in the absence of ligand ($[L^-] = 0$), the value measured by the method is λ_0 .

Comparison of equation 2.25 and 2.31 shows that they are identical. Thus whether MOH^+ is sorbed or not, the measured distribution ratio, D , will be proportional to the free metal ion concentration because MOH^+ will always be present in the same ratio to the free metal ion as long as pH is constant.

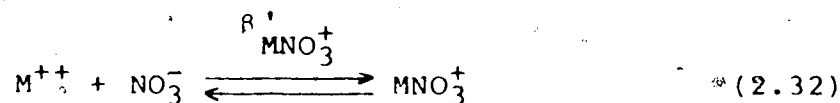
2.4 Effect of Metal Complexation with Electrolyte Anion

Usually the swamping electrolyte is a salt such as an alkali metal nitrate or perchlorate the anion of which is relatively non-complexing. However due to the high concentration of electrolyte used even a very low formation constant of the metal-electrolyte anion complex may tie up a sizable fraction of the total metal. In this section the effect of metal association with electrolyte anion (NO_3^-) is examined.

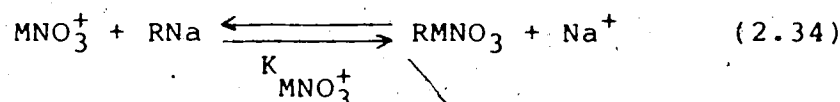
If the concentration of the swamping electrolyte is the same for "sample" ($[L^-] \neq 0$) and "standard" ($[L^-] = 0$) then, as shown below, no problem arises. However, if the ligand $[L^-]$ under study is a weak complexer then it is

necessary to use a high concentration of Na_2L in the sample in order to produce a significant concentration of ML. The requirement of constant $[\text{Na}^+]$ means that a lower concentration of NaNO_3 swamping electrolyte is required in the sample than in the standard.

In the absence of foreign ligands and hydrolysis products the following equilibria will be considered:



$$\beta'_{\text{MNO}_3^+} = [\text{MNO}_3^+] / ([\text{M}^{++}] [\text{NO}_3^-]) \quad (2.33)$$



where $\beta'_{\text{MNO}_3^+}$ is the conditional formation constant of MNO_3^+ while $K_{\text{MNO}_3^+}$ is the distribution constant of MNO_3^+ between the resin and the aqueous phases.

The distribution ratio for the equilibria involved in the absence of complexing ligands, $D_{L=0}$, is given by

$$D_{L=0} = \frac{[\text{R}_2\text{M}] + [\text{RMNO}_3]}{[\text{M}^{++}] + [\text{MNO}_3^+]} \quad (2.35)$$

Defining $\lambda_{\text{M}^{2+}}$ and $\lambda_{\text{MNO}_3^+}$ as the distribution coefficients between the resin and the solution phases we

can write

$$\lambda_{M^{2+}} = \frac{[R_2M]}{[M^{2+}]} \quad (2.36)$$

$$\lambda_{MNO_3^+} = \frac{[RMNO_3]}{[MNO_3^+]} \quad (2.37)$$

Substituting for $[R_2M]$ from equation 2.36, for $[RMNO_3]$ from equation 2.37, and for $[MNO_3^+]$ from equation 2.33 we get:

$$D_{L=0} = \frac{\lambda_{M^{2+}} \cdot [M^{++}]_{L=0} + \lambda_{MNO_3^+} \cdot \beta'_{MNO_3^+} \cdot [M^{++}]_{L=0} [NO_3^-]}{[M^{++}]_{L=0} + \beta'_{MNO_3^+} \cdot [M^{++}]_{L=0} [NO_3^-]} \quad (2.38)$$

Under trace ion exchange conditions $MNO_3^+ \ll NO_3^-$ and, assuming complete dissociation of electrolyte, NO_3^- equals the analytical concentration of added nitrate in the system (0.1 M). Equation 2.38 can be arranged as

$$D_{L=0} = \frac{[M^{++}]_{L=0} \lambda_{M^{2+}} + \lambda_{MNO_3^+} \cdot \beta'_{MNO_3^+} (0.1)}{[M^{++}]_{L=0} + \beta'_{MNO_3^+} (0.1)} \quad (2.39)$$

In the column flow through method the resin is equilibrated with an unperturbed solution phase which consists of all metal species. Thus the denominator of equation 2.39 is simply equivalent to M_T , and

$$D_{L=0} = \frac{[M^{++}]_{L=0} \cdot \lambda_{M^{2+}} + \lambda_{MNO_3^+} \cdot \beta'_{MNO_3^+} \cdot (0.1)}{M_T} \quad (2.40)$$

In the presence of an excess of a complexing ligand, H_2L , which forms a single non sorbed species ML (see equations 2.13-2.16), an expression for the distribution ratio $D_{L \neq 0}$, can be derived in a similar way:

$$D_{L \neq 0} = \frac{[R_2M] + [RMNO_3]}{[M^{++}]_{L \neq 0} + [MNO_3^+] + [ML]} \quad (2.41)$$

$$D_{L \neq 0} = \frac{\lambda_{M^{2+}} \cdot [M^{++}]_{L \neq 0} + \lambda_{MNO_3^+} \cdot \beta'_{MNO_3^+} \cdot [M^{++}][NO_3^-]}{[M^{++}]_{L \neq 0} + \beta'_{MNO_3^+} \cdot [M^{++}]_{L \neq 0} [NO_3^-] + \beta_{ML} \cdot [M^{++}]_{L \neq 0} [L^-]} \quad (2.42)$$

$$D_{L \neq 0} = \frac{[M^{++}]_{L \neq 0} \cdot \lambda_{M^{2+}} + \lambda_{MNO_3^+} \cdot \beta'_{MNO_3^+} \cdot (0.1)}{[M^{++}]_{L \neq 0} \cdot [1 + \beta'_{MNO_3^+} \cdot (0.1) + \beta_{ML} \cdot [L^-]]} \quad (2.43)$$

At breakthrough conditions the denominator of equation 2.43 is equal to the total metal species concentration in the solution phase (M_T), thus

$$D_{L \neq 0} = \frac{[M^{++}]_{L \neq 0} \left\{ \lambda_0 + \lambda_{MNO_3^+} \cdot \beta'_{MNO_3^+} \cdot (0.1) \right\}}{M_T} \quad (2.44)$$

In equations 2.40 and 2.44, $\lambda_{M_2^+}$, $\lambda_{MNO_3^+}$, and $\beta'_{MNO_3^+}$ will be constant as long as both $[Na^+]$ and $[NO_3^-]$ are kept constant. Under this condition the ratio of the two distribution ratios $D_{L \neq 0}/D_{L=0}$ is equal to the ratio of the free metal ion concentration $[M^{++}]_{L \neq 0}/[M^{++}]_{L=0}$. Thus the method will still yield the free metal ion concentration. This conclusion is valid as long as $H_2L \ll 0.1 \text{ M}$ so that $[NO_3^-]$ is essentially constant (0.1 M).

If the ligand concentration is appreciable then in order to keep $[Na^+]$ constant, a lower concentration of electrolyte must be used in the test solution. In this case $[NO_3^-]$ will be 0.1 M in the "standard" solution but less than 0.1 M in the "sample" solution, and the distribution ratio for the "sample" solution will be expressed as:

$$D_{L \neq 0} = \frac{[M^{++}]_{L \neq 0} \lambda_0 + \lambda_{MNO_3^+} \cdot \beta'_{MNO_3^+} (0.1 - [HL^-] - 2[L^{=}])}{M_T}$$

(2.45)

In equation 2.45 the numerator changes with a change in the ligand concentration added and the ratio of the distribution ratios $D_{L \neq 0}/D_{L=0}$ is not proportional to the ratio of the free metal concentration $[M^{++}]_{L \neq 0}/[M^{++}]_{L=0}$.

CHAPTER 3

CHARACTERIZATION OF ION EXCHANGE/ATOMIC ABSORPTION SYSTEM FOR FREE-COPPER DETERMINATION

3.1 Introduction

In an ideal species sensitive technique the measurement step should be performed without perturbation of the existing equilibria in the test solution. The flow-through column method of ion exchange equilibration offers this distinct advantage since, at breakthrough condition, the resin is in equilibrium with fresh unperturbed test solution. That is, the last portion of the test solution in contact with the resin beads did not lose any of its species to the resin.

Initial work in this laboratory led to the development of a semi-automated ion exchange column equilibration system with atomic absorption detection for free-copper ion determination [74]. The system involved a miniaturized ion exchange column (2-10 mg resin weight) through which test solution is forced by a peristaltic pump. The effluent from the column is directly connected to the nebulizer of an atomic absorption spectrophotometer. The system is thus made not only rapid

and simple, but also contamination-free. This is a very important advantage especially when dealing with sub part per billion levels of free metal ions.

In this chapter the effect of various instrumental and test solution variables are thoroughly studied.

3.2 Experimental

3.2.1 Chemicals and Resins

Copper foil was ACS reagent grade supplied by Matheson, Coleman and Bell, Richmond, N.J.

Nickel certified atomic absorption standard solution, 1000 $\mu\text{g/mL}$ (Fisher Scientific Co.) was used in some tests.

Sodium nitrate, NaNO_3 (Fisher Scientific Co. or British Drug Houses), sodium perchlorate, NaClO_4 (G. Frederick Smith Chemical Co.) were used as received. Reagent grade nitric acid, HNO_3 , hydrochloric acid, HCl , sulfuric acid, H_2SO_4 (Fisher Scientific Co.), and sodium hydroxide, NaOH (J.T. Baker Chemical Co.) were also used.

2,6-Dimethylpyridine (2,6-Lutidine) supplied by Terochem Laboratories Inc. was distilled at atmospheric pressure and the middle fraction was collected (boiling range 132-136°C).

Benzyl alcohol, reagent grade (McArthur Chemical Co. Ltd. Montreal), and p-toluene sulfonic acid, practical

grade (Anachemia, Montreal) were also used.

Analytical grade 100-200 mesh Dowex 50W-X8 strong acid type cation exchange resin was supplied by J.T. Baker Chemical Co. in the hydrogen form. The ion exchange capacity is 5.1 milliequivalents per gram on a dry basis.

Analytical grade Chelex 100, (100-200 mesh, sodium form) chelating ion exchange resin was used as supplied (BioRad Laboratories). Nominal total ion exchange capacity is 2.9 milliequivalents per gram of dry resin.

Amberlite XAD-4 non ionic polymeric adsorbent, 20-50 mesh size, and Amberlyst 15 sulfonated ion exchange resin, -325 mesh (Rohm and Haas Co., Philadelphia PA) were both used as well.

3.2.2 Reagents and Solvents

Water was distilled and passed through a mixed bed ion exchange resin column (Amberlite MB-1, analytical reagent, Rohm and Haas Co., Philadelphia, PA).

Stock copper solution (0.100 M) was prepared by dissolving pure copper foil in nitric acid (1% v/v).

Sodium nitrate stock solution (0.500 M) was prepared by dissolving 84.99 g of the salt in 2 L of solution. The solution was then passed through a column of Chelex 100 ion exchange resin which had first been treated with HNO_3 , H_2O and several bed volumes of 0.5 M NaNO_3 solution.

2,6-Lutidine stock solution (0.05 M) was prepared by dissolving the neat liquid (5.358 g) in water and diluting to 1 L.

Nitric acid eluent solution (2 M), was prepared by diluting 128 mL of the concentrated acid (70%) to 1 L.

Analytical reagent grade acetone, methanol, and benzene (British Drug Houses) were used as received.

3.2.3 Apparatus

The instrumental setup used is shown schematically in Figure 18. The variable speed peristaltic pump (Minipuls 2, Gilson, Villiers-le-Bel, France) was fitted with three 0.09 inch i.d. clear standard (PVC) tubes (Technicon Corp.). One tube pumped the test solution. The second pumped either water or eluent, depending on the position of the rotary valve V_1 (Model R6031V6, Laboratory Data Control, Riviera Beach, FL). The third line maintained a continuous supply of water to the nebulizer of the atomic absorption spectrophotometer (AAS). Flow rates were measured with a buret and stopwatch by diverting the flow through the three-way Teflon slider valve V_5 (CAV3031, Laboratory Data Control). The two coupled four-way Teflon slider valves V_2 and V_3 (CAV4031, Laboratory Data Control) are used to direct the flow of either the sample line or the wash-eluent line through the column while diverting

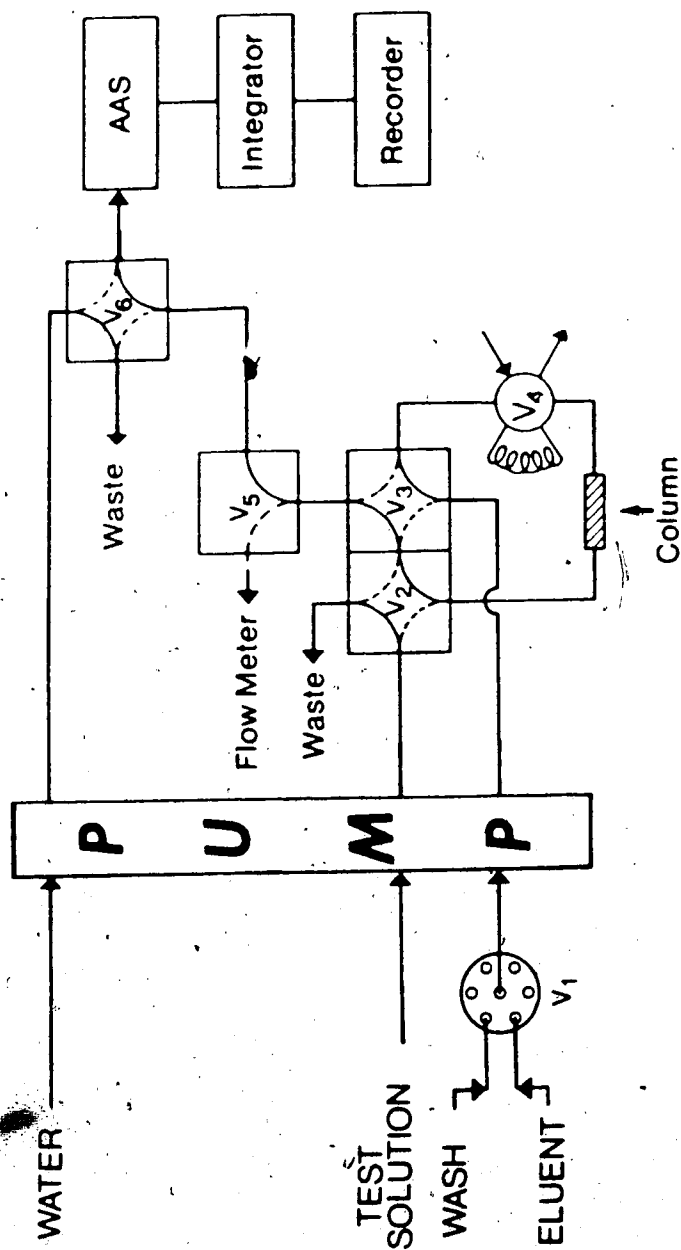


Figure 18. Diagram of the flow-through column ion exchange equilibration for free-copper determination. V_1 is a six-way rotary valve used to choose between wash and eluent. V_2 , V_3 and V_6 are four-way slider valves, V_4 is a standard solution rotary injection valve, and V_5 is a three-way slider valve.

the other to waste. The sample injection valve V_4 (Altex Model 202-00, Altex Inc., Berkeley, CA) is used to inject a standard metal solution to check for flow rate or other instrumental variation. The four-way valve V_6 is similar to V_2 and V_3 and used here to choose the feed line to the AAS. Details of column design and construction are given in Section 3.3.4. Metal concentration was monitored with a flame atomic absorption spectrophotometer (AAS) Model 4000 (Perkin-Elmer Corp.) equipped with a separate burner control unit and Westinghouse copper and nickel hollow cathode lamps (Westinghouse Canada Ltd., Burlington, Ontario). A printer Model PRS 10 (Perkin-Elmer Corp.) was used to provide a printout of the desired signal while a stripchart recorder Model 7101BM (Hewlett-Packard Corp.) was also used to trace the analog signal. The AAS was directly coupled to the flow system by means of a narrow (0.3-mm i.d.) Teflon tube connecting V_6 to the nebulizer tube. A Haake circulating thermostat Model R20 was used to provide a constant temperature of $25^\circ \pm 0.5^\circ \text{C}$ for both the test solution and water jacket surrounding the resin column. Where possible the test solution delivery line was insulated with glass wool. pH measurements were made with a Fisher Accumet Model 320 Expanded Scale Research pH meter using a combination electrode (Model 13-639-90, Fisher Scientific Co.) calibrated with a set of certified

buffer solutions (Fisher Scientific Co.).

A Hewlett Packard Model HP 8451A diode array spectrophotometer and a HP 7470A plotter (Hewlett Packard Corp.) were also used.

3.2.4 Cleaning of Equipment

All laboratory equipment used for solution handling was first cleaned by washing with liquid detergent solution and then thoroughly rinsing with tap water. It was then soaked overnight in 30% (v/v) HNO_3 and rinsed thoroughly with distilled-deionized water. The flow system and resin column were cleaned by pumping nitric acid solution (2 M) through all lines for 15 min followed by thorough rinsing by pumping distilled water. The procedure was repeated whenever contamination of the water reservoirs was suspected. The Chelex 100 ion exchange column was regenerated and reconditioned prior to its use on each new 2-L batch of sodium nitrate stock solution. Attempted relaxation of the washing procedures resulted in higher blank signals and spurious results.

3.2.5 Resin Preparation

A suitable weight of the coarse (>325 mesh) resin was ground in a clean, dry agate mortar and pestle until most of the material passed a 325 mesh sieve. Next, the fines were removed by repeated suspension and decantation in

three bed volumes of solution until the supernatant solution was clear in less than 20 min. The resin was then placed in a borosilicate glass column and washed with 4 M HCl until the effluent was colorless (~100 mL). Then it was converted to the sodium form by washing with 2 M NaOH to constant pH of both the effluent and the influent solutions. This was followed by a water wash to constant pH. Finally the resin was washed with 200 mL of methanol, followed by a water wash and then dried in a convection oven at 45°C for 48 h. The dry resin was stored in a tightly closed glass bottle.

3.2.6 Sulfonation of XAD-4 Resin

A 10-gram sample of XAD-4 non-ionic resin (20-50 mesh) was wetted with 15 mL of absolute methanol. Then 100 mL of water was added. The mixture was stirred at room temperature for 60 min after which most of the liquid was decanted (~4 mL of liquid left).

The resin was then added in portions to 500 mL of 94-95% H_2SO_4 , chilled in an ice bath to 5°C, and stirred magnetically. The portions of resin turned light red, purple, and finally to a purple-black color. When magnetic stirring was stopped and the resin beads floated. The temperature of the acid was then raised to 35°C and the mixture was stirred vigorously for 7 h.

After cooling the mixture to room temperature the beads were scooped off the surface and thrown into a stirred ice-water mixture (~1.5 L). Due to the heat of dilution the final temperature rose to 60°C and the black beads turned to brick red color. The resin was then filtered on a 10 to 20 μ m sintered glass disc using air suction and washed with water until the filtrate was neutral. The beads on the funnel were next washed with 1:1 HCl until the effluent was colorless in order to get rid of any iron. They were washed to neutrality with water which yielded light orange beads. Finally, the beads were washed with methanol (~300 mL) and air-dried to yield a light beige colored product. The sulfonated resin was stored in a glass bottle.

3.2.7 Esterification of Amberlyst 15 Resin

This procedure was adapted from that of Zervas et al. [208] for the selective esterification of the carboxyl group. In a 1-L three-necked round-bottom flask, 1 g of Amberlyst 15 (-325 mesh) resin, 100 mL of benzene, 50 mL of benzyl alcohol and 48.5 g of p-toluenesulfonic acid were introduced. When the brown colored mixture was refluxed (78°C) in a Dean-Stark azeotropic distillation apparatus it turned black. The solution was refluxed for 10 or 80 hours as water collected in the side-arm the

boiling point of the mixture increased from 78° to 110°C. During that period ~15 mL of water was collected. The system was then cooled to room temperature and a lump of tarry product solidified in the bottom. Ten mL of benzene was added and the resulting mixture was filtered through a 10 μ m sintered glass Buchner funnel, washed several times with 30-mL portions of benzene, acetone, methanol, 2 M HNO₃, water, acetone, and methanol respectively.

The grey-black powdery product was dried at 70°C for several hours. The product was de-fined as described in Section 3.2.5, dried and stored.

3.2.8 Column Construction

The column design was patterned after that reported in the literature [74]. A 50-mm long Teflon tube (1.5 mm i.d.) was flared at both ends (Figure 19). This length of tubing is necessary to accommodate the two end fittings, A (Cheminert, Laboratory Data Control, Riviera Beach, FL). Approximately 2-mm long cylindrical glass frits (~1.5 mm diameter) were made by drilling cores from a sintered glass plate (nominal pore size 50 μ m). A snug fitting frit was gently pressed into the 50-mm Teflon tube and placed close to the centre (~20 mm from one end). From the other end the desired weight of the dry (~325 mesh, de-fined) resin, B, was introduced using a fine spatula.

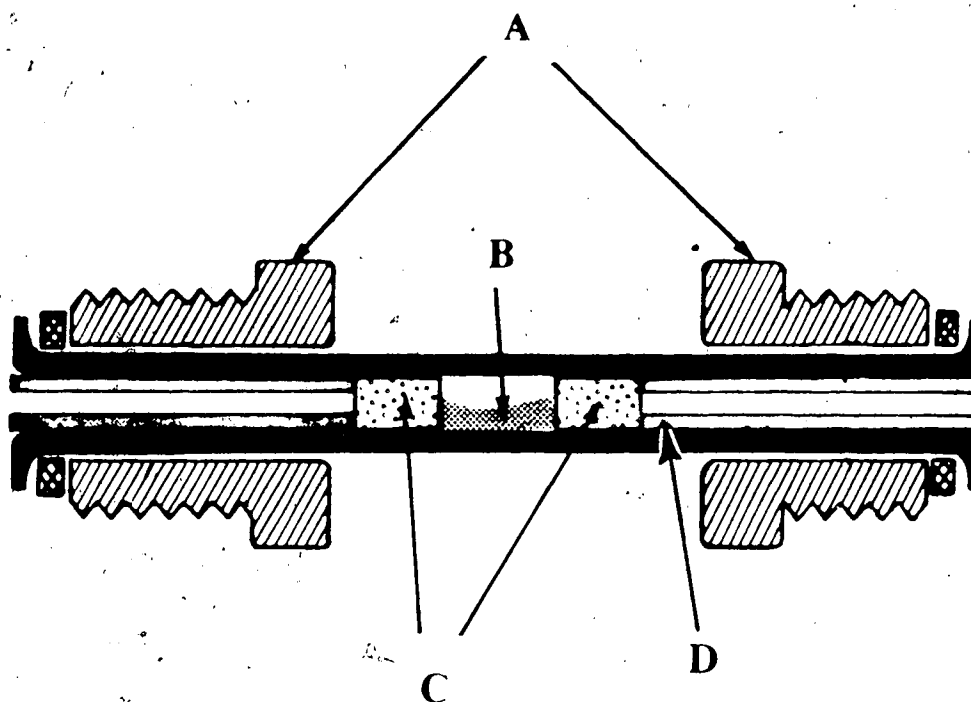


Figure 19. Details of column construction; A are two connectors (including two stainless steel washers). The resin particles, B, are sandwiched very loosely between two porous silica frits, C, in a narrow 1.5-mm i.d. Teflon tube (shown in black). The two Teflon tubes, D, are inserted from both ends to reduce the dead volume of the column.

The end of the tube was tapped lightly to collect most of the resin particles in the centre of the tube. This was followed by pushing another tightly fitting frit into the tube so that all the resin particles were sandwiched very loosely between the two frits, C, leaving extra space about equal to the volume of the resin to allow for swelling of the resin. This minimized flow rate variations. Finally a tightly fitting Teflon tube, D, (0.063 inch o.d., 0.02 inch i.d.) was introduced into each end of the column to reduce the dead volume.

3.2.9 Instrumental Conditions

The peristaltic pump setting was maintained at 666 throughout. Flow rates in all three lines varied between 5 to 6 mL/min depending on solution viscosity and the degree of resin compression in the column. Resin compression varies with resin bed length and pumping time. The atomic absorption spectrophotometer conditions used for monitoring copper and nickel signals are tabulated in Table 4.

3.2.10 Test Solution Preparation

The test solution was generally prepared by dispensing 50.0 mL of sodium nitrate stock solution (0.5 M) and 5 mL of 2,6-Lutidine stock solution (0.05 M) into a 400-mL beaker. About 100 mL of water was added and the pH

Table 4. Instrumental parameters of the atomic absorption spectrophotometric determination of copper.^a

Lamp current, mA	10
Wavelength, nm	324.7
Spectral slit width, Å	7 (high)
Aspiration rate, mL/min	6.3
Mode	Absorbance
Signal	Peak height and Peak area
Integration time, s	50
Acetylene pressure, psig	12
Air pressure, psig	23

a. For the determination of nickel lamp current was 15 mA and the wavelength was 232.0 nm.

was adjusted to the desired value with dilute HNO_3 . Then the appropriate volume of daily-prepared dilute copper (or nickel) solution was added slowly to the magnetically stirred mixture. A final adjustment of pH was necessary in some cases. The beaker contents were then quantitatively transferred to a clean 250-mL volumetric flask, diluted to volume with water, and shaken well. The pH of the test solution was then rechecked and readjusted if necessary using very small volumes of HNO_3 or NaOH solution so as to cause negligible further dilution of the metal ion.

3.2.11 Free Metal Determination

The test solution was first pumped through the column via V_2 and V_3 with V_1 in the wash position (dotted lines in Figure 18). The resin equilibration step required 15 minutes for complete breakthrough. Normally the column effluent was diverted to the flowmeter by valve V_5 during the equilibration cycle to prevent fouling of the nebulizer and burner slit by the high salt concentration. During this cycle the nebulizer was supplied with water from the H_2O line via V_6 .

After the equilibration cycle was completed V_2 and V_3 were switched to the other positions (solid lines in Figure 18) and the column was backwashed with water for 1

minute to remove interstitial test solution. Next, V_5 and V_6 were switched to divert the flow to the atomic absorption spectrophotometer and the water washing was continued for three more minutes to remove the remainder of interstitial test solution. During the water washing the baseline of the AAS was set to zero. The AAS was also set to measure the area of the oncoming signal by setting the integration time (50 seconds). V_1 was then switched to the eluent position (2 M HNO_3) to start the elution cycle. Integration was triggered 15 seconds after switching to the elution cycle. After the peak had eluted and the eluent baseline was re-established V_1 was switched back to the wash position until the wash baseline was re-established. Valves V_6 , V_5 , V_3 , and V_2 were then switched back to their initial position for the next test solution.

To save on acetylene consumption during the equilibration cycle it was found sufficient to turn on the AAS burner five minutes before the elution step. The blank was run in exactly the same manner.

3.3 Results and Discussion

3.3.1 Choice of Eluent

It is desirable to employ a strong eluent in the system in order to obtain sharp peaks and a better

detection limit. This depends primarily on the type as well as on the concentration of the eluent. In an earlier report [74] ethylene diaminetetraacetate was used as eluent for Cu^{2+} because of the high formation constant with the analyte. Since a noble metal capillary nebulizer became available on the PE4000 spectrophotometer it is possible to use routinely a strong acid eluent. Several concentrations of nitric acid were investigated as potential eluents. It was observed that the higher the acid concentration the sharper and narrower the eluted peaks. 2 M and 4 M HNO_3 gave almost identical peak widths. However, 4 M HNO_3 caused cloudiness of the pump tubing in a short time. It was decided to use 2 M HNO_3 eluent because pump tube cloudiness was less severe, yet the elution times were short. Generally pump tubes were replaced every 2 to 3 months depending on the frequency of usage.

3.3.2 Buffering of the Test Solutions

Although the flow-through column method does not require the test solution to be buffered it is desirable to maintain a constant pH of the test solution for characterization purposes, especially when the pH itself is a variable. In general, buffers should have several important properties. These include an appropriate pH,

adequate buffering capacity, and solubility in the medium of interest [209-210]. For metal ion speciation studies another characteristic of the buffer is important; it should not complex the metal ion of interest since this will affect the species distribution in the system. No buffer is known to have this characteristic but there are some buffers developed which have low formation constants with metal ions [211,212]. 2,6-Dimethylpyridine (2,6-Lutidine) has often been used as a buffer in the pH range 6.5 to 8 ($pK_a = 6.96$). The steric hindrance of the two methyl group substituents neighboring the nitrogen donor atom makes it a poor ligand. The formation constant of 2,6-lutidine with Cu^{2+} is not available in the literature. However, for substituted lutidines it is relatively low: β_1 is 1.3 for 3-nitro-2,6-dimethylpyridine; 1.4 for 3-nitro-2,4,6-trimethylpyridine, and 1.6 for 3-sulfonato-2,6-dimethylpyridine. Also the formation constant for 2,6-dimethylpyridine (2,6-lutidine) with nickel(II) is 1.6 [211].

Since it is desirable to keep the added buffer concentration low, an experiment was done to determine the concentration of 2,6-lutidine needed for adequate buffering action. It was found that as low as 4×10^{-4} M of 2,6-lutidine in the test solution was sufficient to maintain a constant pH of 6.0 ± 0.05 for more than 8 h in

a solution exposed to air. At pH 8 the same buffer concentration was inadequate; the pH gradually dropped to 7.8 over the same period, presumably due to uptake of CO_2 . The test solutions used in these experiments contained 0.1 M NaNO_3 and $2 \times 10^{-6} \text{ M}$ copper.

An attempt was made to investigate copper complexation with 2,6-lutidine by UV-Vis molecular absorption spectrophotometry (Section 3.2.3). Figure 20A shows the absorption spectrum of lutidine solution ($2 \times 10^{-2} \text{ M}$) at pH 6. Figure 20B shows three spectra; (1) is the absorption spectrum for a solution containing $10^{-3} \text{ M Cu(NO}_3)_2$ and $2 \times 10^{-2} \text{ M}$ lutidine adjusted to pH 6 with nitric acid. (2) is the absorption spectrum for the above solution except for the absence of lutidine. Spectrum (3) is obtained by mathematical subtraction of (2) from (1). The intense absorption of 2,6-lutidine and nitrate group below 340 nm made the task of monitoring the ligand concentration an impossible one. Spectrum 20B(2) shows that there is no wavelength shift in the copper absorption spectrum upon addition of 2,6-lutidine. Bjerrum [213] showed that the addition of pyridine to a copper nitrate solution (10^{-2} M) resulted in a blue shift and a three-fold increase in absorbance for a 1:1 complex. Spectrum (3) clearly shows that there is no increase in absorbance on addition of lutidine. The slight vertical shift of (1)

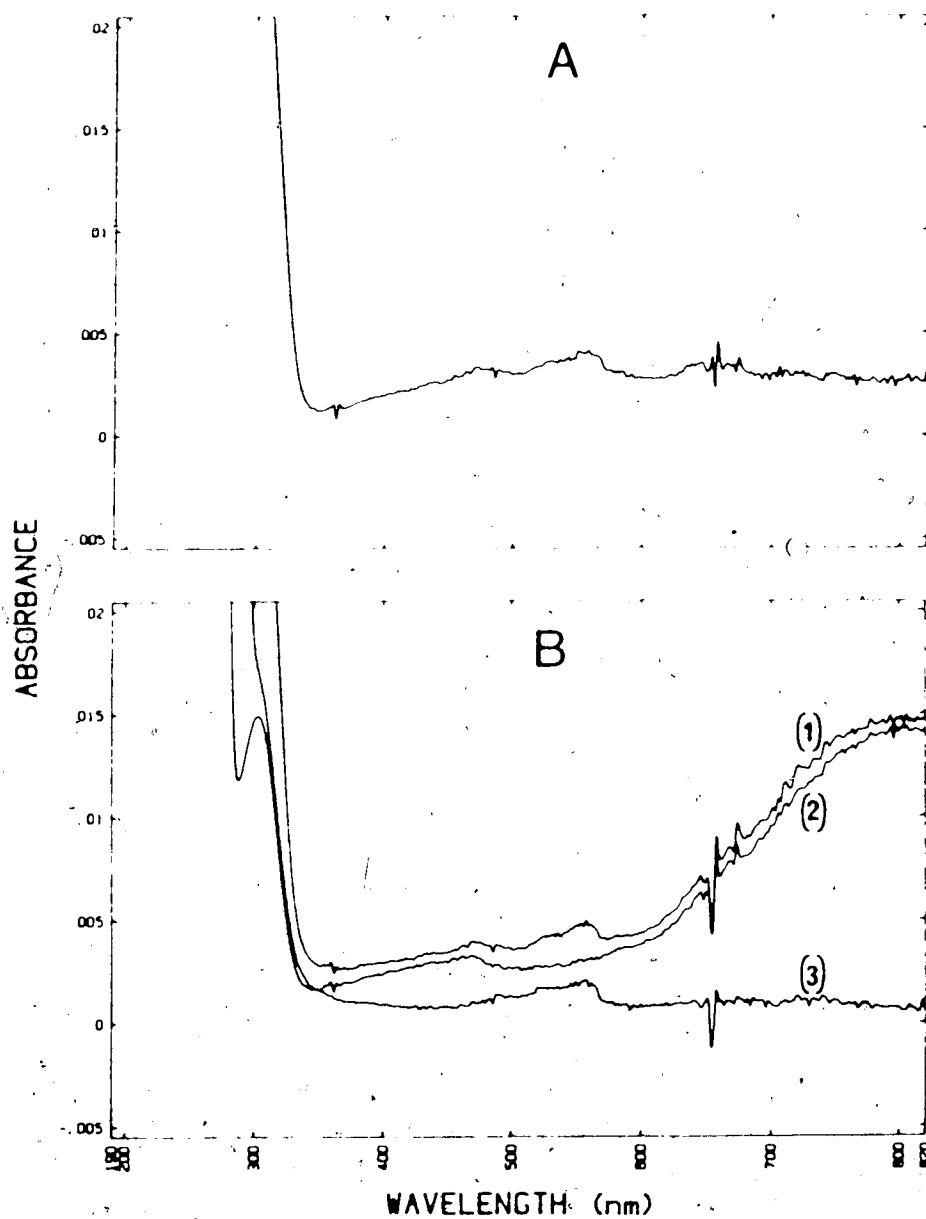


Figure 20. (A) absorption spectrum for 2,6-lutidine ($2 \times 10^{-2} \text{ M}$), (B) spectra for 10^{-3} M $\text{Cu}(\text{NO}_3)_2$ solution (2), and 10^{-3} M $\text{Cu}(\text{NO}_3)_2$ plus $2 \times 10^{-2} \text{ M}$ lutidine at pH 6 (1). Spectrum (3) is the net subtraction of (2) from (1).

and (2) on the absorbance scale (0.0007 absorbance units) is constant over the copper ion absorption region and is probably due to mismatching of blanks or cells, or to light scattering. A slight turbidity was observed in the copper solution containing lutidine. Higher concentrations of copper could not be used because addition of lutidine (pH 6) causes hydrolysis and precipitation of blue copper hydroxide. The above experimental results adds more evidence for the poor ligand characteristics of 2,6-lutidine.

In the ion exchange column equilibration method of free-copper determination the concentration of lutidine buffer employed in the test solutions is twenty times less than that used in the above experiment (Section 3.2.10). Assuming a β value of 2.0 for the copper-2,6-lutidine complex it was calculated that the millimolar concentration of 2,6-lutidine used would only complex 0.02% of the total copper in the test solution. Consequently 2,6-lutidine complexation with copper was neglected.

3.3.3 Effect of Copper Concentration on Column-Test

Solution Equilibration Times at pH < 6

As indicated in Chapter 2 it is necessary to pump the test solution through the resin column until complete breakthrough is attained. In this section the effect of

change in copper concentration on the equilibration time to achieve complete breakthrough is examined. Using a 2-mg resin column three test solutions of fixed pH (6.0), ionic strength (0.1 M), and lutidine buffer concentration (4×10^{-4} M) were prepared. The copper concentrations used were 2×10^{-6} M, 1×10^{-6} M and 2×10^{-7} M. The test solutions were loaded for different periods of time. Figure 21 shows the results obtained for the three test solutions. Breakthrough is achieved when the column is fully equilibrated and the copper content of the resin does not increase with time. The breakthrough regions are therefore seen as plateaus in Figure 21. There is little difference in equilibration times for the different copper concentrations. In subsequent experiments a 15-minute equilibration time was adopted. Equilibration curves obtained at pH values lower than 6 are essentially similar to those at pH 6.

3.3.4 Effect of pH on Column-Test Solution Equilibration Times

To investigate the effect of test solution pH on equilibration time three test solutions of the same copper concentration (1×10^{-6} M), ionic strength (0.1 M), and lutidine concentration (10^{-3} M) were prepared. The pH values of the solutions were 6.0, 7.0, and 8.0. A 2-mg

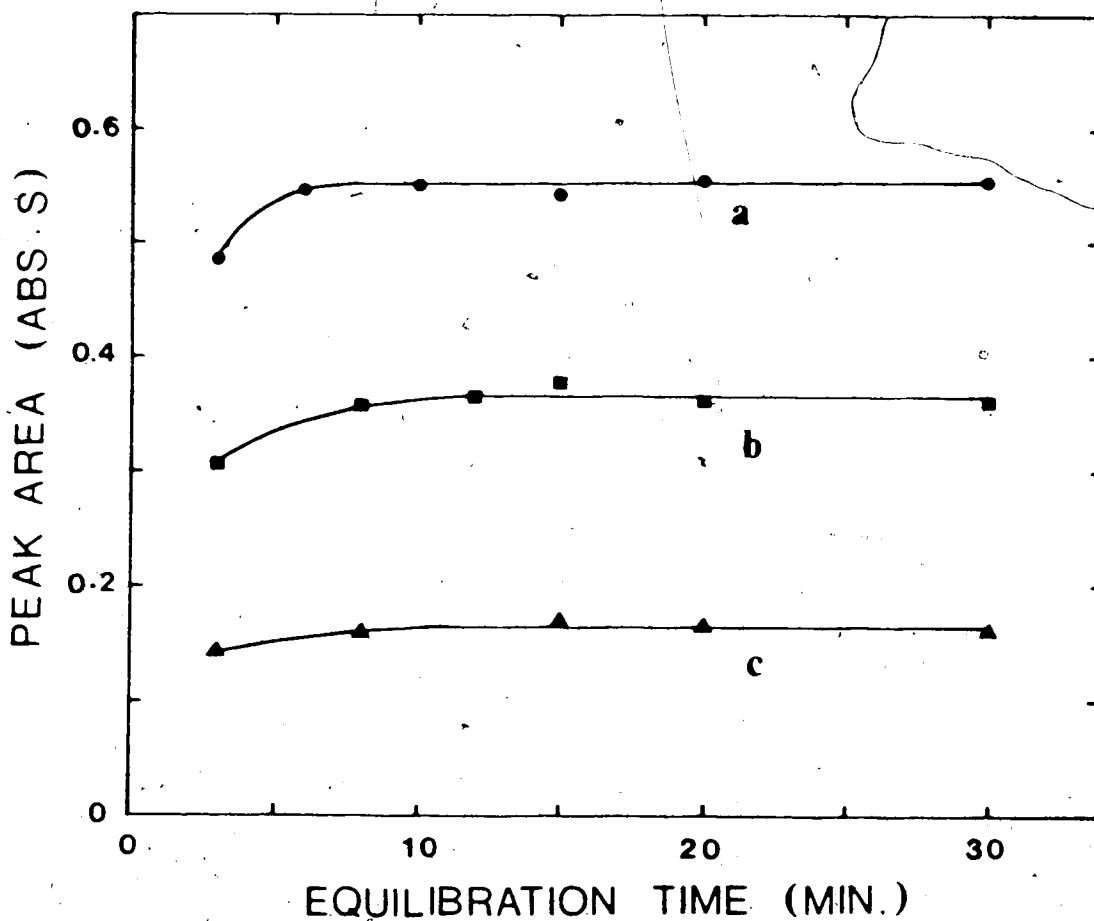


Figure 21. Effect of copper concentration on equilibration time for a 2-mg resin column at pH 6. Total copper concentration 2×10^{-6} M (a), 1×10^{-6} M (b), and 2×10^{-7} M (c).

resin column was equilibrated with each test solution for various periods of time at a fixed flow rate of about 5.5 mL/min and the corresponding peak area upon elution of sorbed copper was recorded. Figure 22 shows a graphical representation of the results obtained.

At pH 6, as reported in Section 3.3.3, a complete breakthrough of copper was reached in less than 15 min. For the test solutions at pH 7 and pH 8 breakthrough was not attained even after 30 minutes of flow through the resin column. Furthermore the peak areas obtained for these test solutions tend to increase with pH. This is contrary to the expected trend; as the pH is increased copper hydroxy species are formed and the fraction of free copper is decreased. Species distributions for two different total concentrations of copper in 0.1 M NaNO_3 solution are shown in Figure 23 (refer to Section 4.2.4 for method of calculation). If complexation of copper with 2,6-lutidine and nitrate is ignored it can be seen from Figure 23 that the free-copper fraction is 96% at pH 6, 65 to 70% at pH 7, and only 12 to 16% at pH 8.

There are two possible explanations for the results in Figure 23:

- (a) The resin has additional, weak-acid functional groups [187,214,215] which are protonated at low pH but free at higher pH. These groups increase the ion exchange

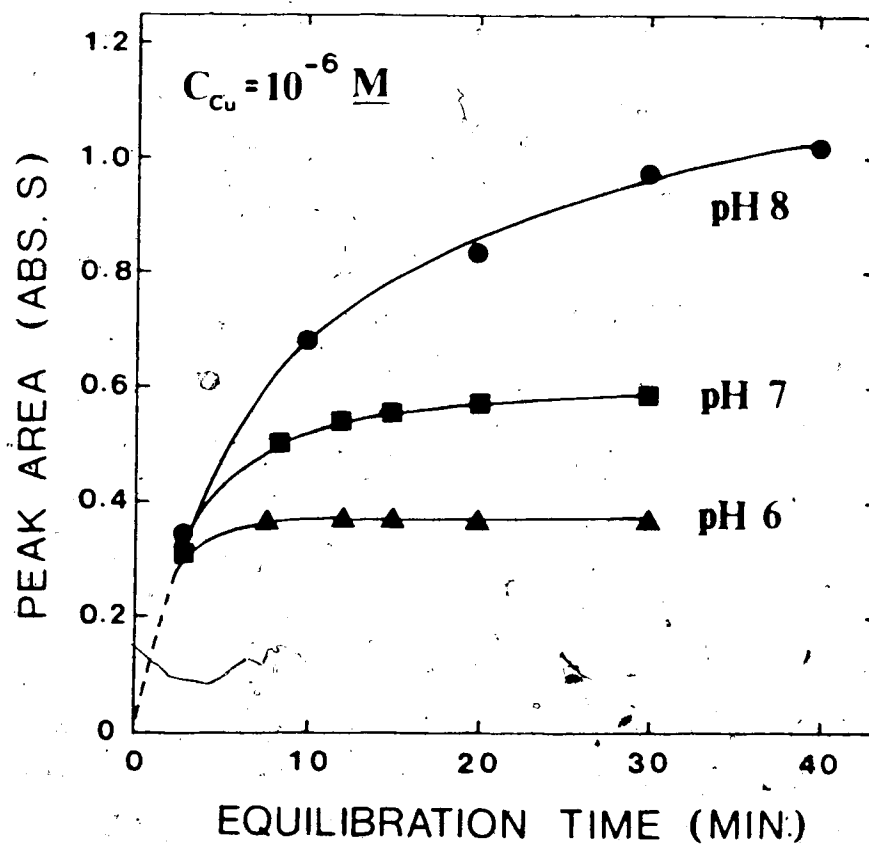


Figure 22. Effect of pH of test solution on column equilibration time. Total copper concentration is constant (10^{-6} M).

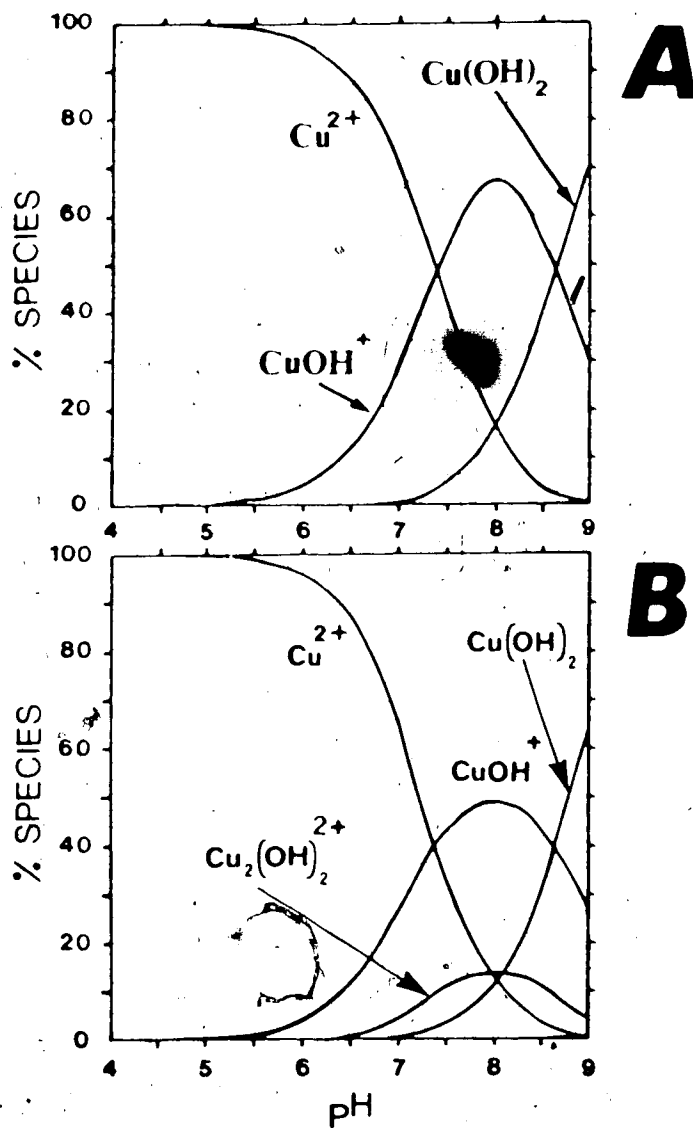


Figure 23. Calculated copper species distributions as a function of pH in 0.1 M NaNO_3 solution. Total copper concentration 10^{-7} M (A), 10^{-4} (B).

capacity and perhaps the resin selectivity for Cu^{2+} .

(b) Colloidal particulates of copper hydroxide are

trapped in the resin phase and are not washed off.

The presence of weak acid (probably carboxylic) groups in addition to strong acid sulfonic groups is believed to result from oxidation of the chain ends of the polymer [187]. This is likely in light of the strong oxidizing conditions used in the sulfonation process [214]. However sulfonated resins prepared by us under milder conditions (Section 3.2.6) behaved in the same way as commercially available ones. Furthermore, derivatization of the suspected carboxylate groups of commercially available resin (Section 3.2.7) did not change the copper-ion exchange characteristics. Thus, it seemed more likely that the effects seen in Figure 22 arise from the presence of a filterable solid phase.

3.3.5 Testing for Presence of Copper-Containing Colloids

To investigate the possibility of colloidal copper particulate formation in the test solution, which might be trapped on the resin column and eluted as free copper, two test solutions of identical composition were prepared.

For both, the copper concentration was 2×10^{-6} M, the pH was 7.8 and the lutidine concentration was 10^{-3} M. One test solution was filtered through a 0.45- μm pore size

Nylon 66 filter (Rainin Instruments Co. Inc., Woburn, MA). Filtration did not affect the pH of the test solution. Using a 2-mg resin column, equilibration curves were obtained for both filtered and unfiltered solutions under identical conditions. A slightly lower final pumping rate of the unfiltered test solution was observed, especially at long equilibration times (4.9 mL/min instead of 5.7 mL/min). The equilibration curves obtained are depicted in Figure 24. It is evident that in the filtered test solution particulate copper was almost completely eliminated. The striking difference in the shape of the two curves clearly indicates the uptake of particulate copper by the column, and the continuously rising copper signal with time for the unfiltered test solution indicates the collection of this colloidal copper form. In the copper determination step, following a given loading time increasing the column washing cycle from 4 to 15 min did not wash off the trapped copper colloids in the unfiltered test solution and essentially the same peak area is observed.

The copper residue on the filter was leached with 2 M HNO_3 solution and quantified by directly aspirating the solution into the atomic absorption spectrophotometer. 10.25% of the total copper in the 1000 mL of test solution passed through the filter was filtered out.

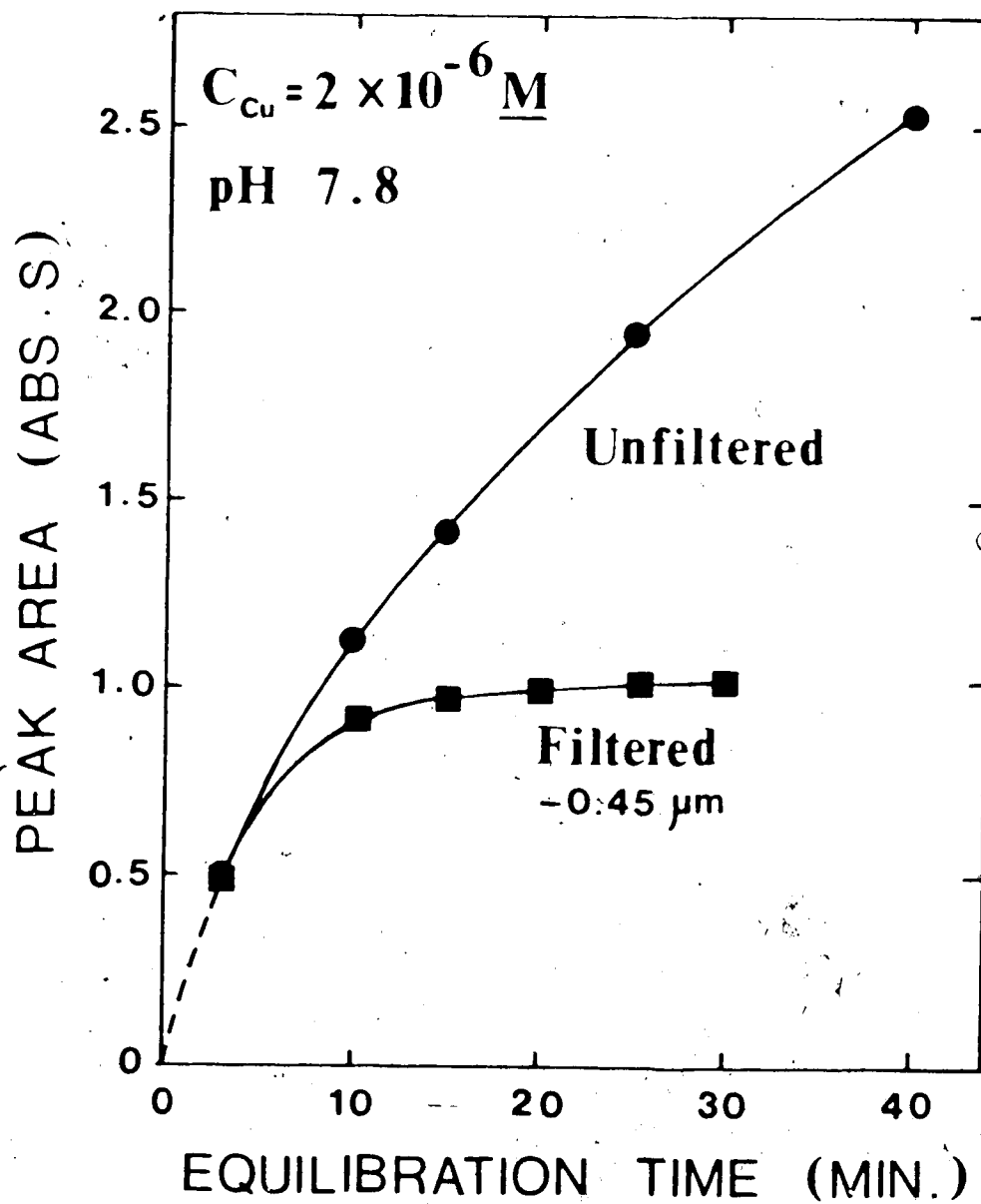


Figure 24. Effect of filtration of the test solution on the shape of the equilibration curve. Total copper concentration was $2 \times 10^{-6} M$ and the pH was 7.8.

There was evidence that a colloidal copper precipitate also forms at pH 7. However at pH 6 there was no evidence for the presence of such a precipitate; the equilibration curves for the filtered and unfiltered solutions were identical. It should be stated here that not all colloidal copper is expected to be trapped by a 0.45- μ m filter.

Paulson et al. [171], studying the hydrolysis of copper in sodium perchlorate solutions (0.05 M or 0.7 M), reported a procedure for preparation of an essentially precipitate-free copper solution (up to 4×10^{-6} M) in the pH range of 6.8-8.4. The procedure involved ultra violet light irradiation to destroy organic matter and purified nitrogen purging to eliminate dissolved carbon dioxide. They reported 1% residual copper on a 0.1- μ m Nucleopore filter. Recently Gulens et al. [170] reported the presence of copper-hydroxy colloids both in the presence and absence of atmospheric carbon dioxide. Their observations were confirmed by light scattering measurements, even for a 10^{-6} M copper solution at pH 8.5. Also Buffle et al. [129,131] studied the complexation of copper with humic and fulvic acid substances and concluded that, contrary to earlier reports, slow hydrolysis of copper probably plays a role at pH values > 6 .

The solubility of colloidal copper is affected by several physical and chemical parameters including surface area, ionic strength, pH, copper concentration and the presence of complexing agents [129,170,171,216,217]. It is expected that in more dilute solutions less colloidal copper precipitate will be formed. Using a 2-mg resin column equilibration curves for four test solutions at pH 8 were obtained. The total copper concentrations of the test solutions were 2×10^{-6} M, 1×10^{-6} M, 4×10^{-7} M, and 2×10^{-7} M. The curves obtained are shown in Figure 25. A plateau was obtained for the solution with a total copper concentration of 2×10^{-7} M, but not for the higher concentrations. Comparison of the loading curves for 2×10^{-7} M copper in Figures 25d and 21c reveals that the plateau peak area at pH 8 is higher than that at pH 6. This may be due to the presence of multiply charged soluble polymeric copper-hydroxo species at the higher pH. Thus it seems that at pH 8 filterable colloidal copper hydroxides form at concentrations higher than 2×10^{-7} M, but that copper-hydroxo species formed at lower copper concentrations are soluble. It should therefore be possible to use the ion exchange method at pH 8 or less given that the total copper concentration does not exceed 2×10^{-7} M.

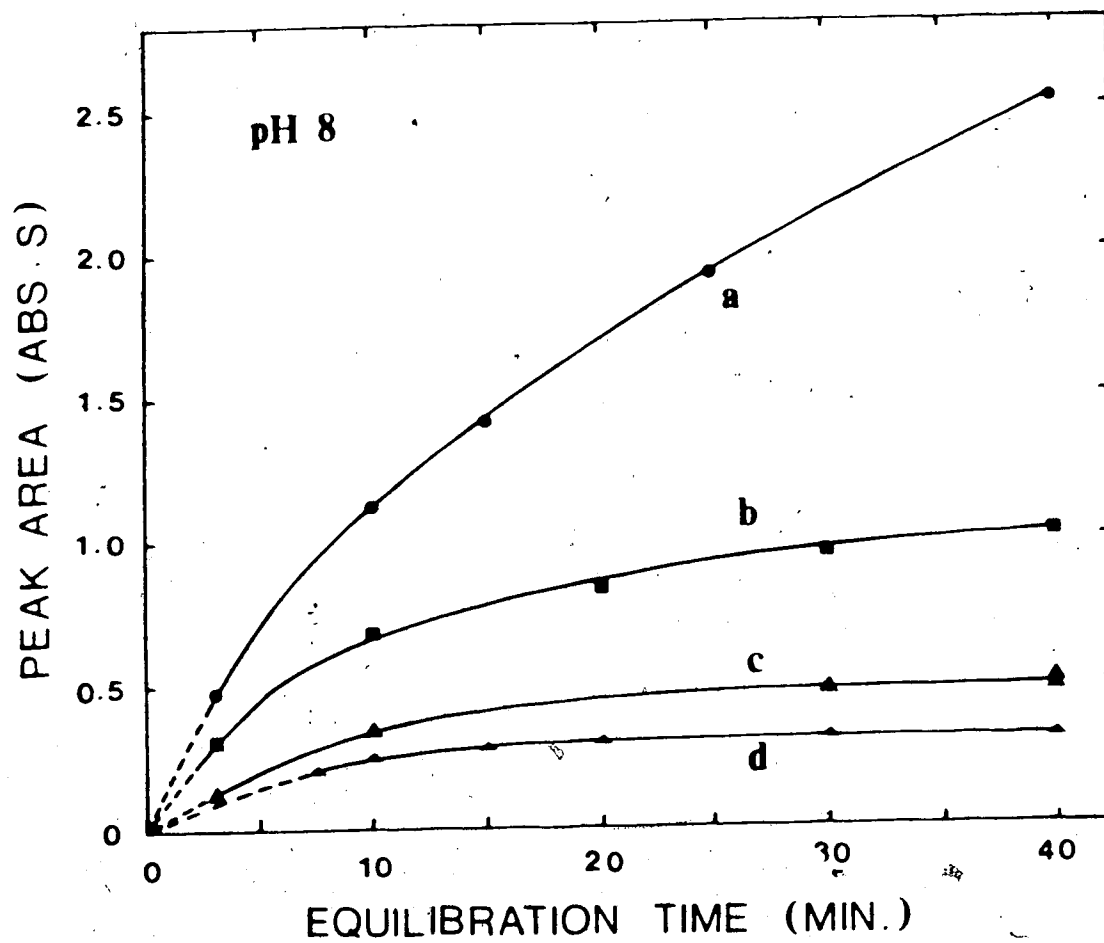


Figure 25. Equilibration curves for various total copper concentrations: $2 \times 10^{-6} \text{ M}$ (a), $1 \times 10^{-6} \text{ M}$ (b), $4 \times 10^{-7} \text{ M}$ (c), $2 \times 10^{-7} \text{ M}$ (d), at constant pH.

3.3.6 Effect of Aging of Test Solutions

Further evidence for the formation of particulate copper in the test solution came from aging studies described below. Six 1-L volume test solutions having a fixed total copper concentration of 2×10^{-6} M but different pH values (4.0 to 9.0) were prepared in polyethylene bottles according to Section 3.2.10. These test solutions were analyzed for free copper immediately after preparation, and again after aging for different periods. The equilibration time employed for the analyses in these experiments was 15 minutes. At the same time the undisturbed bulk test solutions were analyzed for total copper by direct aspiration using the same instrumental settings (Table 4). Figure 26 depicts the results obtained for the ion exchange method of analysis for free copper. From Figure 26 it is evident that:

- (a) As the pH is increased the copper signal is increased.
- (b) For test solutions with pH < 6.5 there is no change in the copper signal with aging.
- (c) For test solutions with pH values above 6.5 there is a decrease in copper signal with aging. The decrease in signal is larger for higher pH values. This clearly indicates that copper is lost from the test solutions at high pH values. This conclusion is

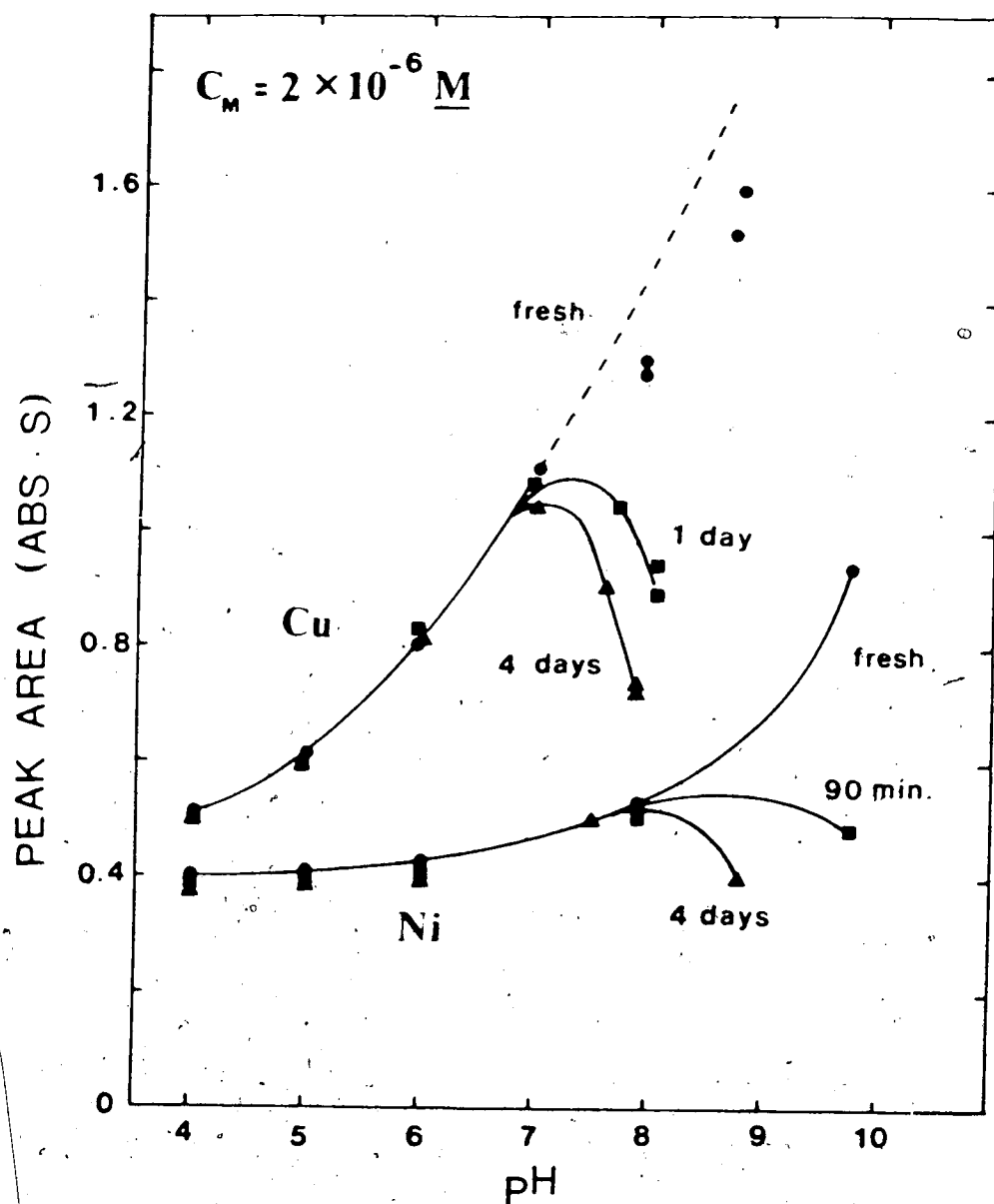


Figure 26. Effect of aging of test solution on the relation between metal uptake and pH for copper and nickel. Total metal concentration $2.00 \times 10^{-6} \text{ M}$ for copper and $2.04 \times 10^{-6} \text{ M}$ for nickel.

confirmed by the results of direct aspiration determination of copper in the still solution.

A similar aging study was performed for nickel under the same flow conditions. The instrumental conditions are listed in Table 4, and the results are plotted in Figure 26. The same behavior was observed for nickel as for copper except for a shift of the ascending curves to higher pH. This agrees with the fact that nickel undergoes less hydrolysis than copper.

The gradual decrease in pH of the aged solution (Table 5) indicates that copper hydrolysis is kinetically slow. The complications arising from copper hydroxy colloids at pH values > 6.5 must be overcome before the method can be applied for free-copper determination at higher pH values. Further work is required in this area.

3.3.7 Assessment of a Larger Ion Exchange Resin Column to Increase Sensitivity

For the ion exchange method to be applicable to natural water samples it must be sensitive enough to determine free-copper concentrations on the order of 10^{-7} to 10^{-8} [218]. The ion exchange method can be made more sensitive by employing a larger resin column, thus sorbing more copper at equilibrium. However this will require longer equilibration times. For a 10-mg resin column the

Table 5. The effect of test solution aging on pH for metals in 0.1 M NaNO_3 and 10^{-3} M lutidine. Total metal concentrations were 2.00×10^{-6} M and 2.04×10^{-6} M for copper and nickel respectively.

Aging Time (h)	Copper	Nickel
0.0	9.05	9.75
0.5	8.75	9.75
1.5	--	9.75
24	8.05	--
96	7.85	8.80

equilibration time for complete breakthrough of a 2×10^{-8} M copper solution at pH 6 is 15 min. For a 2-mg resin column the above test solution requires 10 minutes for complete breakthrough. The equilibration time will also depend on other factors such as flow rate of the test solution. Equilibration time is shorter for faster flow rate. The upper limit of column size is governed by the practical pumping rate and by copper peak signal broadening induced by elution from the column.

3.3.8 Effect of Ionic Strength

Decreasing the ionic strength of the test solution is another way of increasing the sensitivity of the method. As the ionic strength is decreased the distribution coefficient of copper between the aqueous and the resin phases is increased. Thus the absolute amount of copper sorbed onto the resin will be larger. However, two other factors need to be taken into consideration. The first is the need to maintain trace ion exchange conditions and thus a linear distribution isotherm. The second factor is the need to establish complete breakthrough (equilibrium) which will require a longer time as the distribution coefficient is made larger.

The quantitative relationship between copper uptake and ionic strength can be obtained by rearranging equation

2.4 into the form

$$\frac{[R_2M]}{[M^{2+}]} = K_{IE}^{Th} \cdot \frac{[RNa]^2}{[Na^+]^2} \cdot \frac{\gamma_{M^{2+}} \cdot \gamma_{RNa}^2}{\gamma_{R_2M} \cdot \gamma_{Na^+}^2} = \lambda_o \quad (3.1)$$

An experiment was conducted to examine the effect of ionic strength on the distribution coefficient of copper between the resin and solution phases. The sodium nitrate concentration in the test solution was varied from 0.1 M to 0.4 M at a fixed copper concentration of 1×10^{-7} M, a lutidine concentration of 10^{-3} M, and a pH of 6.0.

From the peak areas obtained upon analysis of the test solutions, the amount of copper sorbed at various ionic strengths was calculated by comparison with peak areas obtained by injection into the eluent stream via valve V (Figure 18) of a known volume (135 μ L) of standard copper solution (4×10^{-4} M). A plot of the experimentally measured distribution coefficient of copper (λ_o) vs ionic strength (μ) is shown in Figure 27.

Equation 3.1 suggests that if one knows the value of the activity coefficients then a plot of

$$\lambda_o \cdot \frac{\gamma_{R_2M} \cdot \gamma_{Na^+}^2}{\gamma_{M^{2+}} \cdot \gamma_{RNa}^2} \text{ vs } \frac{1}{[Na^+]^2}$$

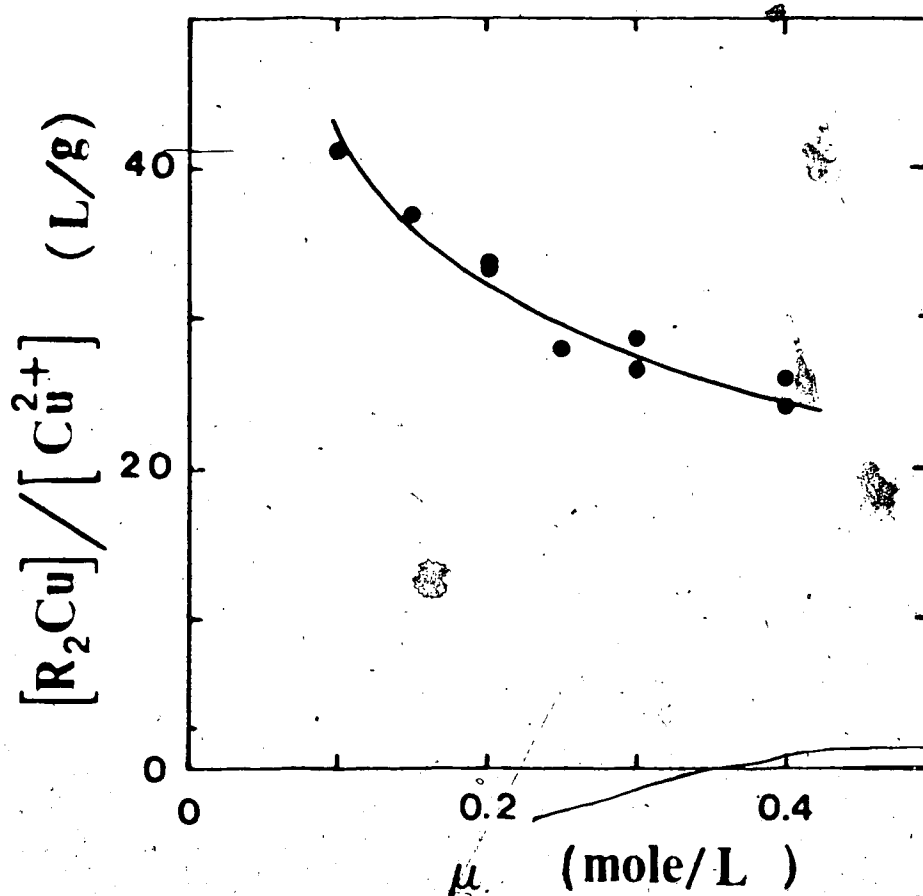


Figure 27. The distribution coefficient of free copper between the resin and the aqueous phases as a function of ionic strength.

should be linear with zero intercept. The resin phase activity coefficients γ_{R_2M} and γ_{RNA} cannot readily be evaluated as this requires knowledge of electrolyte sorption and swelling characteristics in addition to the selectivity coefficients [185,203]. Activity coefficients in the solution phase, γ_{Na^+} and $\gamma_{M^{2+}}$, can be estimated at different ionic strengths [219,220] up to 0.1 M or by the Stokes and Robinson formula [221] for ionic strengths up to 4 M. Therefore, neglecting the resin phase activity coefficients, a plot was made of $\lambda_o \cdot \gamma_{Na^+}^2 / \gamma_{M^{2+}}$ vs $1/[Na^+]^2$ (plot not shown). The plot was not linear but rather showed a deviation from linearity. There are three possible reasons for non-linearity of the above plot:

- (a) Neglect of correction for variation in the resin phase activity coefficients with ionic strength.
- (b) Sorption of other charged species such as $CuNO_3^+$.
- (c) Sorption of colloidal species.

An experiment which was performed to investigate the possibility of sorption of $CuNO_3^+$ species will first be described. The formation constant of $CuNO_3^+$, as compiled in the literature [222,223] is relatively low (3.47 to 3.16 at $\mu = 0$) and literature values vary widely for the same ionic strength. For example at $\mu = 3$ M $CuNO_3^+$ values from 0.40 to 0.96 are reported. Using the individual

activity coefficients of Kielland [219] and taking the activity coefficient of CuNO_3^+ as being equal to that of CdCl^+ the thermodynamic formation constant of CuNO_3^+ (3.47) was corrected for ionic strength and found to be 1.34 at $\mu = 0.1 \text{ M}$. Correction for ionic strength was also done by a form of the Davies equation [220, 224a]; the values of the Debye-Huckel constants used were those listed by Bates [209] at 25°C . The calculated formation constant obtained was 1.70 in fairly good agreement with that obtained by the first method.

It is generally believed that sodium perchlorate, NaClO_4 , is a completely dissociated salt [220] with a non-complexing anion. For this reason NaClO_4 was chosen as a swamping electrolyte in this experiment conducted to check the degree of complexation of copper ion by nitrate ion. Four solutions were prepared as detailed in Section 3.2.10; all had the same total copper concentration of $1 \times 10^{-7} \text{ M}$, pH of 6.0, lutidine concentration of 10^{-3} M , and ionic strength of 0.10 M but different proportions of NaNO_3 to NaClO_4 (Table 6). Upon running these test solutions following the procedure in Section 3.2.11 the peak areas of the copper signals obtained were statistically equal. These results mean either that NO_3^- is as non-complexing as ClO_4^- or that CuNO_3^+ does form but sorbs onto resin to the same extent as does Cu^{2+} . The

Table 6. Composition of test solutions used to test the possibility of copper complexation with nitrate ion.

Test Solution #	NaClO ₄ (M)	NaNO ₃ (M)	2,6-Lutidine (M)	[Cu] _T (M)
1	0.10	0.00	10 ⁻³	10 ⁻⁷
2	0.07	0.03	10 ⁻³	10 ⁻⁷
3	0.04	0.06	10 ⁻³	10 ⁻⁷
4	0.00	0.10	10 ⁻³	10 ⁻⁷

second explanation is unlikely in light of the charge difference between the two species [203].

Sorption of colloidal copper containing species is possible. Schubert [184] suggested use of ion exchange for detection and interpretation of colloidal behavior. In contrast to the sorption of cations the sorption of colloids may be increased with increasing electrolyte concentration by virtue of enhancing coagulation. This possibility was ruled out as an explanation of the non-linearity of the plot of $\lambda_o \cdot \gamma_{Na^+}^2 / \gamma_{M^{2+}}$ vs $1/[Na^+]^2$ in the present case because equilibration curves obtained for high ionic strength (0.4 M) showed a flat plateau after 10 minutes of loading. If colloidal particles are sorbed a flat plateau will not be obtained (refer to Section 3.3.5 and Figure 24).

Thus it is likely that the explanation of non-linearity in the present case lies in correction of resin-phase activity coefficients with ionic strength. Upon increasing ionic strength electrolyte invasion of the resin [203] gives rise to a change in the activity coefficients.

In a previous study of the sorption of nickel(II) on a cation exchanger a linear relationship between λ_o and $[Na^+]^{-2}$ was observed in the ionic strength range of 0.01 to 0.5 M [224b]. However, closer examination of the

results obtained for nickel over the same ionic strength range studied here (0.1 to 0.4 M) showed a curvature similar to that observed for copper. This behavior, of course, does not prevent the use of the ion exchange method for free-copper determination as long as the ionic strength is constant for all samples and standards. In natural water samples the salt content is so low that the ionic strength will be equal to the concentration of the added swamping electrolyte (0.100 M) and will not change from one sample to another.

3.3.9 Calibration Curve, Detection Limit, and Precision

Seven calibration standards of pH 6 containing 0 to 2×10^{-7} M copper were made as described in Section 3.2.10 and run as described in Section 3.2.11 using the instrumental conditions listed in Table 4. Figure 28 shows a photo reproduction of the peaks obtained for duplicate runs of these solutions. The solutions contained 0.1 M NaNO_3 and 10^{-3} M lutidine buffer. The calibration curve obtained was linear at least up to 2×10^{-7} M copper with a correlation coefficient of 0.995. The slope was 4.1×10^6 absorbance \cdot second \cdot mole $^{-1}\cdot$ L with a relative standard deviation of 1.57%. The intercept with the peak area axis was 0.002 ± 0.017 at the 95% confidence level. Each standard was run twice and the

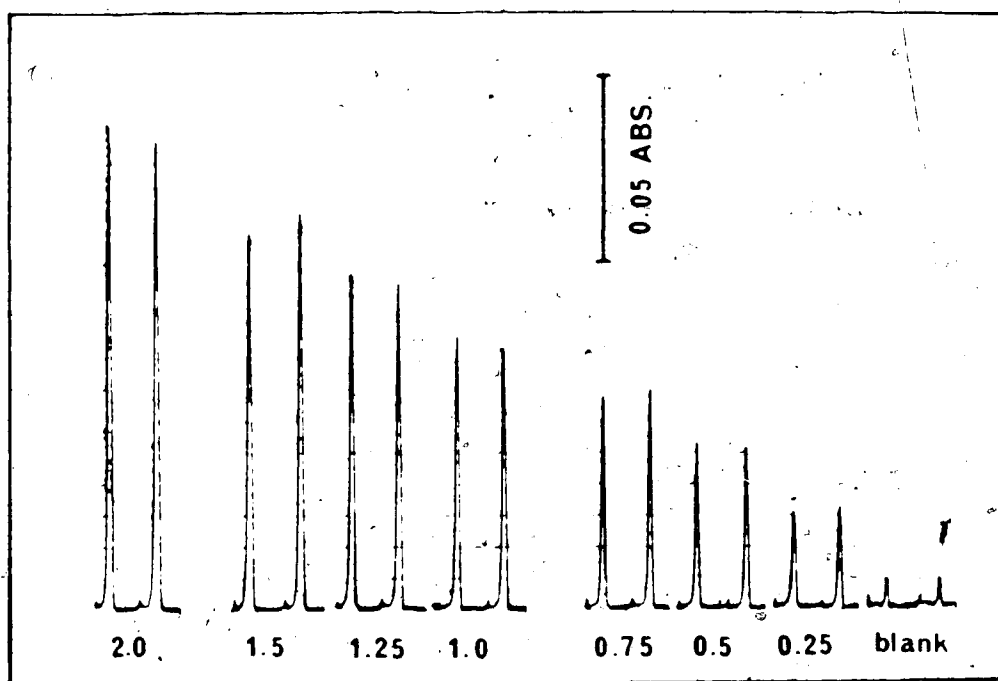


Figure 28. Chart recorder tracings for duplicate runs of standard copper solutions (0 to 2×10^{-7} M) at pH 6 containing 0.1 M NaNO_3 and 10^{-3} M lutidine buffer using the ion exchange column equilibration/AAS method.

average peak area (corrected for the blank signal) was used in the calculations.

The detection limit (2×10^{-8} M copper concentration) was calculated as the sum of the average blank signal plus three standard deviations [225,226]. The relative standard deviation of the blank, calculated from eleven blank test solutions run over a period of 3 months, was 16%.

The precision of the method was evaluated at 1×10^{-7} M copper concentration. For four test solutions analyzed in duplicate the relative standard deviation of the average peak area was 3.4%.

CHAPTER 4

EFFECT OF COMPLEXING LIGANDS ON FREE-COPPER DETERMINATION BY THE ION EXCHANGE COLUMN EQUILIBRATION/AAS METHOD

4.1 Introduction

In the ion exchange column equilibration method of free-copper determination it is assumed that only the free metal is exchanged onto the resin while the complexed forms are not. The addition of a complexing ligand to a solution containing free copper will result in the complexation of some of the copper ions, rendering them unexchangeable and thus giving a lower value for free copper.

As mentioned in Section 2.1, cationic copper complexes are likely to sorb onto the resin by mechanisms similar to those of free copper [203]. Cockerell and Walton [227] observed that the presence of ethylenediamine (en) in the test solution drives more copper into the resin phase than when ethylenediamine is absent. The distribution coefficient of Cu(en)_2^{2+} is evidently larger than the distribution coefficient for hydrated Cu^{2+} . Maes and Cremers [228] concluded that the enhanced sorption of Cu(en)_2^{2+} on inorganic clay cation exchangers can be

explained in terms of greater delocalization of the charge on the complex in the exchanger and poor hydration relative to Cu^{2+} . In the present ion exchange method of free-copper determination sorption of cationic complexes causes an interference by giving a falsely high free-copper concentration.

Neutral copper complexes may also sorb onto ion exchange resins. Although a quantitative theory of such a process has not yet been presented, sorption of neutral species has been explained in terms of physical forces and interactions such as London forces, dipole-dipole interactions, salting in, salting out, and sieve action [203]. As with cationic complexes, sorption of neutral copper complexes will interfere in the selectivity of the ion exchange method of free-copper determination, giving high results. Anionic complexes are not expected to sorb to a significant extent onto a cation exchange resin because they bear the same sign of charge as the resin matrix and will therefore experience coion exclusion [203].

Natural water systems contain variable concentrations of different organic and inorganic ligands which are capable of complexing copper(II) [95,115]. Depending on the ligand charge, the copper complex formed with these ligands may be positive, neutral, or negative. In this

chapter the ion exchange column equilibration technique is tested for its specificity for free copper in the presence of various organic and inorganic complexing ligands. The ligands chosen were those often found in natural waters such as chloride, phosphate, sulfate, and fulvic acid or simple organic ligands with functional groups similar to those present in humic substances, such as glycine, phthalic acid, citric acid, and salicylic acid.

The testing scheme is composed of two major steps. The first involves mathematical calculations of the copper species distributions in the presence of various concentrations of complexing ligand. The second step involves preparation and analysis of test solutions containing copper(II) and various ligand compositions in order to compare the free-copper concentrations obtained by the ion exchange method with those predicted by calculation.

In the last three sections of this chapter analyses for total and free copper are reported for a water sample from Bonnevill Lake in Quebec. The complexation capacity of this water sample was also determined by titration with copper(II) using the ion exchange technique to monitor the titration.

4.2 Experimental

4.2.1 Chemicals

Aminoacetic acid, $\text{NH}_2\text{CH}_2\text{COOH}$ (glycine) was analytical reagent grade (British Drug Houses) and sodium salicylate, $\text{C}_6\text{H}_4(\text{OH})\text{COONa}$ was certified reagent grade (Fisher Scientific Co.). Phthalic acid; $\text{C}_6\text{H}_4\text{-1,2-(COOH)}_2$ was Baker Grade (J.T. Baker Co.); citric acid, $\text{HOCOCH}_2\text{C(OH)(COOH)CH}_2\text{COOH}\cdot\text{H}_2\text{O}$ (Caledon Laboratories Ltd.) was reagent grade, sodium chloride; NaCl (Amachem Co.); anhydrous sodium sulfate, Na_2SO_4 (Amachem Co.); anhydrous di-sodium hydrogen orthophosphate, Na_2HPO_4 (British Drug Houses); and monohydrated sodium dihydrogen orthophosphate, $\text{NaH}_2\text{PO}_4\cdot\text{H}_2\text{O}$ (British Drug Houses) were either analytical or reagent grades. All of the above were used as received, without further purification.

A sample of fulvic acid was supplied by Dr. C.H. Langford, Department of Chemistry, Concordia University, Montreal, Quebec and used without further treatment. The material was extracted from the Bh horizon of a podzol from Armadale, Prince Edward Island, Canada.

4.2.2 Reagents

Sodium chloride stock solution (0.500 M) was prepared by dissolving 29.220 g of the salt in water and diluting to 1 L.

Di-sodium hydrogen orthophosphate stock solution (0.025 M) was prepared by dissolving 3.549 g of the dried anhydrous powder in a 1-L volumetric flask and diluting to volume with water.

Sodium dihydrogen orthophosphate stock solution (0.050 M) was prepared by dissolving 6.899 g of the monohydrated salt in water and diluting to 1-L.

Sodium sulfate stock solution (0.25 M) was prepared by dissolving 35.510 g of the dried salt and diluting to 1 L with water.

Glycine stock solution (10^{-2} M) was prepared by dissolving 0.1878 g of glycine in water in a 250-mL volumetric flask and diluting to volume with water. Working standards of glycine were prepared by serial dilution of this stock solution.

Phthalic acid stock solution (10^{-2} M) was prepared by dissolving 0.8306 g of the crushed crystals in a 500-mL volumetric flask and diluting to volume with water.

Citric acid stock solution (10^{-3} M) was prepared by dissolving 0.1501 g of the monohydrated acid in a 500-mL volumetric flask and diluting to volume with water. The freshly prepared stock solution was used to prepare more dilute standards as required.

Sodium salicylate stock solution (10^{-2} M) was prepared by weighing 1.601 g of the salt and dissolving in

water with the aid of an ultrasonic bath. The volume was brought to 100 mL with water. This stock was used to prepare fresh dilute standards.

Fulvic acid stock solution (1g/L) was prepared by dissolving 0.1000 g of the material in a 100-mL volumetric flask using an ultrasonic bath. The solution was then diluted to volume with water. More dilute stock solutions were freshly prepared by serial dilution of the original preparation.

Other reagents and solvents used were described in Chapter 3.

4.2.3. Apparatus

As well as the equipment described in Section 3.2, a Perkin-Elmer Model 5000 atomic absorption spectrophotometer with a graphite furnace unit (Model HGA 2200), an autosampler (Model AS-1), and a Perkin-Elmer copper hollow cathode lamp were used for the determination of total copper in the Bonneville Lake water sample. The instrumental conditions are listed in Table 7.

4.2.4 Calculation of Copper Species Distributions as a Function of Ligand Concentration

For varying ligand concentrations the soluble mononuclear copper-containing species distributions (in percent) were calculated at 0.1 M ionic strength and pH 6

Table 7. Instrumental conditions for the Perkin-Elmer 5000 graphite furnace AAS for the determination of total copper in lake water.

Wavelength (nm)	324.7
Spectral slit width (nm)	0.7 (low)
Lamp current (mA)	15
Furnace	Pyrolytic graphite with platform
Furnace temperature (°C)	
Dry	110
Ash	1000
Atomize	2650
Time (s)	
Dry	40
Ash	20
Atomize	8
Integration time (s)	8
Purge gas	Argon

following the general scheme in Appendix A. Values for total copper concentrations were 1×10^{-7} M and 1×10^{-6} M. The formation constants of CuOH^+ and Cu(OH)_2 used were $10^{6.4}$ and $10^{11.6}$ respectively [170] and the autoprotolysis constant of water k_w was taken as $10^{-13.78}$ [222].

Formation constants of various copper-ligand species were taken from data compilations or from specific references, as indicated. If necessary, an ionic strength correction was made using individual ionic activity coefficient values based upon computations by Kielland [219] or calculated from the Davies equation [220]. Both lutidine and nitrate ion were considered as non-complexing ligands (Sections 3.3.2 and 3.3.8). Calculations of species distributions obtained by the procedure of Appendix A were checked by computer calculations (University of Alberta Amdahl) using a slightly modified version of the speciation program COMICS [134]. The modification was the inclusion of an additional subroutine which provided fractional species distributions of the metal in a tabular form. For both total copper concentrations used the species distributions were identical for all ligands studied except citrate. For a 1×10^{-6} M total copper concentration the relative free copper curve in the presence of citrate is higher than that of the 1×10^{-7} M total copper by a maximum of 6% (Figure 34(b)). This shift is due to the higher metal-to-ligand ratio for the 1

$\times 10^{-6}$ M total copper solution.

4.2.5 Preparation of Test Solutions and Blanks

On the basis of the species distributions calculated for a given ligand, a series of test solutions was prepared containing variable ligand concentrations but constant total sodium concentration (0.100 M) and lutidine buffer (10^{-3} M) in the following way.

A suitable volume of 0.500 M NaNO_3 solution was delivered into a 400-mL beaker. The volume of NaNO_3 was calculated such that the total sodium concentration, including that from the ligand solution, was always 0.100 M after dilution to 250 mL. This was followed by an appropriate volume of the ligand solution. Five mL of lutidine solution (0.05 M) were then added and, if necessary, a volume of water to give a total volume of approximately 200 mL. The pH was then adjusted to 6.0 by addition of dilute HNO_3 except for NaH_2PO_4 ligand system where NaOH was used. This was followed by dropwise addition to the stirred solution of 10 mL of daily-prepared standard copper solution (2.5×10^{-6} M). A final pH adjustment was necessary after addition of the copper in some cases. The contents of the beaker were quantitatively transferred to a 250-mL volumetric flask, diluted to volume and shaken well. For each test solution

a corresponding blank was prepared in exactly the same manner except for the absence of copper standard.

4.2.6 Determination of Free Copper by Ion Selective Electrode (ISE) Potentiometry

This work was carried out by D. Lucyk [229] to provide comparative measurements to the ion exchange column equilibration/AAS measurements for the determination of free copper. An Orion 94-29 cupric selective electrode, an Orion 90-02 double junction Ag-AgCl reference electrode and a Fisher 825 MP Accumet pH meter were used. The measurement and electrode cleaning procedures were similar to those of Blaedel and Dinwiddie [172].

Since the ISE measurements were designed to provide comparison data for the ion exchange column equilibration method, the test solutions used for ISE measurements were of the same composition as those for the ion exchange method (Sections 4.25 and 4.3). However due to the lower sensitivity of the ISE method for copper determination, a 10 fold higher total copper concentration (10^{-6} M) had to be used. Of the seven ligands studied by the ion exchange method, only chloride was not investigated by ISE. Several researchers have noted abnormal cupric-ISE response in chloride media and it was feared that

performing such a study might foul the electrode.

4.2.7 Treatment of the Bonneville Lake Water Sample and Standard

The Bonneville Lake water sample was supplied by M. Papineau of Environment Canada, Inland Waters Directorate, Quebec Region. It was an integrated sample (0 to 4 m) collected by a helicopter on October 3, 1985, divided into four 1-L subsamples and shipped in ice [230]. In our laboratory the subsamples were allowed to stand at room temperature for several hours before the pH was measured (5.2). The subsamples were then filtered ($\sim 0.45 \mu\text{m}$) using acid-washed 47-mm diameter Nylon 66 filters (Rainin Instruments Co., Woburn, MA). For each 1-L subsample a new filter was used. The first 200 mL of filtrate were used to rinse the receiving flask and were discarded.

The sample solutions for free-copper determination were prepared as follows: To 20 mL of 0.500 M NaNO_3 solution was added 2.0 mL of lutidine buffer (0.05 M); the pH was adjusted to 5.2 by dropwise addition of dilute nitric acid; into this solution was delivered 78.0 mL of the filtered water sample, which gave a final pH of 5.25 ± 0.05 . A blank test solution was prepared by the same procedure, but replacing the water sample with an equivalent volume of filtered distilled water. A standard

copper test solution (1.0×10^{-7} M) was also prepared for calibration as described in Section 3.2.10 except for pH adjustment to 5.2.

4.2.8 Preparation of Sample Solutions for the Determination of the Complexing Capacity of the Water Sample

Eighty milliliters of the filtered lake water sample were dispensed into each of eight 100-mL polyethylene bottles and spiked with 0, 10, 25, 50, 100, 200, 300, and 400 μ L of a standard copper solution (5×10^{-5} M). A variable volume Finnpiptette (Labsystem Oy, Helsinki, Finland) and yellow disposable plastic tips were used. The final pH did not drop by more than 0.06 unit. The next day 20.0 mL of a solution composed of 0.500 M NaNO_3 and 0.005 M lutidine with a pH of 5.2 was added to each bottle and the bottles were shaken well.

4.3 Results and Discussion

4.3.1 Effect of Chloride on Free-Copper Determination

Cupric ion forms a very weak 1:1 complex with chloride ion. From the compiled data [222,223] the formation constant, β_{CuCl^+} , is $10^{-0.06}$ at an ionic strength, μ , of 2 and lies in the range of $10^{0.00}$ to $10^{0.4}$ at $\mu = 0$. Makashev et al. [231] reported a formation constant of $10^{0.12}$ at $\mu = 0.1$ for the inner-sphere

complex. This value was used in the calculation of species distribution presented in this section. HCl was assumed to be totally dissociated ($k_a = 10^{6.1}$) [222]. The copper species distributions in the presence of chloride ion (0 to 0.1 M) were calculated as described in Section 4.2.4 and the results are plotted in Figure 29(a).

Test solutions and blanks containing 0, 0.02, 0.04, 0.07, and 0.1 M chloride concentrations were prepared as in Section 4.2.5. These solutions were analyzed for free copper (Section 3.2.11) using the ion exchange column equilibration/AAS method described in Sections 3.2.3 and 3.2.9. The peak area (corrected for the corresponding blank) of the test solution in the presence of the ligand was divided by that in the absence of the ligand to obtain the relative free copper (in percent). For each ligand concentration used the relative free copper was plotted against the ligand concentration (Figure 29(b)). The solid curve in Figure 29(b) is the relative free copper calculated from the Cu^{2+} species distribution in (a) as detailed in Appendix B. The solid circles are experimental points.

The good agreement between the solid curve and the experimental points of Figure 29(b) must be considered fortuitous in light of the high uncertainty ($\pm 5\%$) in the calculation of the copper species distribution. The error

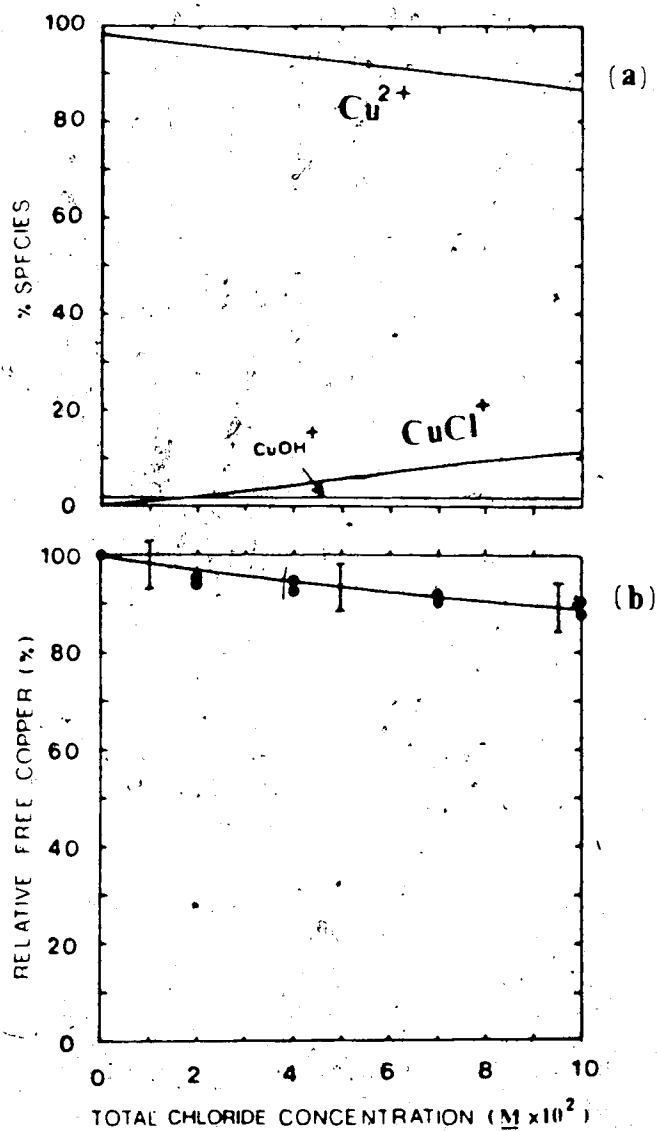


Figure 29. (a) Calculated copper species distribution as a function of chloride concentration at pH 6; (b) decrease in free-copper concentration with increasing chloride concentration as measured by the ion exchange method (●). The solid line in (b) is calculated from the Cu^{2+} species distribution in (a). Error bars are the uncertainty in the calculated solid line.

bars shown in Figure 29(b) are based on a calculated relative standard deviation of 0.44 in β_{CuCl^+} . This uncertainty was estimated from evaluation of the various values of β_{CuCl^+} compiled at $\mu = 0$ [222,223].

The uncertainty in β_{CuOH^+} was also taken into account. Gulens et al. [170] determined β_{CuOH^+} for dilute copper solutions ($\sim 5 \times 10^{-7}$ M) in 0.1 M NaNO_3 . The values reported were $10^{6.3}$ and $10^{6.8}$. On the other hand, Smith and Martell [233] listed β_{CuOH^+} as $10^{6.1 \pm 0.0}$. The value of $10^{6.4 \pm 0.35}$ was used in this work. The results in Figure 29(b), however, show that chloride ion does not interfere in the determination of free copper by the ion exchange column equilibration method. That is, the sorption of CuCl^+ by the ion exchanger under these conditions is slight enough to be ignored even at fairly high chloride concentrations.

4.3.2 Effect of Orthophosphate on Free-Copper

Determination

Copper forms two orthophosphate complexes [222], CuHPO_4 with a β value of $10^{3.2}$ at $\mu = 0.1$ and $\text{CuH}_2\text{PO}_4^+$ with a β value of $10^{1.3}$ at $\mu = 0.15$. For the latter complex Kriss and Yastrimirskii [232] reported a β value of $10^{1.7}$ at $\mu = 0$. This value was corrected for ionic strength, taking the activity coefficient of $\text{CuH}_2\text{PO}_4^+$ to be equal to

that of CdCl^+ [219]. The resulting formation constant of $\text{CuH}_2\text{PO}_4^+$ was $10^{1.3}$ the same as that reported at $\mu = 0.15$. The stepwise phosphoric acid dissociation constants used for $\mu = 0.1$ were those listed by Martell and Smith [233]: $k_{a1} = 10^{-2.00}$, $k_{a2} = 10^{-6.73}$, and $k_{a3} = 10^{-11.74}$. The copper species distributions in the presence of various phosphate concentrations were calculated as outlined in Appendix A and Section 4.2.4. Figure 30(a) shows a plot of these results.

Test solutions and blanks containing 0, 0.5, 2, 3.5, 5, 7.5, and 10 mM concentrations of orthophosphate were prepared as described in Section 4.2.5 and analyzed for free copper (Section 3.2.11) by the ion exchange column equilibration/AAS method described in Chapter 3. The relative free copper, defined in Section 4.3.1, is plotted against the total orthophosphate concentration in Figure 30(b). The solid line in (b) was obtained by calculating the relative free copper from the Cu^{2+} species distribution curve in Figure 30(a) (Appendix B). The solid circles are experimental points for the system using Na_2HPO_4 as the starting material, while the open circles are the experimental points for the system using NaH_2PO_4 as the starting material. The ion selective electrode results are also shown in Figure 30(b); the solid triangles are experimental points for the Na_2HPO_4 ligand

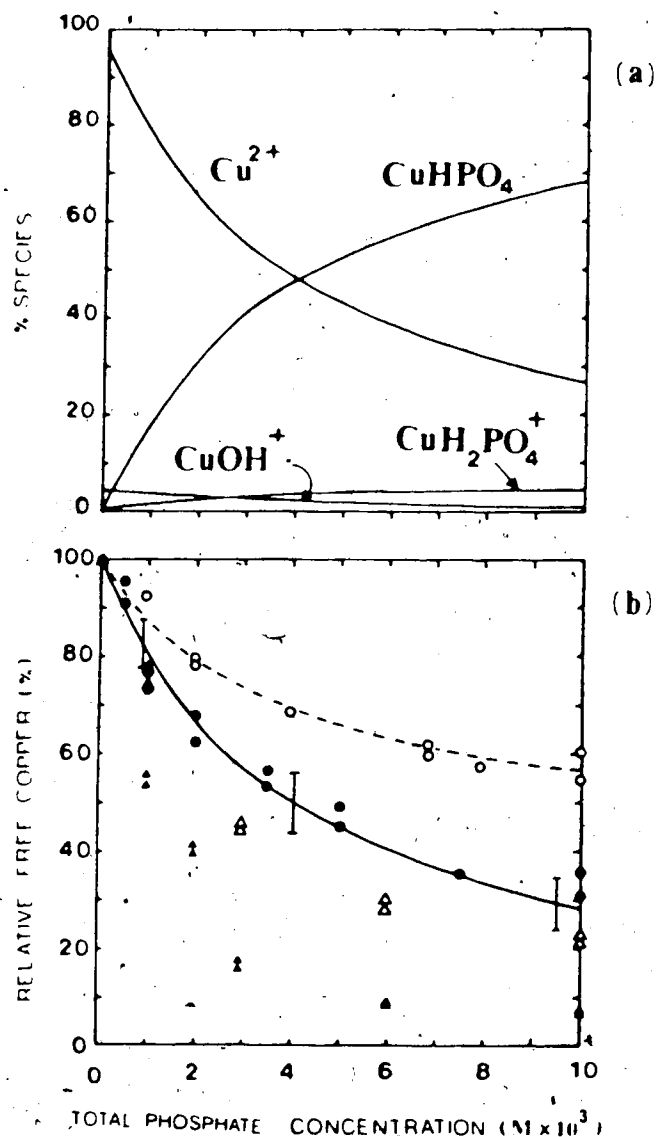


Figure 30. (a) Copper species distribution as a function of orthophosphate concentration at pH 6; (b) the decrease in free-copper concentration with phosphate concentration as obtained by the ion exchange method (O) and the ion selective electrode method (Δ). The solid symbols denote values obtained when Na₂HPO₄ stock solution was used as a source of phosphate while the open symbols denote values obtained when NaH₂PO₄ was used. The solid line in (b) is the relative free copper calculated from the Cu²⁺ species distribution in (a) and the dashed line is calculated from the solid line assuming CuHPO₄ sorbs as well.

system while the open triangles are those for the NaH_2PO_4 ligand system.

Figure 30(b) shows that the ISE results are always lower than those of the ion exchange method. Furthermore, the relative free copper is dependent on the type of salt added to provide the orthophosphate ligand. For both techniques use of NaH_2PO_4 as a source of orthophosphate ion yields higher relative free-copper values than those obtained when Na_2HPO_4 is used. In the NaH_2PO_4 system the pH of the test solution was adjusted by addition of dilute NaOH while in all other ligand systems, including Na_2HPO_4 , the pH was adjusted by addition of dilute HNO_3 (Section 4.2.5). This would result in about 5% higher $[\text{Na}^+]$ for the Na_2HPO_4 system. In this case a slightly lower (~2.5%) free-copper signal is expected by the ion exchange method which is contrary to the 75% higher relative free copper values found (Figure 30(b)). The possibility that NaH_2PO_4 is contaminated with copper was ruled out because blanks of both orthophosphate salts (Section 4.2.5) showed a similar free-copper signal and therefore similar total copper concentrations. This peculiar observation was not pursued further.

The uncertainty in the solid curve of Figure 30(b) was estimated by taking into consideration the errors in $\text{p}K_{\text{CuOH}^+}$ (Section 4.3.1), in k_{a2} for phosphoric acid and in

β_{CuHPO_4} as the major species formed. The error in $\alpha_{\text{HPO}_4^{2-}}$ was taken as equal to that of the uncertainty in K_{a2} for phosphoric acid which was calculated as 0.21 relative standard deviation (r.s.d.) based on six values compiled in the literature [222,223] at $\mu = 0.1$. The uncertainty in β_{CuHPO_4} was taken as 0.18 r.s.d. based on a single value of $10^{3.2}$ reported at $\mu = 0.1$ [222]. The overall absolute uncertainty ranges from 5 to 6% (one standard deviation) and is shown as error bars in Figure 30(b) for three phosphate concentrations.

The dotted line in Figure 30(b) is the new position of the solid line, assuming that CuHPO_4 does sorb onto the resin with a distribution coefficient of 19 L/g. It was calculated according to equation B.18 in Appendix B using the experimentally determined value of 41 L/g for the distribution coefficient of free copper, $\lambda_{\text{Cu}^{2+}}$ (or λ_0).

4.3.3 Effect of Sulfate on Free-Copper Determination

Copper forms a single 1:1 complex with sulfate ion with a formation constant of $10^{0.95}$ at $\mu = 1$ and $10^{2.36}$ at $\mu = 0$ [222]. At $\mu = 0.1$ a corrected β value of $10^{1.52}$ was calculated using activity corrections [219]. The first proton of sulfuric acid (H_2SO_4) was assumed to be completely dissociated while the acid dissociation constant of HSO_4^- was taken as $10^{-1.55}$ [222]. The copper

species distributions at different total sulfate concentration were calculated as described in Section 4.2.4 and plotted in Figure 31(a).

Test solutions and blanks containing 0, 0.01, 0.02, 0.03, and 0.05 M sulfate were prepared as described in Section 4.2.5 and analyzed for free copper using the instrumentation and conditions in Chapter 3. A plot of the relative free copper (derived in Appendix B) vs total sulfate concentration is presented in Figure 31(b). The dots are experimental values obtained by the ion exchange method while the solid triangles were obtained by the ISE method (Section 4.2.6). The solid line was obtained by calculating the relative free copper from the Cu^{2+} species distribution curve of Figure 31(a) as detailed in Appendix B. The ion exchange method gave 64% higher results than expected while the ion selective electrode gave 34% lower results.

Sodium ion has a fairly large formation constant with sulfate ion ($\beta = 10^{0.7}$ at $\mu = 0$). This value was corrected for ionic strength [219] and a β value of $10^{0.25}$ was used to calculate the free-sodium and sulfate concentrations available at $\mu = 0.1$. Table 8 shows the species distributions obtained in the absence of copper (blank test solutions). As NaNO_3 is gradually replaced by Na_2SO_4 the free-sodium ion concentration drops from 0.1 M

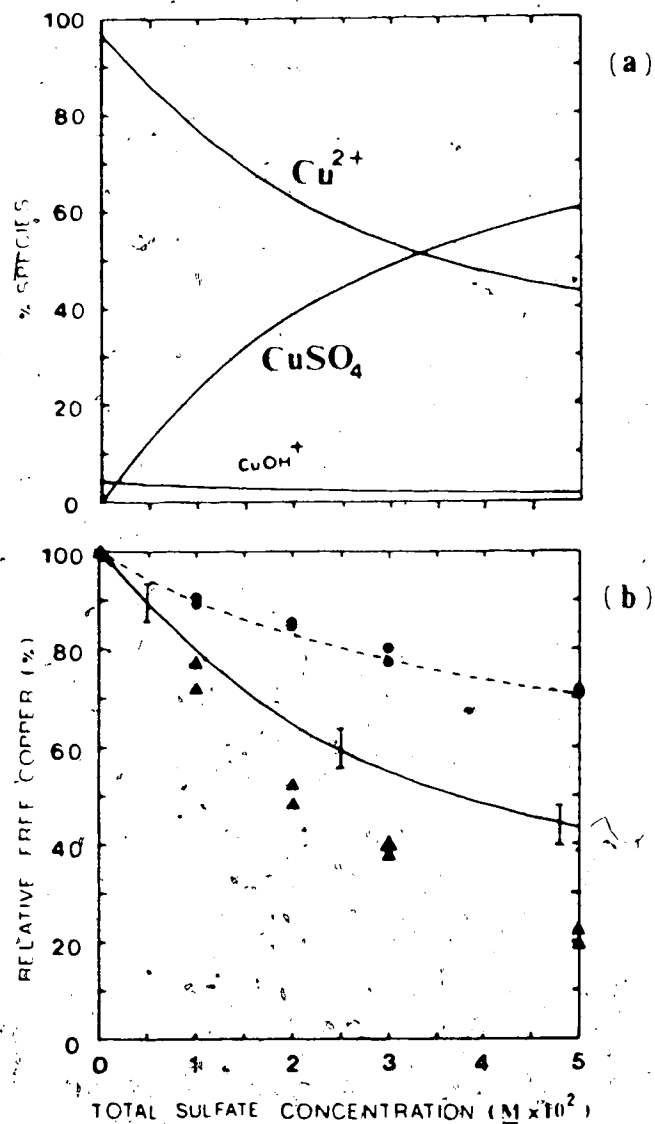


Figure 31. (a) Copper species distribution as a function of sulfate concentration at pH 6; (b) the decrease in free-copper concentration with increase in sulfate concentration as measured by the ion exchange (●) and by the ion selective electrode (▲) methods. The solid line in (b) is calculated from Cu^{2+} species distribution in (a). The dashed line is calculated assuming that CuSO_4 also sorbs.

Table 8. Species distribution of sodium and sulfate at constant total sodium concentration but variable total sulfate concentration.

Salt Concentration (M)		Species Concentration (M)				Ionic Strength (μ)
Na_2SO_4	NaNO_3	NaSO_4^-	Na^+	$\text{SO}_4^{=}$	NO_3^-	
0.00	0.10	0.000	0.100	0.000	0.10	0.100
0.01	0.08	0.002	0.098	0.008	0.08	0.106
0.02	0.06	0.004	0.096	0.016	0.06	0.112
0.03	0.04	0.005	0.095	0.025	0.04	0.120
0.05	0.00	0.009	0.091	0.041	0.00	0.132

to 0.091 M (Column 4). Furthermore, about 20% of the sulfate added is tied up as NaSO_4^- ion. The higher free-copper signal observed in Figure 31(b) in the ion exchange method is partly due to a decrease in $[\text{Na}^+]$ upon addition of sulfate. At 0.09 M $[\text{Na}^+]$ the calculated free-copper signal was 4% higher than at 0.1 M $[\text{Na}^+]$. Also, replacement of NO_3^- by SO_4^{2-} results in an increase in ionic strength (Column 7). This change is too small, however, to affect the free-copper concentration significantly (see Figure 27).

Uncertainties in the calculated relative free-copper curve in Figure 31(b) arise mainly from uncertainty in the values for β_{CuOH^+} (Section 4.3.2), $\beta_{\text{NaSO}_4^-}$, and β_{CuSO_4} . Smith and Martell [222] list β_{CuSO_4} as $10^{2.36 \pm 0.03}$ at $\mu = 0$ while for the same ionic strength the IUPAC compilation [223] lists a range of values from $10^{2.25}$ to $10^{2.36}$. The corresponding uncertainty in the free copper calculation is 0.12 r.s.d., which is the same as that used for the uncertainty in $\beta_{\text{NaSO}_4^-}$. The absolute error in the relative free copper value, calculated for three sulfate concentrations, is shown as error bars in Figure 31(b).

It is possible that the neutral species CuSO_4 sorbs onto the exchanger. The dotted line in Figure 31(b) is the new position of the solid line assuming that CuSO_4 sorbs onto resin with a distribution coefficient of 19

L/g. The calculations are similar to those used for the phosphate system and are detailed in Appendix B. In natural water systems sulfate concentrations are generally less than 8×10^{-3} M, even for CuSO_4 -treated lakes [115] and sulfate will be mainly associated with calcium, which is more abundant than copper and equally strongly complexing. Thus sulfate is not expected to cause severe interference in the determination of free-copper concentration by the ion exchange column equilibration method.

4.3.4 Effect of Glycine on Free-Copper Determination

Copper and glycinate ion, $\text{NH}_2\text{CH}_2\text{COO}^-$, (GLY^-) form a 1:1 complex ($\beta = 10^{8.13}$) and a 1:2 complex ($\beta = 10^{15.03}$) at 0.1 M ionic strength [234]. The acid dissociation constants, k_{a1} and k_{a2} of glycinium ion, $\text{H}_3^+\text{NCH}_2\text{COOH}$ (H_2GLY^+) are $10^{-2.36}$ and $10^{-9.56}$ respectively [233,234] at $\mu = 0.1$. Copper species distribution calculations were performed for various total glycine concentrations following the scheme in Section 4.2.4; the results are presented in Figure 32(a).

Test solutions and blanks were prepared to contain 0, 10, 15, 60 and 100 μM total glycine according to Section 4.2.5. Since the total concentration of ligand added is low relative to the swamping electrolyte no correction was

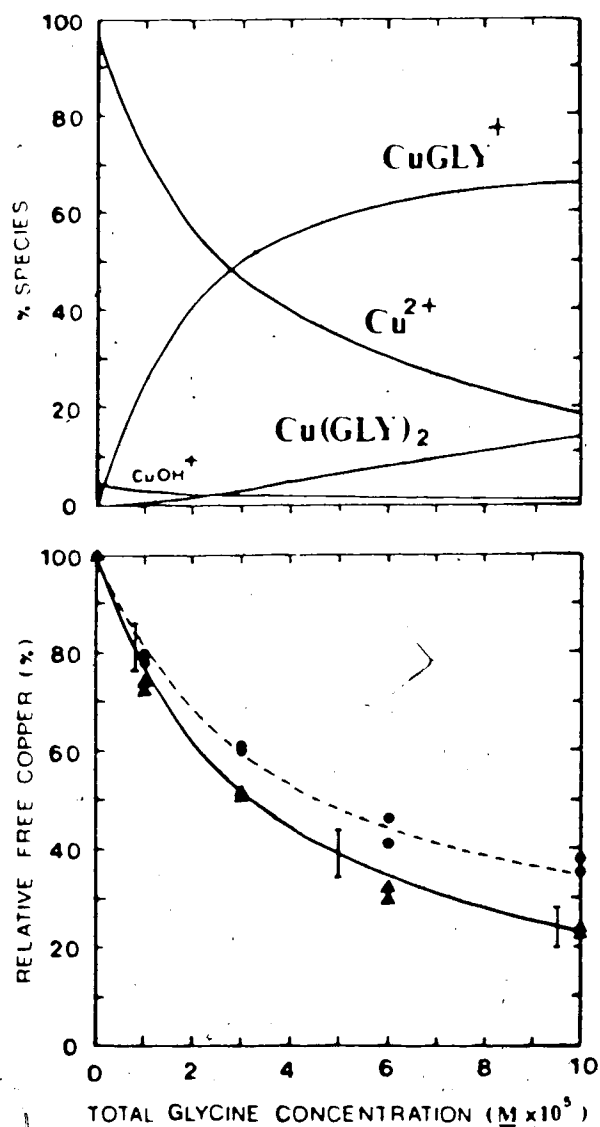


Figure 32. (a) Copper species distribution as a function of total glycine concentration at pH 6; (b) the decrease in relative free-copper with increase in glycine concentration as obtained by the ion exchange (●) and by ion selective electrode (▲) methods. The solid line in (b) is calculated from the Cu^{2+} species distribution in (a) while the dashed line accounts for sorption of CuGLY^+ .

made for total $[Na^+]$ (compare with Table 8). The above test solutions and blanks were analyzed for free copper by the ion exchange column equilibration/AAS method (Section 3.2). The relative free copper, defined in Section 4.3.1 is plotted against the total glycine concentration in Figure 32(b) (solid circles) while the ion selective electrode results (Section 4.2.6) are shown as solid triangles. The solid line in (b) is obtained by calculating the relative free copper from the Cu^{2+} distribution curve in Figure 32(a). The ISE results agree well with those predicted by calculations (solid line in Figure 32(b)) while the ion exchange results are slightly higher, probably due to exchange of positively charged copper glycinate species ($CuGLY^+$ in Figure 32(a)). Assuming a value of 9 L/g for the distribution coefficient of $CuGLY^+$ between the resin and the aqueous phase, the dotted line in Figure 32(b) was calculated according to equation B.18 in Appendix B. This line fits well the experimental data obtained by the ion exchange method, which suggests that positively charged complex species do sorb on the exchanger.

A $\pm 5\%$ absolute standard deviation in the solid line in Figure 32(b) was estimated and is shown as error bars at three total glycine concentrations. The error calculations took into account the uncertainty in β_{CuOH^+}

(Section 4.3.1), in β_{CuGLY^+} ($10^{8.15 \pm 0.09}$) [234], and in the acid dissociation constant of glycine ($10^{-9.61 \pm 0.06}$), which was calculated from eight compiled values at $\mu = 0.1$ [236].

4.3.5 Effect of Phthalate on Free-Copper Determination

Phthalic acid (H_2PTH) is a dibasic acid with dissociation constants of $10^{-2.75}$ and $10^{-4.92}$ at an ionic strength of 0.7 [235]. At pH 6, 92% of the acid is completely dissociated as the phthalate ion (PTH^-). Copper forms three complexes with phthalate ion; CuPTH with a β value of $10^{3.22}$, CuH(PTH)^+ with a β value of $10^{1.33}$, and Cu(PTH)_2^- with a β value of $10^{5.46}$, all at 0.1 M ionic strength [235]. The copper-phthalate species distributions versus phthalate concentration, calculated as in Section 4.2.4 and Appendix A, are plotted in Figure 33(a). For the highest phthalate concentration used in the calculation, CuH(PTH) was less than 0.1%. Therefore this species was not included in Figure 33(a).

Test solutions and blanks containing 0, 0.2, 0.5, 1.2, and 2 mM phthalic acid were prepared as described in Section 4.2.5 and analyzed for free copper by the ion exchange column equilibration method (Section 3.2). The relative free copper (defined in Appendix B) was plotted against the total phthalate concentration (Figure 33(b),

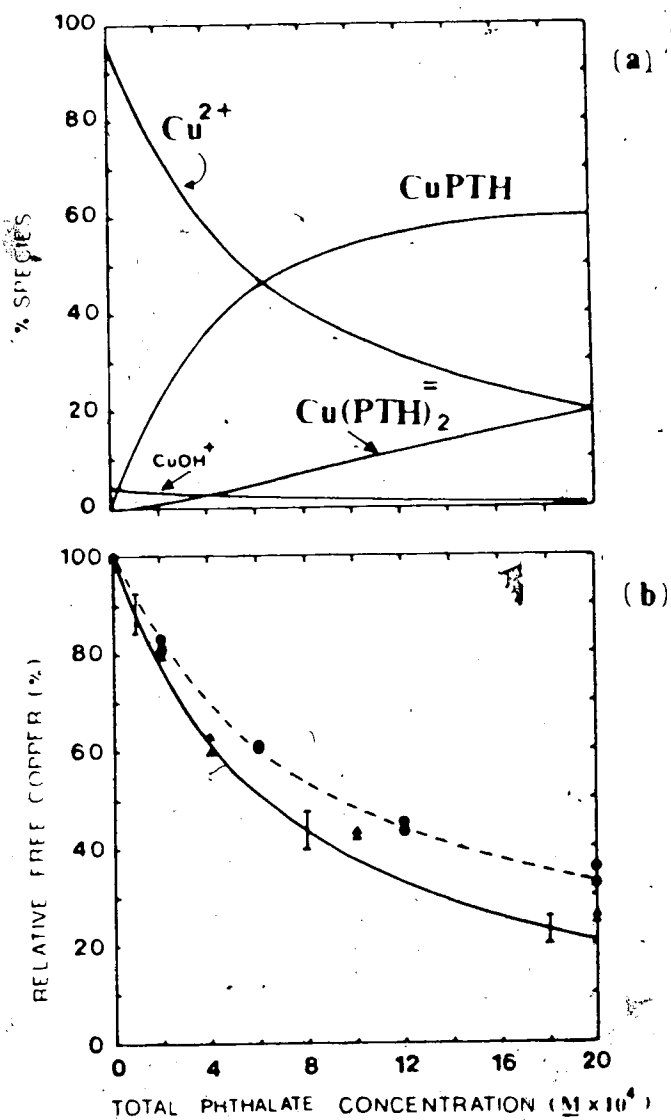


Figure 33. (a) Copper species distributions as a function of total phthalate concentration; (b) the decrease in free-copper concentration with increasing phthalate concentration as obtained by the ion exchange method (●) and by the ion selective electrode method (▲). The solid line in (b) is the relative free copper as obtained from Cu^{2+} species distribution curve in (a) while the dashed line accounts for sorption of CuPTH as well as free copper.

solid dots). The solid triangles were obtained by the ISE method (Section 4.2.6), while the solid line in (b) is the relative free copper expected at various ligand concentrations as calculated from the Cu^{2+} species distribution curve in Figure 33(a) (Appendix B). The ISE method gives results that are closer to the theoretical calculation line than does the ion exchange method. The higher results obtained by the ion exchange method are probably due to sorption of the neutral species CuPTH . This is not surprising in light of the skeletal similarity of phthalic acid and the styrene-divinylbenzene copolymer. The dashed line in Figure 33(b) was calculated from equation B.18 in Appendix B with the assumption that CuPTH sorbs onto the resin with a distribution coefficient of 8 L/g. This value was arbitrarily chosen to give the best fit to the experimental data.

The uncertainty in the solid line of Figure 33(b) was calculated as ± 3 to 4% (one absolute standard deviation) and is shown as error bars at three different phthalate concentrations. β_{CuPTH} was reported as $10^{3.15 \pm 0.05}$ [235] and more recently as $10^{3.22}$ by the same authors [233]. The uncertainty in α_{PTH^-} was taken as equivalent to the uncertainty in k_{a2} of phthalic acid, which was estimated as 0.11 r.s.d. This dissociation constant was listed as $10^{-4.92}$ in one case [235] and $10^{-5.0}$ in another [236].

The error in β_{CuOH^+} was discussed in Section 4.3.1, and amounts to 1.2 r.s.d.

4.3.6 Effect of Citrate on Free-Copper Determination

Citric acid H_3CIT is a tribasic acid with stepwise dissociation constants of $10^{-2.87}$, $10^{-4.35}$, and $10^{-5.69}$ at an ionic strength of 0.1 [235]. At pH 6 CIT^- is the major species (67%) while HCIT^- comprises 32.6%. Copper forms three mononuclear complexes with citrate; CuCIT^- with a β value of $10^{5.9}$, CuHCIT with a β value of $10^{3.42}$, and CuH_2CIT^+ with a β value of $10^{2.26}$ [235]. The species distributions of copper as a function of total citrate concentration were calculated as described in Section 4.2.4 and plotted in Figure 34(a). For the citrate concentration range used in the calculation, % CuHCIT and % CuH_2CIT^+ are too low to be plotted in Figure 34(a).

Test solutions and blanks containing 0, 0.25, 0.5, 1, 5, and 10 μM citric acid were prepared as described in Section 4.2.5. The presence of this low concentration of citric acid does not change the total sodium ion concentration from 0.1 M . Therefore 50 mL of 0.5 M NaNO_3 stock were added to all test solutions and blanks regardless of the citric acid concentration in the test solution. The above solutions were analyzed for free copper by the ion exchange column equilibration method

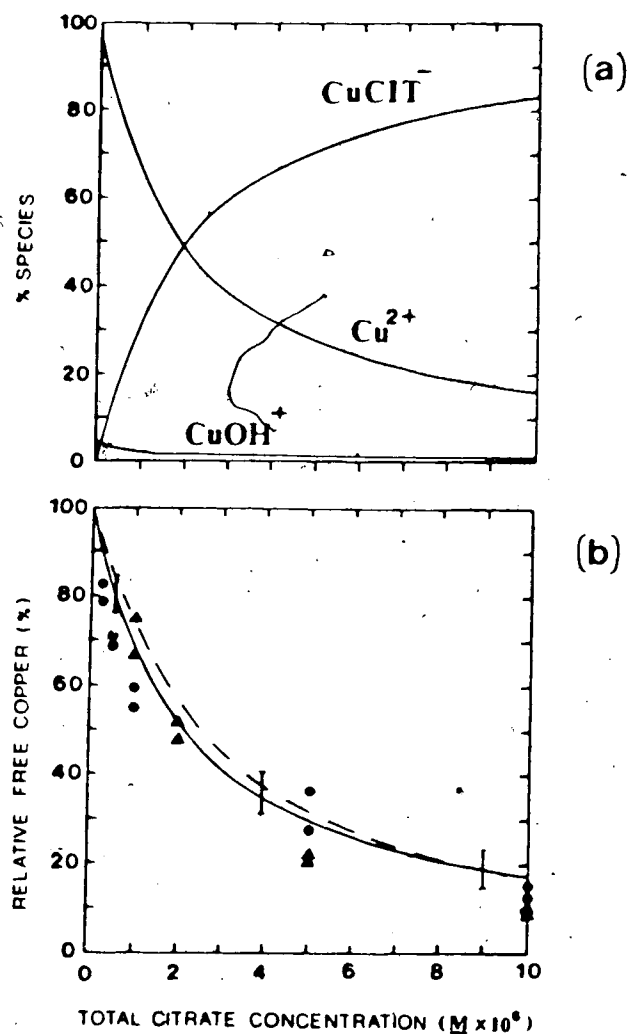


Figure 34. (a) Copper species distribution vs total citrate concentration for $1 \times 10^{-7} M$ total copper at pH 6.0; (b) the decrease in relative free copper with increase in total citrate concentration as obtained by the ion exchange method (●) and by the ion selective electrode method (▲). The solid line in (b) is calculated from the Cu^{2+} species distribution in (a) as outlined in Appendix B. The dashed line in (b) is calculated from the Cu^{2+} species distribution curve (not shown) for $1 \times 10^{-6} M$ total copper.

(Section 3.2) and the relative free copper was plotted against the total citrate concentration (solid dots in Figure 34(b)). The solid and the dashed lines in Figure 34(b) are the relative free copper curves as calculated from the Cu^{2+} species distribution curves for $1 \times 10^{-7} \text{ M}$ and $1 \times 10^{-6} \text{ M}$ total copper concentrations respectively. The solid triangles are the results obtained by ISE (Section 4.2.6). Both the ion exchange and the ion selective electrode methods gave results close to those predicted by calculation. As seen from Figure 34(a) the major species formed upon addition of citric acid is CuCIT^- , which is excluded from the resin phase because of its negative charge.

The absolute standard deviation in the solid line of Figure 34(b) was calculated to be $\pm 5\%$ to $\pm 7\%$ based on estimated uncertainties in β_{CuOH^+} (Section 4.3.1), α_{CIT^-} , and β_{CuCIT^-} . The uncertainty in α_{CIT^-} was calculated as 0.12 r.s.d. based on an equivalent uncertainty in the k_{a3} of citric acid [235]. At $\mu = 0.1$ β_{CuCIT^-} was reported to be $10^{5.90}$ [235] while at $\mu = 0.5$ it was reported as $10^{5.95}$ [236]. The value of β_{CuCIT^-} used in these calculations was $10^{5.9 \pm 0.1}$, corresponding to 0.27 r.s.d. The absolute standard deviations in the relative free copper are shown as error bars in Figure 34(b).

4.3.7 Effect of Salicylate on Free-Copper Determination

Salicylic acid (H_2SAL) has two acidic hydrogens, one a carboxylic hydrogen ($k_{a1} = 10^{-2.81}$) and the other a phenolic hydrogen ($k_{a2} = 10^{-13.4}$) [235]. At pH 6 salicylic acid is 99.9% in the $HSAL^-$ form. Copper ion forms two complexes with salicylate ion, $CuSAL$ with a formation constant of $10^{10.6}$ and $Cu(SAL)_2^{=}$ with a formation constant of $10^{18.5}$ [235]. Following the general procedure described in Section 4.2.4 and Appendix A the copper species distribution vs total salicylate concentration was calculated; the results obtained are plotted in Figure 35(a).

Test solutions and blanks containing 0, 0.5, 1, 3, and 5 mM sodium salicylate were prepared as described in Section 4.2.5 and analyzed for free copper by the ion exchange column equilibration method of Section 3.2. The results obtained, expressed as relative free copper (Section 4.3.1) are plotted against total salicylate concentration in Figure 34(b) (solid circles). The solid line in (b) is the relative free copper as calculated from the Cu^{2+} species distribution curve of Figure 35(a) (Appendix B) while the solid triangles are experimental results obtained by the ion selective electrode method (Section 4.2.6).

Good agreement is found between the ISE method and

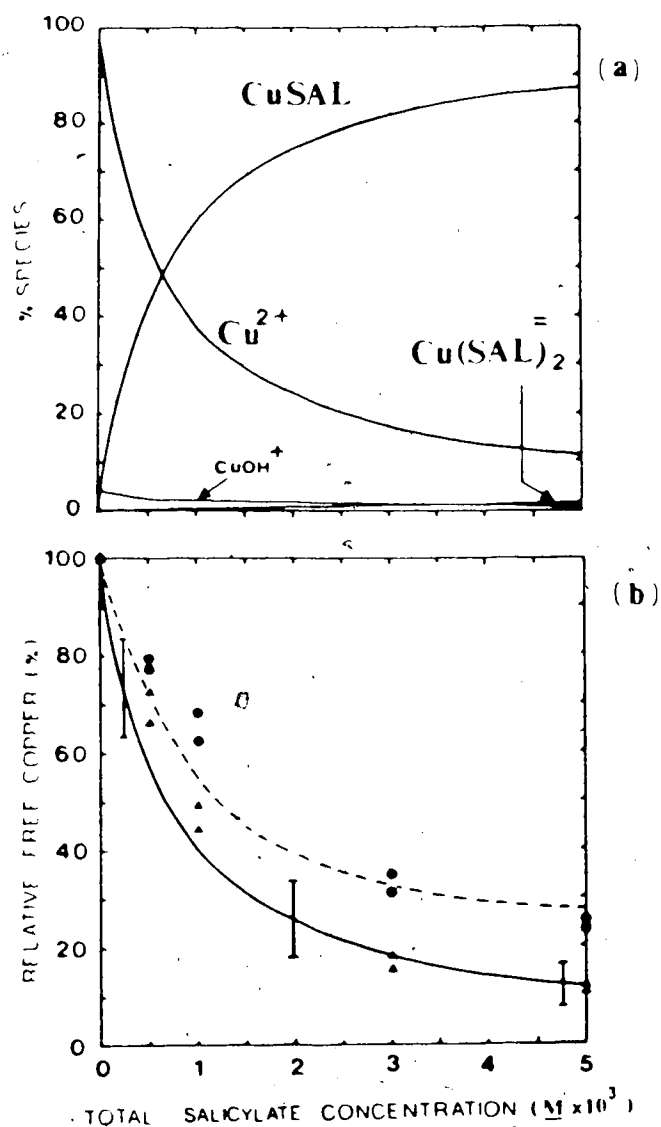


Figure 35. (a) Copper species distribution vs total salicylate concentration at pH 6; (b) the decrease in relative free copper as total salicylate concentration is increased as obtained by the ion exchange method (●) and by the ion selective electrode method (▲). The solid line in (B) was calculated from the Cu²⁺ species distribution in (a) while the dashed line was calculated taking into account sorption of CuSAL as well as Cu²⁺.

the calculation method, but ion exchange gave higher relative free copper. This may be attributed to sorption of the neutral species CuSAL.

An experiment was conducted to test the possibility of removal of sorbed neutral complexes during the column washing cycle. The experiment involved washing the loaded column with different solvent mixtures and pure solvents for periods of time ranging from 4 to 15 min. The solvents studied were water, 50:50 methanol/water, and 95:5 methanol/water. In each case there was no change in the eluted copper signal from that obtained in the normal washing cycle of 4 min using distilled water. This indicates that either there are no sorbed neutral complexes or that such sorbed complexes are not removed by the solvents used.

The dashed line in Figure 35(b) was calculated from the solid line by taking into account the sorption of CuSAL with a distribution coefficient of 8 L/g, a value arbitrarily chosen to fit the experimental data of the ion exchange method. Details of the calculation procedure are given in Appendix B. The dashed line does not fit the experimental data of the ion exchange method very closely, partly because of the relatively high uncertainty in the calculations of the solid line, especially in the low salicylate concentration region ($\pm 11\%$ absolute standard

deviation). The standard deviation in the relative free copper curve of Figure 35(b) was calculated taking into account errors in β_{CuOH^+} (1.2 r.s.d., Section 4.3.1), $\alpha_{\text{SAL}} = (0.25 \text{ r.s.d.})$, and β_{CuSAL} (0.38 r.s.d.). As before, the uncertainty in α_{SAL} was taken as the uncertainty in k_{a2} for salicylic acid which was evaluated from five values reported at $\mu = 0.1$ [235,236]. For β_{CuSAL} Martell and Smith [235] listed the value $10^{10.62 \pm 0.02}$ at $\mu = 0.1$ while in the IUPAC compilation [236] the listed value is $10^{10.80 \pm 0.03}$ at the same ionic strength. For this calculation the value used was $10^{10.6 \pm 0.1}$.

4.3.8 Effect of Fulvic Acid on Free-Copper Determination

Fulvic acid is the soluble fraction of the humic substances in soil or water. It is a polydispersed polymer with a molecular weight of a few hundred to a few thousand atomic units containing phthalic and salicylic acid-type functional groups [128,133]. Because of the ill-characterized nature and of the very complex behavior of fulvic acid [131,201] no attempt was made to utilize the formation constants reported in the literature to predict the variation of free-copper concentration with fulvic acid concentration. It was decided simply to compare the results of the ion exchange column equilibration method with those of the copper ion

selective electrode method.

Test solutions and blanks containing 0, 0.25, 0.5, 1.25, and 2 mg/L of fulvic acid were prepared as described in Section 4.2.5 except that 50 mL of NaNO_3 stock solution were added to all test solutions and blanks. These solutions were stored in polyethylene bottles for 24 h, after which they were analyzed for free copper by the ion exchange column equilibration method (Section 3.2). A plot of relative free copper against fulvic acid concentration is presented in Figure 36 (solid dots). The solid triangles are those obtained by the ion selective electrode method (Section 4.2.6).

The relative free copper obtained by the ion exchange method is similar to, or even slightly lower than, that obtained using the ISE. The selectivity of the ion exchange method for free copper in the presence of fulvic acid may be due to the fact that copper-fulvate complexes formed are anionic and therefore are excluded from the cation exchange resin. Gamble [237] showed that Armadale fulvic acid in 0.1 M KCl is almost completely ionized for H^+ concentrations less than 1×10^{-5} molal and has a total of 6.5 milliequivalents of acidic functional groups per gram. The concentration of copper in the test solution (1×10^{-7} M) is too small to neutralize the negatively charged fulvate ligand since the latter is available in 6

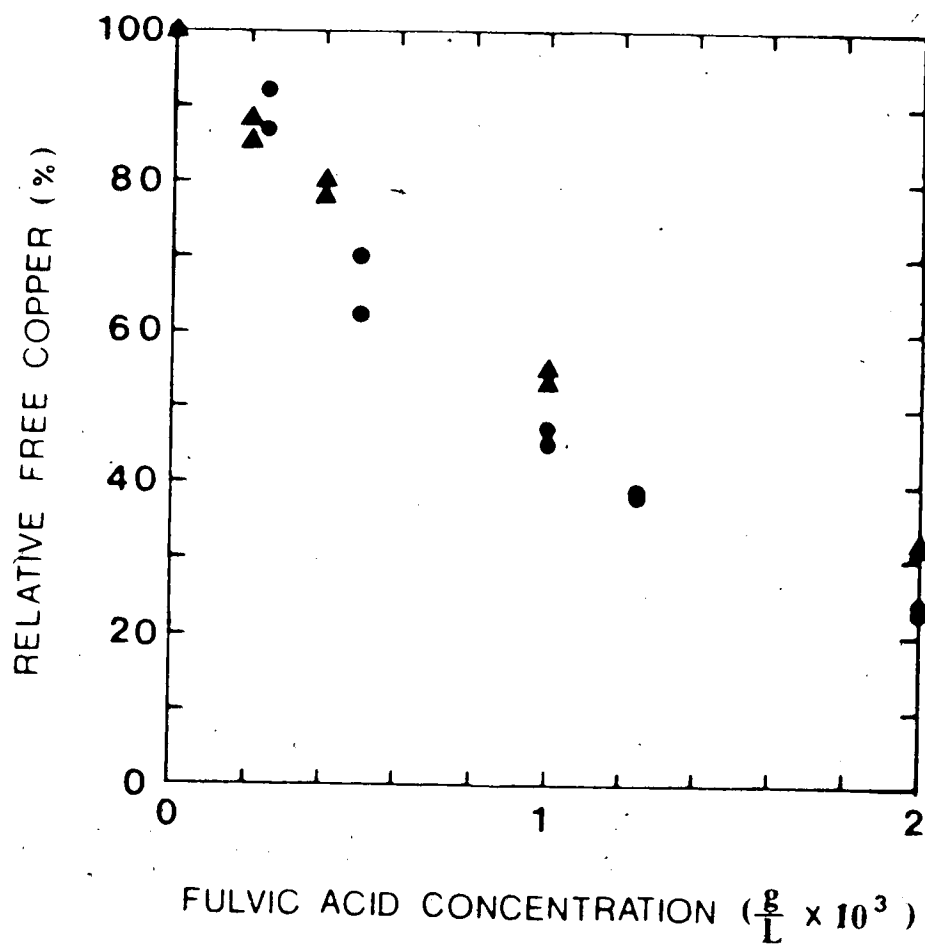


Figure 36. The decrease in relative free copper as a function of fulvic acid concentration by the ion exchange method (O) and by the ion selective electrode method (Δ).

to 120 fold excess. The fact that model organic ligands such as salicylate and phthalate (with the same functional groups as fulvic acid) interfere in the ion exchange method while fulvate apparently does not means that such simple ligands cannot be used here to simulate the behavior of fulvic acid. This is not surprising in light of the polymeric nature of fulvic acid.

The agreement between the results obtained by the two methods in Figure 36 is within about 10% over the ligand concentration range studied. For these measurements, as for all of the ion selective electrode measurements in this chapter, the copper concentration employed had to be a factor of 10 larger than that used in the ion exchange method because of the insensitivity of the electrode. Thus the ion exchange method, which has the same selectivity for free copper in the presence of fulvic acid, can be used at the lower copper concentrations more commonly encountered in natural waters.

In the pH range of 6 to 8 speciation modelling in natural water has shown that the major copper fraction is associated with soluble organic matter such as fulvic acid [167]. Experimental studies have confirmed the above statement. It was reported that 58 to 98% of the copper in fresh water [166,238] and 67% of the copper in salt water [148], may be organically bound. This means that

the fraction bound to inorganic ligands such as sulfate ion may be relatively small and the interference observed in that system may be small or nonexistent. This further supports use of the ion exchange method for free-copper speciation in natural water samples.

Based on the results obtained in this chapter, as well as in other studies, one can conclude that dicationic copper species such as $\text{Cu}(\text{en})_2^{2+}$ interfere strongly in the ion exchange method. That is, the distribution coefficient of this complex between the resin and the solution phase is higher than that of free copper, which was determined in this work as 41 ± 1 L/g (Section 3.3.8) for Dowex 50W-X8. Monocationic species such as CuGLY^+ and neutral copper species such as CuPTH and CuSAL interfere to varying degrees, with distribution coefficients ranging from 8 to 9 L/g. Anionic copper species such as CuCIT^- do not interfere, i.e., the distribution coefficient is less than 8 L/g.

4.3.9 Determination of Free Copper in a Lake Water Sample

The Bonneville Lake water sample, filtered and prepared as described in Section 4.2.7, was analyzed for free copper by the ion exchange column equilibration method (Section 3.2). The peak area obtained for the sample solution was 0.035 ± 0.003 absorbance•second which

is smaller than that of a blank test solution (0.055 + 0.004 absorbance·second) used in the calibration curve (Section 4.2.7). This is probably due to complexation of the copper impurities from the reagents with the available ligands in the sample solution. Another blank, prepared by the same procedure except using unfiltered distilled water, gave the same peak area as the above blank, which eliminates the possibility of copper contamination by the filter or adsorption on the filter. The above results indicate that free copper in the lake water sample is below the detection limit of the system, and that the water sample is capable of complexing the copper impurities that are introduced into the sample solution through the addition of lutidine buffer and swamping electrolyte.

4.3.10 Determination of the Complexing Capacity of a Bonneville Lake Water Sample by Copper Titration

The copper-spiked lake water sample solutions (Section 4.2.8) were analyzed for free copper by the ion exchange column equilibration method (Section 3.2). As observed in the previous section the unspiked samples showed a lower copper signal than the blank. Sample solution (100 mL) spiked with 1.25×10^{-9} moles of copper showed a free-copper signal comparable to the blank. The

free-copper concentration was calculated from a calibration curve at pH 5.2. A plot of the free-copper concentration obtained vs the total copper concentration added to the sample solutions is presented in Figure 37. The total copper concentration in each sample solution was calculated as the sum of the copper spike and the copper impurity from the reagents. The copper contribution by the reagents was evaluated by graphite furnace AAS (Section 4.3.11) as $(1.8 \pm 0.3) \times 10^{-8} \text{ M}$.

The intersection point of the two segments of the curve was used to calculate the complexing capacity of the water sample ($3.0 \times 10^{-8} \text{ M}$). This value is very low compared to that of many lakes around the world which range from $1.0 \times 10^{-7} \text{ M}$ to $1.26 \times 10^{-4} \text{ M}$ [120]. This is not surprising since the water sample is poorly mineralized and has a low total organic carbon. Table 9 shows the chemical assay report that accompanied the sample of Bonneville Lake water. For comparison an assay of another lake (#108) reported by Wagemann and Barica [167] is also included in the table. The low complexing capacity of the Bonneville Lake water sample means that the lake is susceptible to metal ion pollution more than others. This is also evident from the low pH of this lake, it is poorly buffered.

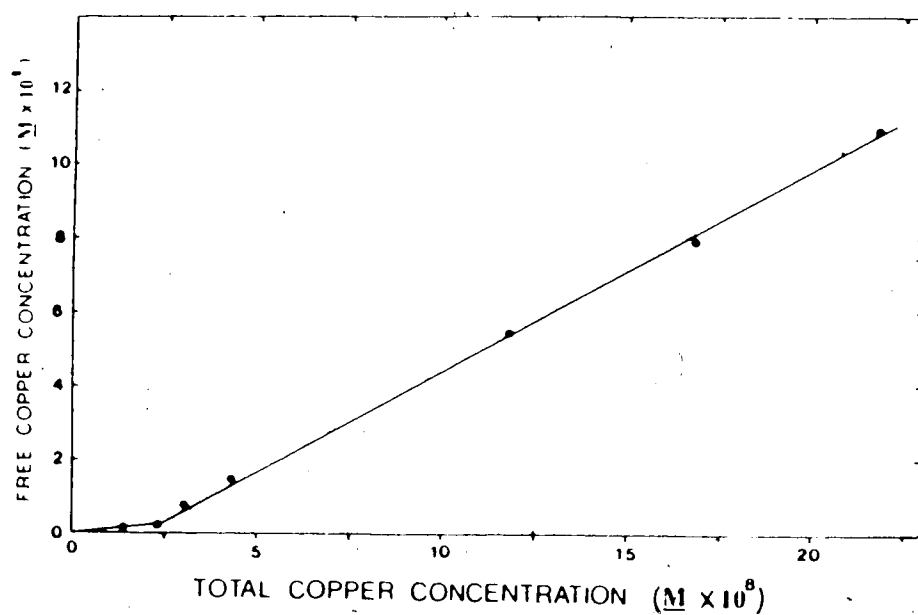


Figure 37. Relation between the total copper concentration in the sample solution and the free-copper concentration as determined by the ion exchange column equilibration/AAS method.

Table 9. Chemical composition of Bonneville Lake water, Quebec and a pothole lake near Erickson, Manitoba [167].

	Bonneville	Lake #108 [167]
Ca^{2+} (mg/L)	0.93	72
Mg^{2+} (mg/L)	0.24	180
Na^{+} (mg/L)	0.44	24
K^{+} (mg/L)	0.38	32
NH_4^{+} (mg/L)	0.015	0.073
SO_4^{2-} (mg/L)	4.00	710
Cl^{-} (mg/L)	0.30	34
Dissolved organic carbon (mg/L)	3.9	28
Dissolved inorganic carbon (mg/L)	--	51
Conductivity ($\mu\text{mhos}\cdot\text{cm}^{-1}$)	13.6	1470
Alkalinity (mg/L)	1.60	921
pH	5.6	8.1-8.5

4.3.11 Determination of the Total Copper Concentration in Lake Water by Graphite Furnace AAS

It was necessary to determine the total copper concentration of the sample solutions used in Section 4.3.9. This would allow accurate determination of the total copper concentration in the sample and the exact contribution of reagent contamination.

The filtered sample, the treated sample (Section 4.2.7), and its blank solution were analyzed for total copper using a Perkin-Elmer 5000 AAS (Section 4.2.3) with the experimental conditions listed in Table 7. The determination was carried out by N. Motkosky of the Department of Chemistry, University of Alberta. A linear calibration curve was obtained using copper concentrations of 0, 2.5, 5, 7.5, and 10 ng/mL in dilute nitric acid (1% v/v).

No copper could be detected in the filtered sample. For the treated sample and its blank a small copper concentration of 1.2 ng/mL was detected for both. This is, obviously, a copper contribution by the reagents added in the treatment process, and is equivalent to 1.8×10^{-8} M. The general conclusion in this section is that the Bonneville Lake water sample contains no detectable copper.

CHAPTER 5

CONCLUSIONS AND FUTURE WORK

In the first part of this thesis it has been demonstrated that solvent extraction in the flow injection analysis (FIA) mode can be effectively used to eliminate interferences prior to flame atomic absorption spectrophotometry (AAS). In the work reported this technique was used to eliminate spectral line interference from iron in the determination of zinc. However, it should be evident that the technique can just as easily be used to remove other types of spectral interferences and also matrix effects in general. Another significant discovery made in this work is the fact that flow compensation using the extracting organic solvent provides a convenient and reliable means of interfacing solvent extraction/FIA with the nebulizer of an atomic absorption spectrophotometer without sacrificing signal stability.

The effect of various chemical, instrumental, and flow parameters on peak height in solvent extraction/FIA has been quantitatively described by an equation developed during this work. This equation has been experimentally verified. Such a quantitative understanding is useful for

optimization of solvent extraction/FIA systems interfaced with various detectors.

Another significant contribution of this work is development of a semiquantitative model of phase segment formation in solvent extraction/FIA based on consideration of both the interfacial and hydrodynamic forces operating in the segmentor. This model represents a viable basis for a theoretical understanding of the segmentation process and provides a guide for the design of new and modified segmentors for use in continuous flow systems.

The solvent extraction/FIA method developed here can be adapted for preconcentration and elimination of various interferences in the analysis of extractable trace elements in natural water, biological, soil, and geological samples. It can also be used to investigate solvent extraction processes since the method is rapid and because extraction parameters can be easily changed. Interfacing of solvent extraction/FIA should be feasible with other spectroscopic techniques such as graphite furnace AAS and inductively coupled plasma atomic emission spectroscopy, where matrix and spectral interferences are encountered more frequently.

In the second part of this thesis a previously developed semiautomated method for free-copper ion determination by an ion exchange column equilibration

technique was characterized, particularly with respect to its selectivity for the free Cu^{2+} species in the presence of copper(II)-containing complexes. It was found that the method is selective for free copper in the presence of negatively charged complexes but that neutral and positively charged copper complexes may interfere. The method is applicable to natural waters with pH values less than 6 which do not contain a high concentration of complexing ligands that form neutral or positively charged copper complexes. This condition is likely to be met for many natural waters where complexation arises primarily from humic and fulvic acids. The total concentration of sulfate in natural waters usually ranges from 10^{-3} to 10^{-4} M, although it may be as high as 7×10^{-3} M for waters treated with copper sulfate. However, even in this case the error in Cu^{2+} concentration due to uptake of CuSO_4 will be < 5%. Furthermore, complexing ligands will associate with the major cations in natural water such as Ca^{2+} and Mg^{2+} to further reduce the available ligand concentration.

The ion exchange column equilibration method is an order of magnitude more sensitive than the copper ion selective electrode method. However, the ion exchange method requires addition of a swamping electrolyte which may perturb the chemical equilibria in the system. It

also requires longer analysis times than the ion selective electrode method and is not as selective for the Cu^{2+} species.

Since the pH of natural waters may range between 4 and 9 it is desirable to extend the applicability of the ion exchange method to pH values above 6. This would require further investigation into the formation of colloidal species that can adsorb onto the column, along with investigation of means of eliminating them. Based on the filtration study reported in this work, an on-line filter might be used to remove colloidal copper from the sample solution. At $\text{pH} > 6$ complexation of copper with carbonate and bicarbonate ions becomes important. Thus if future studies were conducted in this region it would be necessary to assess the specificity of the ion exchange method in the presence of these ligands.

Specificity of the method for free-copper ion could be improved by replacement of the resin used here by a column packing which would be expected to be more selective for Cu^{2+} , such as porous glass beads containing chemically bonded ligands. The method could also be adapted to multi-element free metal ion measurements by coupling the ion exchange flow system to an inductively coupled plasma atomic emission spectrophotometric detector. Specificity of the resin for other free metal

ions would have to be verified in a similar way to that outlined in this thesis. There also exists the possibility of replacing the atomic absorption spectroscopic detection with electrochemical, colorimetric, or even neutron activation detection. The possibility of measuring much lower concentrations of free metal ions than can be measured by ion selective electrodes provides motivation for further studies of the column equilibration technique.

REFERENCES

1. J. Ruzicka and E.H. Hansen, Anal. Chim. Acta 78, 145 (1975).
2. K.K. Stewart, G.R. Beecher and P.E. Hare, Anal. Biochem. 70, 167 (1976).
3. D. Betteridge, Anal. Chem. 50, 832A (1978).
4. J. Ruzicka and E.H. Hansen, Chemtech. Dec., 756 (1979).
5. C. Ranger, Anal. Chem. 53, 20A (1981).
6. C. Ranger, Amer. Lab. 14, 56 (1982).
7. B. Rocks and C. Riley, Clin. Chem. 28, 409 (1982).
8. J. Ruzicka and E.H. Hansen, Anal. Chim. Acta 145, 1 (1983).
9. B.I. Karlberg, Amer. Lab. 15, 73 (1983).
10. C. Riley, B.F. Rocks and R.A. Sherwood, Talanta 31, 879 (1984).
11. M. Gallego, M.D. Luque de Castro and M. Valcarcel, Atomic Spectrosc. 6, 16 (1985).
12. M.D. Luque de Castro and M. Valcarcel Cases, Analyst 109, 413 (1984).
13. J. Ruzicka and E.H. Hansen, "Flow Injection Analysis", John Wiley and Sons, New York (1981).

14. J.M. Reijn, W.E. Van der Linden and H. Poppe, Anal. Chim. Acta 123, 229 (1981).
15. R. Tijssen, Anal. Chim. Acta 114, 71 (1980).
16. J.H.M. Van den Berg, R.S. Deelder and H.G.A. Egberink, Anal. Chim. Acta 114, 91 (1980).
17. L.R. Snyder and H.J. Adler, Anal. Chem. 48, 1022 (1976).
18. A Sodergren, Analyst 91, 113 (1966).
19. B. Karlberg and S. Thelanders, Anal. Chim. Acta 98, 1 (1978).
20. H. Bergamin F°, J.X. Medeiros, B.F. Reis and A.E.G. Zagatto, Anal. Chim. Acta 101, 9 (1978).
21. L. Fossey and F.F. Cantwell, Anal. Chem. 54, 1693 (1982).
22. L. Fossey and F.F. Cantwell, Anal. Chem. 55, 1882 (1983).
23. J. Kawase, A. Nakae and M. Yamanaka, Anal. Chem. 51, 1640 (1979).
24. M. Bengtsson and G. Johansson, Anal. Chim. Acta 158, 147 (1984).
25. F.F. Cantwell and J.A. Sweileh, Anal. Chem. 57, 329 (1985).
26. J.A. Sweileh and F.F. Cantwell, Anal. Chem. 57, 420 (1985).

27. D.C. Shelly, T.M. Rossi and I.M. Warner, Anal. Chem. 54, 87 (1982).
28. T.M. Rossi, D.C. Shelly and I.M. Warner, Anal. Chem. 54, 2056 (1982).
29. L. Nord and B. Karlberg, Anal. Chim. Acta 164, 233 (1984).
30. L. Snyder, J. Levine, R. Stoy and A. Conetta, Anal. Chem. 48, 942A (1976).
31. L. Nord and B. Karlberg, Anal. Chim. Acta 118, 285 (1980).
32. K. Ogata, S. Tanabe and T. Imanari, Chem. Pharm. Bull. 31, 1419 (1983).
33. K. Backstrom, L-G. Danielsson and L. Nord, Anal. Chim. Acta 169, 43 (1985).
34. J.L. Burgnera and M. Burgnera, Anal. Chim. Acta 153, 207 (1983).
35. J.A. Sweileh and F.F. Cantwell, Can. J. Chem. 63, 2559 (1985).
36. A.C. West, V.A. Fassel and R.N. Kniseley, Anal. Chem. 45, 1586 (1973).
37. M. Yanagisawa, M. Suzuki and T. Takeuchi, Talanta 14, 933 (1967).
38. G.R. Kornblum and L. DeGalan, Spectrochim. Acta 28B, 139 (1973).

39. R.J. Lovett, D.L. Welch and M.L. Parsons, Appl. Spectrosc. 29, 470 (1975).
40. G.K. Billing, At. Absorpt. Newsl. 4, 357 (1965).
41. V.A. Fassel, J.O. Rasmuson and T.O. Cowley, Spectrochim. Acta 23B, 579 (1968).
42. W.R. Kelly and C.B. Moore, Anal. Chem. 45, 1274 (1973).
43. G. Wibetoe and F.J. Langmyhr, Anal. Chim. Acta 165, 87 (1984).
44. S.R. Koirtyohan and E.E. Pickett, Anal. Chem. 37, 601 (1965).
45. R. Stephen, CRC Crit. Rev. Anal. Chem. 9, 167 (1980).
46. J.J. Sotera and H.L. Kahn, Amer. Lab. 14, 100 (1982).
47. H. Massmann, Talanta 29, 1051 (1982).
48. J. Nix and T. Goodwin, At. Absorpt. Newsl. 9, 119 (1970).
49. P. Hannaker and T.C. Hughes, Anal. Chem. 49, 1485 (1977).
50. J.R. Clark, J.G. Viets, Anal. Chem. 53, 61 (1981).
51. L. Zhou, T.T. Chao and R.F. Sanzolone, Talanta 32, 475 (1985).
52. M.S. Cresser, "Solvent Extraction in Flame Spectroscopic Analysis", Butterworths, London (1978).

53. J.E. Allan, Spectrochim. Acta 17B, 467 (1961).
54. A. Ringbom, "Complexation in Analytical Chemistry", Interscience, New York (1963); Chemical Analysis Series, Vol. 16.
55. G.H. Morrison and H. Freiser, "Solvent Extraction in Analytical Chemistry", Wiley, New York (1966).
56. P. Stary, "The Solvent Extraction of Metal Chelates", Pergamon Press, New York (1964).
57. Y. Marcus and A.S. Kertes, "Ion Exchange and Solvent Extraction of Metal Complexes", Wiley-Interscience, New York (1964).
58. O. Klinghoffer, J. Ruzicka and E.H. Hansen, Talanta 27, 169 (1980).
59. L. Nord and B. Karlberg, Anal. Chim. Acta 125, 199 (1981).
60. L. Nord and B. Karlberg, Anal. Chim. Acta 145, 151 (1983).
61. K. Backstrom, L-G. Danielsson and L. Nord, Analyst 109, 323 (1984).
62. M. Gallego and M. Valcarcel, Anal. Chim. Acta 169, 161 (1985).
63. M.S. Taylor, Proc. Anal. Div. Chem. Soc., 342 (1976).
64. K.J.R. Rosman and P.M. Jeffery, Chem. Geol. 8, 25 (1972).

65. W.J. Price, "Spectrochemical Analysis by Atomic Absorption", Hayden, London (1979), p. 356.
66. J.B. Headridge and A. Sowerbutts, *Analyst*, 97, 442 (1972).
67. N. Yoza and S. Ohashi, *Anal. Lett.* 6, 595 (1973).
68. D. Thornburn-Burns, F. Glockling and M. Harriott, *Analyst* 106, 921 (1981).
69. J.A. Koropchak, and G.N. Coleman, *Anal. Chem.* 52, 1252 (1980).
70. J.D. Messman and T.C. Rains, *Anal. Chem.* 53, 1632 (1981).
71. D.R. Jones IV, H.C. Tang and S.E. Manahan, *Anal. Chem.* 48, 7 (1976).
72. K. Fukamachi and N. Ishibashi, *Anal. Chim. Acta* 119, 383 (1980).
73. (a) N. Yoza, Y. Aoyagi and S. Ohashi, *Anal. Chim. Acta* 111, 163 (1979).
(b) "CRC Handbook of Chemistry and Physics", 64th Ed., R.C. Weast Editor-in-Chief, CRC Press Inc., Boca Raton, FL (1983).
(c) J.A. Riddick and W.B. Bunger, "Organic Solvents, Physical Properties and Methods of Purification", 3rd Ed., Techniques of Chemistry Series, Vol. II, Wiley-Interscience, New York (1970).

- (d) K.B. Yatsimirskii and V.D. Korableva, *Z. Neorg. Khim.* 3, 339 (1958); (Eng. p. 139).
- (e) P. Ulmgren and O. Wahlberg, *Acta Chem. Scand.* A28, 631 (1974).
74. J. Treit, J.S. Nielsen, B. Kratochvil and F.F. Cantwell, *Anal. Chem.* 55, 1650 (1983).
75. J. Ruzicka and E.H. Hansen, *Anal. Chim. Acta* 99, 37 (1978).
76. H. Yamada, K. Uchino, H. Koizumi, T. Noda and K. Yasuda, *Anal. Lett.* A11, 855 (1978).
77. F. Fernandez and R. Giddings, *At. Spectrosc.* 3, 61 (1982).
78. A.W. Boorn and R.F. Browner, *Anal. Chem.* 54, 1402 (1982).
79. P.W.J.M. Boumans and M. Ch. Lux-Steiner, *Spectrochim. Acta* 37B, 97 (1982).
80. T.R. Gilbert and B.A. Penney, *Spectrochim. Acta* 38B, 297 (1983).
81. C.J. Sternberg, Chapter 6 in Giddings, J.C., Keller, R.A., Ed. "Advances in Chromatography", Vol. 2, Marcel Dekker, New York (1966).
82. W.R. Wolf and K.K. Stewart, *Anal. Chem.* 51, 1201 (1979).
83. M. Brown and J. Ruzicka, *Analyst* 109, 1091 (1984).

84. A. Leo, C. Hansch and D. Elkins, Chem. Rev. 71, 525 (1971).
85. J. Kawase, Anal. Chem 52, 2124 (1980).
86. L. Fossey and F.F. Cantwell, Anal. Chem. 57, 922 (1985).
87. J.T. Davies and E.K. Rideal, "Interfacial Phenomena", 2nd ed., Academic Press, New York (1963), Chapter 1.
88. A.W. Adamson, "Physical Chemistry of Surfaces", 2nd ed., Academic Press, New York (1967), Chapters 1 and 7.
89. F.W. Kieth, Jr. and A.N. Hixon, Ind. Eng. Chem. 47, 258 (1955).
90. "International Critical Tables", 1st ed., Vol. 4, McGraw-Hill, New York (1928), pp. 432-475.
91. H. Peper and J. Berch, J. Phys. Chem. 48, 1586 (1964).
92. C.B. Hayworth and R.E. Treybal, Ind. Eng. Chem. 42, 1174 (1950).
93. T.B. Drew, H.H. Dunkle and R.P. Genereaux, Chapter 5 in J.H. Perry, Ed., "Chemical Engineer's Handbook", 3rd ed., McGraw-Hill, New York (1950).
94. J.R. Partington, "An Advanced Treatise on Physical Chemistry", Vol. 1, Longman, New York (1951), pp. 881-887.

95. F. Daniels, J.W. Williams, P. Bender, R.A. Alberty and C.D. Cornwell, "Experimental Physical Chemistry", 6th ed., McGraw-Hill, New York (1962), Chapter 8.
96. J.R. Partington, "An Advanced Treatise on Physical Chemistry", Vol. 2, Longman, New York (1951), pp. 72-80.
97. T.M. Florence and G.E. Batley, CRC Crit. Rev. Anal. Chem. 9, 212 (1980).
98. A. Mudroch, N. Arafat and S. Davies, Environ. Technol. Lett. 5, 237 (1984).
99. N.M. Arafat, Water Pollut. Res. J. Canada 20, 1 (1985).
100. M.W. Lewis, Jr. and M.C. Grant, Science 207, 176 (1980).
101. M. Lachance; B. Bobee and Y. Grimard, Water Air Soil Pollut. 25, 115 (1985).
102. A.C. Rossin, R.M. Sterritt and J.N. Lester, Water Air Soil Pollut. 19, 105 (1983).
103. R.D. Guy and A.R. Kean, Water Res. 14, 891 (1980).
104. D.P. Laxen, Water Res. 19, 1229 (1985).
105. W.G. Sunda and R.B.L. Guillard, J. Marine Res. 34, 511 (1976).
106. D.M. Anderson and F.M.M. Morel, Limnol. Oceanogr. 23, 283 (1978).

107. W.G. Sunda and P.A. Gillespie, *J. Marine Res.* 37, 761 (1979).
108. G.A. Jackson and J.J. Morgan, *Limnol. Oceanogr.* 23, 268 (1978).
109. J. Gavis; R.R.L. Guillard and B.L. Woodward, *J. Marine Res.* 39, 315 (1981).
110. R. Peterson, *Environ. Sci. Technol.* 16, 443 (1982).
111. M. Merlini and G. Pozzi, *Environ. Pollut.* 13, 119 (1977).
112. D.F. Spencer and L.H. Nichols, *Environ. Pollut. Ser. A* 31, 97 (1983).
113. M.A. Anderson, F.M.M. Morel and R.R.L. Guillard, *Nature* 276, 70 (1978).
114. H.E. Allen, R.H. Hall and T.D. Brisbin, *Environ. Sci. Technol.* 14, 441 (1980).
115. R. Wagemann and J. Barica, *Water Res.* 13, 515 (1979).
116. R.W. Andrew, K.E. Biesinger and G.E. Glass, *Water Res.* 11, 309 (1977).
117. E.E. Dodge and T.L. Theis, *Environ. Sci. Technol.* 13, 1287 (1979).
118. H. Borgman and K.M. Ralph, *Water Res.* 17, 1697 (1983).
119. T.M. Florence, *Anal. Chim. Acta* 141, 73 (1982).

120. T.A. Neubecker and H.E. Allen, Water Res. 17, 1 (1983).
121. G. Feick, R.A. Horne and D. Yeaple, Science 175, 1142 (1972).
122. B.T. Hart, Environ. Technol. Lett. 2, 95 (1981).
123. T.M. Florence, Talanta 29, 345 (1982).
124. R.D. Guy and C.L. Chakrabarti, Chemistry in Canada 28, 26 (1976).
125. Proc. Anal. Div. Chem. Soc. 21, 359 (1984).
126. R.M. Sterritt and J.N. Lester, Sci. Total Environ. 34, 117 (1984).
127. D.R. Turner, M. Whitefield and A.G. Dickson, Geochim. Cosmochim. Acta 45, 855 (1981).
128. R.A. Saar and J.H. Weber, Environ. Sci. Technol. 16, 510A (1982).
129. J. Buffle, P. Deladoey, F.L. Greter and W. Haerdi, Anal. Chim. Acta 116, 225 (1981).
130. D.S. Gamble, C.H. Langford and A.W. Underdown, in "Complexation of Trace Metals in Natural Waters", C.J.M. Kramer and J.C. Duinker (eds.), Martinus Nijhoff/Dr. W. Junk The Hague, Boston, 1984, p. 349.
131. J. Buffle, Anal. Chim. Acta 118, 29 (1980).
132. D.S. Gamble, A.W. Underdown and C.H. Langford, Anal. Chem. 52, 1901 (1980).

133. D.S. Gamble, J.A. Marinsky and C.H. Langford in "Ion Exchange and Solvent Extraction", J.A. Marinsky and Y. Marcus (eds.), Vol. 9, Marcel Decker, New York, 1985, Chapter 7.
134. D.D. Perrin and I.G. Sayce, *Talanta* 14, 833 (1967).
135. J.C. Westall, J.L. Zachary and F.M.M. Morel, Technical Note 18, R.M. Parsons Laboratory for Water Resources and Hydrodynamics, Massachusetts Institute of Technology, Cambridge, MA, 1976.
136. J. Buffle and C. Staub, *Anal. Chem.* 56, 2837 (1984).
137. C. Staub, J. Buffle and W. Haerdi, *Anal. Chem.* 56, 2843 (1984).
138. P. Benes and E. Steinnes, *Water Res.* 8, 947 (1974).
139. P. Benes and E. Steinnes, *Water Res.* 9, 741 (1975).
140. J.A. Cox, K. Slonawska, D.K. Gatchell and A.G. Hiebert, *Anal. Chem.* 56, 650 (1984).
141. R.M. Sterritt and J.N. Lester, *Water Res.* 18, 1149 (1984).
142. D.P.H. Laxen and R.M. Harrison, *Sci. Total Environ.* 19, 59 (1981).
143. R.D. Guy and C.L. Chakrabarti, *Proc. Int. Conf. Heavy Metals Environ.* Vol. 1, T. Hutchinson (ed.), University of Toronto, Ontario 1975, pp. 275.
144. S.J. de Mora and R.M. Harrison, *Water Res.* 17, 723 (1983).

145. R.F.C. Mantoura and J.P. Riley, Anal. Chim. Acta 78, 193 (1975).
146. R. Ernst, H.E. Allen and K.H. Mancy, Water Res. 9, 969 (1975).
147. S.A. Wilson, T.C. Huth, R.E. Arndt and R.K. Skogerboe, Anal. Chem. 52, 15115 (1980).
148. G.E. Batley and T.M. Florence, Anal. Lett. 9, 379 (1976).
149. G.A. Bhat; R.A. Saar; R.B. Smart and J.H. Weber, Anal. Chem. 53, 2275 (1981).
150. Y.K. Chau and K. Lum-Shue-Chan, Water Res. 8, 383 (1974).
151. Y.K. Chau, R. Gächter and K. Lum-Shue-Chan, J. Fish. Res. Board Canada 31, 1515 (1974).
152. I.K. Alzand and C.H. Langford, Can. J. Chem. 63, 643 (1985).
153. J.A. Plambeck, "Electroanalytical Chemistry, Basic Principles and Applications", John Wiley and Sons, New York, 1982, Chapter 16.
154. W. Davidson and M. Whitfield, J. Electroanal. Chem. 75, 763 (1977).
155. H.W. Nurnburg, Sci. Total Environ. 12, 35 (1979).
156. H. Blutstein and D.J. Smith, Water Res. 12, 119 (1978).

157. P. Figura and B. McDuffie, *Anal. Chem.* 52, 1433 (1980).
158. M.S. Shuman, *Anal. Chem.* 54, 998 (1982).
159. K.W. Hanck and J.W. Dillard, *Anal. Chim. Acta* 89, 329 (1977).
160. H.E. Allen, M.L. Crosser and T.D. Brisbin, *Proc. Workshop on Toxicity to Biota of Metal Forms in Natural Water, Duluth, Minnesota, October 1975*, pp 33.
161. T.M. Florence, *J. Electroanal. Chem.* 35, 237 (1972).
162. P. Sagberg and W. Lund, *Talanta* 29, 457 (1982).
163. P.L. Brezonik and J.R. Toschall, Jr., *Anal. Chem.* 54, 1000 (1982).
164. G.A. Bhat, J.H. Weber, J.R. Toschall and P.L. Brezonik, *Anal. Chem.* 54, 2116 (1982).
165. R. Stella and M.T. Ganzerli-Valentini, *Pergamon Series on Environmental Science* 3, 581 (1980).
166. M.J. Stiff, *Water Res.* 5, 585 (1971).
167. R. Wagemann and J. Barica, *Water Res.* 13, 515 (1979).
168. W.T. Bresnahan, C.L. Grant and J.H. Weber, *Anal. Chem.* 50, 1675 (1978).
169. S. Ramamoorthy and P.G. Manning, *J. Inorg. Nucl. Chem.* 35, 1279 (1973).

170. J. Gulens, P.K. Leeson and L. Seguin, Anal. Chim. Acta 156, 19 (1984).
171. A.J. Paulson and D.R. Kester, J. Solution Chem. 9, 269 (1980).
172. W.J. Blaedel and D.E. Dinwiddie, Anal. Chem. 46, 873 (1974).
173. M.J. Smith and S.E. Manahan, Anal. Chem. 45, 836 (1973).
174. A. Lewenstam, T. Sokalski and A. Hulancki, Talanta 32, 531 (1985).
175. T. Hepel, Anal. Chim. Acta 123, 151 (1981).
176. J.C. Westall, F.M.M. Morel and D.N. Hume, Anal. Chem. 51, 1792 (1979).
177. P. Lanza, Anal. Chim. Acta 105, 53 (1979).
178. D. Midgley, Anal. Chim. Acta 87, 19 (1976).
179. M. Neshkova and H. Sheytanov, Talanta 32, 937 (1985).
180. R. Wagemann, J. Phys. Chem. 84, 3433 (1980).
181. J. Barica, J. Fish. Res. Board Canada 35, 141 (1978).
182. P. Baccini and U. Suter, Schweiz Z. Hydrol. 41, 291 (1979).
183. B.T. Hart and S.H.R. Davies, Proc. Int. Conf. Management and Control of Heavy Metals in the Environment, London, Sept. 1979, pp. 466.

184. J. Schubert, J. Phys. Colloid Chem. 52, 340 (1948).
185. J. Schubert and A. Lindenbaum, J. Am. Chem. Soc. 74, 3529 (1952).
186. M.L. Crosser and H.E. Allen, Proc. Ind. Waste Conf., Purdue University 32, 345 (1977).
187. S. Fronaeus, Acta Chem. Scand. 7, 469 (1953).
188. M.H. Cheng, J.W. Patterson and R.A. Minear, J. Water Pollut. Control Fed. 47, 362 (1975).
189. F.F. Cantwell, J.S. Nielsen and S.E. Hrudey, Anal. Chem. 54, 1498 (1982).
190. C.M.G. Van den Berg and J.R. Kramer, Anal. Chim. Acta 106, 113 (1979).
191. K.N. Pearce and L.K. Creamer, Anal. Chem. 46, 457 (1974).
192. Y.K. Chan, P.T.S. Wong, G.A. Bengert and O. Kramer, Anal. Chem. 51, 186 (1979).
193. K.L. Jewett and F.E. Brinckman, J. Chromatogr. sci. 19, 583 (1981).
194. F.J. Fernandez, Atomic Absorpt. Newslett. 16, 33 (1977).
195. T.P. Lynch, N.J. Kernoghan and J.N. Wilson, Analyst 109, 839 (1984).
196. J.L. Burguera and M. Burguera, Anal. Chim. Acta 161, 375 (1984).

197. G.E. Pacey and B.P. Bubnis, Amer. Lab. 16, 17 (1984).
198. R.B. Fulton and B. Kratochvil, Anal. Chem. 52, 546 (1980).
199. I. Tabani, M.Sc. Thesis, Department of Chemistry, University of Alberta, Edmonton, Alberta, Canada, Spring 1986.
200. D.K. Ryan and J.H. Weber, Anal. Chem. 54, 986 (1982).
201. W. Fish and F.M.M. Morel, Can. J Chem. 63, 1185 (1985).
202. M.J. Hanson and G.H. Stefan, Water Resources Bull. 20, 889 (1984).
203. F. Helfferich, "Ion Exchange", McGraw-Hill, New York, 1962, Chapter 5.
204. M. Schnitzer and E.H. Hansen, Soil Science 102, 333 (1970).
205. F.J. Stevenson, Soil Science 123, 10 (1977).
206. F.M.M. Morel, "Principles of Aquatic Chemistry", John Wiley and Sons, 1983, Chapter 8.
207. H.A. Laitinen and W.E. Harris, "Chemical Analysis", 2nd Ed., McGraw-Hill, New York, 1974, Chapter 11.
208. L. Zervas, M. Winitz and J. Greenstein, J. Org. Chem. 22, 1515 (1957).

209. R.G. Bates, "Determination of pH", John Wiley and Sons, New York, 1973, Chapter 5.
210. N.E. Good, G.D. Winget, W. Winter, Th.N. Conolly, S. Izawa and R.M. Singh, *Biochemistry* 5, 467 (1966).
211. U. Bips, H. Ilias, M. Hauröder, G. Kleinhans, S. Pfeifer and K.J. Wannowius, *Inorg. Chem.* 22, 3862 (1983).
212. R. Nakon and C.R. Krishnamoorthy, *Science* 221, 749 (1983).
213. J. Bjerrum, *Acta Chem. Scand.* 18, 843 (1964).
214. I.M. Abrams, *Ind. Eng. Chem.* 46, 1469 (1956).
215. F.F. Cantwell and D. Pietrzyk, *Anal. Chem.* 46, 344 (1974).
216. C.F. Baes, Jr. and R.E. Mesmer, "The Hydrolysis of Cations", Wiley, New York, 1976, Chapter 12.
217. N.K. Milic and P. Durdevic, *Bull. Soc. Chim. Beograd* 49, 459 (1984).
218. P.A. Spear and R.C. Pierce, "Copper in the Aquatic Environment", National Research Council of Canada, Publication No. 16454, 1979, p. 41.
219. J. Kielland, *J. Am. Chem. Soc.* 59, 1675 (1937).
220. C.W. Davies, *J. Chem. Soc.* 2039 (1938).
221. R.A. Robinson and R.H. Stokes, "Electrolyte Solutions", 2nd Ed., Butterworth, London, 1959, Chapter 9.

222. A.E. Martell and R.M. Smith, "Critical Stability Constants, Vol. 4, Inorganic Complexes", Plenum Press, New York, 1976.
223. E. Högfeltdt, "Stability Constants of Metal-Ion Complexes Part A", IUPAC Chemical Data Series No. 21, Pergamon Press, Oxford, 1982.
224. (a) V.A. Fedorov, A.M. Robov, I.I. Shmyd'ko, and V.E. Mironov, Russ. J. Inorg. Chem. 18, 180 (1973).
- (b) J.S. Nielsen, Ph.D. Thesis, Department of Civil Engineering, University of Alberta, Edmonton, Alberta, Canada, Fall 1982.
225. "Guidelines for Data Acquisition and Data Quality Evaluation in Environmental Chemistry", Anal. Chem. 52, 2242 (1980).
226. G.L. Long and J.D. Winefordner, Anal. Chem. 55, 712A (1983).
227. L. Cockerell and H. Walton, J. Phys. Chem. 66, 75 (1962).
228. A. Maes and A. Cremers, J. Chem. Soc. Faraday Trans. I 75, 513 (1979).
229. D.S. Lucyk, unpublished research, University of Alberta, 1985.
230. M. Papineau, private communication (1985).

231. Y.A. Makashev, M.I. Shalaevskaya, V.V. Blokhin and V.E. Mironov, Russ. J. Phys. Chem 49, 493 (1975).
232. E.E. Kriss and K.B. Yastrimirskii, Z. Neorg. Khim. 13, 3270 (1968) (Eng. 1223).
233. A.E. Martell and R.M. Smith, "Critical Stability Constants, Vol. 5: First Supplement", Plenum Press, New York, 1985.
234. A.E. Martell and R.M. Smith, "Critical Stability Constants, Vol. 1: Amino Acids", Plenum Press, New York, 1974.
235. A.E. Martell and R.M. Smith, "Critical Stability Constants, Vol. 3: Other Organic Ligands", Plenum Press, New York, 1977.
236. D.D. Perrin, "Stability Constants of Metal-Ion Complexes, Part B, Suppl. 2: Organic Ligands", IUPAC Chemical Data Series No. 22, Pergamon Press, 1979.
237. D.S. Gamble, Can. J. Chem. 50, 2680 (1972).
238. T.M. Florence, Water Research 11, 681 (1977).

APPENDIX A

CALCULATION OF METAL SPECIES DISTRIBUTION

In the studies of specificity of the ion exchange column equilibration technique for metal ion, M^{++} , various organic and inorganic complexing ligands are added to the test solution. It is therefore necessary to calculate the species distribution in the test solution to allow comparison of predicted $[M^{2+}]$ with the experimental value.

Consider that a fixed concentration of a dibasic weakly acidic ligand, H_2L , is added to a test solution containing a trace amount of metal, M^{++} , and a high concentration of a non-complexing electrolyte. If the ligand forms a variety of mononuclear complexes with the metal (e.g., ML , MHL^+ , ML_2^-), then the metal-containing species distribution as a function of pH can be calculated as shown below.

$$M_T = [M^{++}] + [MOH^+] + [M(OH)_2] + \dots + [M(OH)_n]^{-(n-2)} + \\ ML + [MHL^+] + [ML_2^-] \quad (A.1)$$

Substituting for each species concentration in terms of its conditional formation constant and individual ligand concentration we get

$$\begin{aligned}
 M_T = & [M^{++}] + \beta_{MOH^+}' \cdot [M^{++}] [OH^-] + \beta_{M(OH)_2}' \cdot [M^{++}] [OH^-]^2 + \dots + \\
 & \beta_{M(OH)_n}' \cdot [M^{++}] [OH^-]^{2(2-n)} + \beta_{ML}' \cdot [M^{++}] [L^-] + \\
 & \beta_{MHL^+}' \cdot [M^{++}] [HL^-] + \beta_{ML_2}' \cdot [M^{++}] [L^-]^2 \quad (A.2)
 \end{aligned}$$

Substituting for $[OH^-]$ in terms of $[H^+]$ and k_w (the autoprotolysis constant of water) and recognizing that $[M^{++}]$ is common to all terms we get:

$$\begin{aligned}
 M_T = & [M^{++}] \left(1 + \beta_{MOH^+}' \cdot \frac{k_w}{[H^+]} + \beta_{M(OH)_2}' \cdot \left(\frac{k_w}{[H^+]} \right)^2 + \dots + \right. \\
 & \left. \beta_{M(OH)_n}' \cdot \left(\frac{k_w}{[H^+]} \right)^{2(2-n)} + \beta_{ML}' \cdot [L^-] + \beta_{MHL^+}' \cdot [HL^-] + \right. \\
 & \left. \beta_{ML_2}' \cdot [L^-]^2 \right) \quad (A.3)
 \end{aligned}$$

The fraction of the metal present in the free form, $\alpha_{M^{++}}$ is obtained by rearranging equation A.3

$$\alpha_{M^{++}} = 1 / \left(1 + \beta_{MOH^+} \cdot \frac{k_w}{[H^+]} + \beta_{M(OH)_2} \cdot \left(\frac{k_2}{[H^+]} \right)^2 + \dots + \beta_{M(OH)_n}^{-(n-2)} \right. \\ \left. \cdot \left(\frac{k_w}{[H^+]} \right)^n + \beta_{ML} \cdot [L^-] + \beta_{MHL} \cdot [HL^-] + \beta_{ML_2} \cdot [L^-]^2 \right) \quad (A.4)$$

In the above equation $\alpha_{M^{++}}$ is independent of the metal concentration. It is dependent on pH and the complexing ligand concentration, $[L^-]$. If M_T is much less than the total ligand concentration, C_L , the amount of ligand tied up in the form of metal complexes can be neglected and we can assume that

$$C_L = [H_2L] + [HL^-] + [L^-] \quad (A.5)$$

The individual ligand species concentration in equation A.5 can be calculated in a conventional manner from the acid dissociation constants k_a , and pH [207]:

$$[L^-] = \frac{k_{a1} \cdot k_{a2}}{[H^+]^2 + [H^+] \cdot k_{a1} + k_{a1}k_{a2}} \cdot C_L \quad (A.6)$$

If the total ligand concentration, C_L is not in large excess relative to the metal concentration M_T , an iterative procedure is required to determine the individual ligand

species.

The α value for each metal species can be expressed in terms of $\alpha_{M^{++}}$ by rearranging equation A.4

$$\alpha_{MOH^+} = \frac{[MOH^+]}{M_T} = \beta_{MOH^+}' \cdot \frac{k_w}{[H^+]} \cdot \alpha_{M^{++}} \quad (A.7)$$

$$\alpha_{M(OH)_2} = \frac{[M(OH)_2]}{M_T} = \beta_{M(OH)_2}' \cdot \left(\frac{k_w}{[H^+]} \right)^2 \cdot \alpha_{M^{++}} \quad (A.8)$$

$$\alpha_{M(OH)_n^{-(n-2)}} = \frac{[M(OH)_n^{-(2-n)}]}{M_T} = \beta_{M(OH)_n^{-(n-2)}}' \cdot \left(\frac{k_w}{[H^+]} \right)^n \cdot \alpha_{M^{++}} \quad (A.9)$$

$$\alpha_{ML} = \frac{[ML]}{M_T} = \beta_{ML}' \cdot [L^-] \cdot \alpha_{M^{++}} \quad (A.10)$$

$$\alpha_{MHL^+} = \frac{[MHL^+]}{M_T} = \beta_{MHL^+}' \cdot [HL^-] \cdot \alpha_{M^{++}} \quad (A.11)$$

$$\alpha_{ML_2^{=}} = \frac{[ML_2^{=}] }{M_T} = \beta_{ML_2^{=}}' \cdot [L^=]^2 \cdot \alpha_{M^{++}} \quad (A.12)$$

A programmable calculator can be used to calculate

the species distribution of the metal as a function of pH. It is also possible to calculate the species distribution at a fixed pH and variable ligand concentration. The above calculations can also be done using the various computer programs available which are generally used to solve multiple metal-ligand equilibria (Section 1.2.1).

APPENDIX B

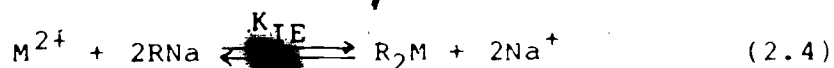
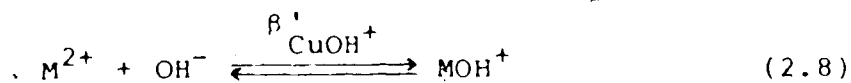
DERIVATION OF AN EXPRESSION FOR THE EFFECT OF SORPTION OF ANOTHER SPECIES IN ADDITION TO FREE METAL

As mentioned in Section 4.1 species other than free metal may also sorb onto a cation exchange resin. It is useful to be able to predict the extent of interference in the measurement of free-copper concentration caused by the sorption of a copper complex. Two cases will be compared here: Case I, where only the free- Cu^{2+} ion is sorbed and Case II, where free- Cu^{2+} and a copper complex species are both sorbed.

Assume a simple system where MOH^+ and ML are the only complexes of a metal ion M^{2+} (such as copper(II)) present at trace concentrations in a buffered test solution that is swamped with a high concentration of non-complexing electrolyte.

Case I: (Only M^{2+} sorbs)

In the absence of complexing ligand, L^- , the following equilibria will be established upon equilibration of the test solution with the resin, RNA , under trace ion exchange conditions.



For the column flow through method of ion exchange equilibration the total concentration of metal species in solution, M_T , is equal to the sum of $[M^{2+}]$ and $[MOH^+]$:

$$M_T = [M^{2+}] + [MOH^+] \quad (2.16)$$

The distribution ratio of the metal between the resin and the solution phases is given by

$$D_{L=0} = \frac{[R_2M]}{[M^{2+}] + [MOH^+]} = \frac{[R_2M]}{M_T} \quad (B.1)$$

Defining $\lambda_{M^{2+}}$ as the distribution coefficient of M^{2+} between the resin and the solution phases:

$$\lambda_{M^{2+}} = \frac{[R_2M]}{[M^{2+}]} \quad (B.2)$$

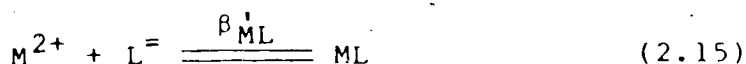
and

$$\alpha_{M^{2+}, L=0} = \frac{[M^{2+}]}{[M^{2+}] + [MOH^+]} = \frac{[M^{2+}]}{M_T} \quad (B.3)$$

where $\alpha_{M^{2+}, L=0}$ is the fraction of the metal in solution present in the free form, M^{2+} in the absence of complexing ligand L^- . Combining equations B.1, B.2, and B.3 we get

$$D_{L=0}^{I} = \lambda_{M^{2+}} \cdot \frac{[M^{2+}]}{M_T} = \lambda_{M^{2+}} \cdot \alpha_{M^{2+}, L=0} \quad (B.4)$$

In the presence of a complexing ligand, L^- , the following equilibrium will be established (Section 2.3) in addition to 2.8 and 2.4 above,



The distribution ratio in this case, $D_{L \neq 0}^{I}$, is given by

$$D_{L \neq 0}^{I} = \frac{[R_2M]}{[M^{2+}] + [MOH^+] + [ML]} = \frac{[R_2M]}{M_T} \quad (B.5)$$

Substituting for $[R_2M]$ from equation B.2 we get

$$D_{L \neq 0}^{I} = \frac{\lambda_{M^{2+}} \cdot [M^{2+}]}{M_T} \quad (B.6)$$

The ratio $[M^{2+}]/M_T$ in equation B.6 is the fraction of

metal present in solution as the free form in the presence of L^- , $\alpha_{M^{2+}, L \neq 0}$, and is a function of $[L^-]$. Equation B.6 can be written as

$$D_{L \neq 0}^I = \lambda_{M^{2+}} \cdot \alpha_{M^{2+}, L \neq 0} \quad (B.7)$$

Dividing equation B.7 by equation B.4 we get

$$\frac{D_{L \neq 0}^I}{D_{L=0}^I} = \frac{\alpha_{M^{2+}, L \neq 0}}{\alpha_{M^{2+}, L=0}} \quad (B.8)$$

In the ion exchange column equilibration method we measure a peak area, P.A., that is proportional to the concentration of the metal in the resin phase, $[R_2M]$ (Section 2.2):

$$P.A. = \frac{G \cdot S}{F} \cdot [R_2M] \quad (2.6)$$

Combining 2.6 and B.1 for a case where the complexing ligand is absent, $L=0$; we get

$$(P.A.)_{L=0} = \frac{G \cdot S}{F} \cdot M_T \cdot D_{L=0} \quad (B.9)$$

Since G , S , F , and M_T are constant it is evident from equation B.9 that in the absence of complexing ligand the

peak area is directly proportional to the distribution ratio $D_{L=0}$. By the same token, combining equations 2.6 and B.5 in the presence of a complexing ligand, i.e., $L \neq 0$, gives

$$(P.A.)_{L \neq 0} = \frac{G \cdot S}{F} \cdot M_T \cdot D_{L \neq 0}^I \quad (B.10)$$

which means that the peak area in the presence of a complexing ligand is proportional to the distribution ratio, $D_{L \neq 0}^I$. Dividing B.10 by B.9 we get

$$\frac{(P.A.)_{L \neq 0}}{(P.A.)_{L=0}} = \frac{D_{L \neq 0}^I}{D_{L=0}^I} \quad (B.11)$$

Combining equations B.11 and B.8 gives

$$\frac{(P.A.)_{L \neq 0}}{(P.A.)_{L=0}} = \frac{D_{L \neq 0}^I}{D_{L=0}^I} = \frac{\alpha_{M^{2+}, L \neq 0}}{\alpha_{M^{2+}, L=0}} \quad (B.12)$$

In panel (a) of Figures 29 to 35 the α values of various species are expressed as % by multiplying each by 100. For a given total ligand concentration, dividing $\alpha_{Cu^{2+}, L \neq 0}$ (in percent) by $\alpha_{Cu^{2+}, L=0}$ yields the corresponding "relative" free copper (%) value used for the solid line in panel (b). As shown by equation B.12, this is proportional to $(P.A.)_{L \neq 0} / (P.A.)_{L=0}$, the ratio of

measured peak area for a test solution containing ligand to that for a test solution not containing ligand.

Case II: (M^{2+} and ML sorb onto resin)

In the absence of complexing ligand just as in Case I, the distribution ratio, $D_{L=0}$, is given by equation B.4.

$$D_{L=0} = \lambda_{M^{2+}} \cdot \alpha_{M^{2+}, L=0} \quad (B.4)$$

In the presence of complexing ligand the following equilibrium, in addition to 2.8, 2.4, and 2.15, must be considered:



where K_{ML} is the distribution constant of the species ML between the resin and the solution phases. Defining λ_{ML} as the distribution coefficient of ML we can write

$$\lambda_{ML} = \frac{[RNaML]}{[ML]} \quad (B.14)$$

In this case the distribution ratio, $D_{L \neq 0}^{II}$, is given by

$$D_{L \neq 0}^{II} = \frac{[R_2M] + [RNaML]}{[M^{2+}] + [MOH^+] + [ML]} = \frac{[R_2M] + [RNaML]}{M_T} \quad (B.15)$$

Substituting for $[R_2M]$ and $[RNaML]$ from equations B.5 and B.14 respectively, we get:

$$D_{L \neq 0}^{II} = \frac{\lambda_{M^{2+}} \cdot [M^{2+}]_{L \neq 0} + \lambda_{ML} \cdot [ML]}{M_T} = \lambda_{M^{2+}} \cdot \alpha_{M^{2+}, L \neq 0} + \lambda_{ML} \cdot \alpha_{ML} \quad (B.16)$$

where α_{ML} is the fraction of the metal in solution present as ML.

Dividing equation B.16 by equation B.4 gives

$$\frac{D_{L \neq 0}^{II}}{D_{L=0}} = \frac{\lambda_{M^{2+}} \cdot \alpha_{M^{2+}, L \neq 0} + \lambda_{ML} \cdot \alpha_{ML}}{\lambda_{M^{2+}} \cdot \alpha_{M^{2+}, L=0}} \quad (B.17)$$

Breaking up the quotient on the right hand side of equation B.17 we get

$$\frac{D_{L \neq 0}^{II}}{D_{L=0}} = \frac{\alpha_{M^{2+}, L \neq 0}}{\alpha_{M^{2+}, L=0}} + \frac{\lambda_{ML} \cdot \alpha_{ML}}{\lambda_{M^{2+}} \cdot \alpha_{M^{2+}, L=0}} \quad (B.18)$$

Comparison of equation B.18 and equation B.8 shows that sorption of ML results in addition of the second term

on the right hand side of equation B.18. $\alpha_{M^{2+}}$ and α_{ML} can be calculated for any ligand concentration (Appendix A).

$\lambda_{M^{2+}}$ (41 L/g for copper(II)) can be determined experimentally by determining the concentration of metal in the resin phase (mole/g) in the absence of complexing ligands and dividing by the free metal concentration in the solution phase (mole/L) in equilibrium with the resin. If experimental results of the type plotted as the points in panels (b) of Figures 29 to 35 do not fit the solid line calculated from equation B.12, which assumes that only M^{2+} is sorbed by the resin, then equation B.18 can be used to evaluate the experimental data. Thus, the dashed line in panel (b) of Figures 30, 31, 32, 33, and 35 was obtained by evaluating the α 's in equation B.18 from literature values of formation constants and assuming a value of λ_{ML} which gives the best fit to the experimental points. The agreement between the dashed lines and experimental points in these cases suggests that the source of deviation from the behavior predicted by equation B.8 is, indeed, the sorption by the resin of a metal-ligand complex in addition to the free metal. The interfering metal-ligand complexes were $CuHPO_4$ (neutral), $CuSO_4$ (neutral), $CuGLY^+$ (cationic), $CuPTH$ (neutral), and $CuSAL$ (neutral).